Institute of Thermoelectricity, Academy of Sciences and Ministry of Education and Science of Ukraine

Journal of THERMOELECTRICITY

International Research

Founded in December, 1993

published 6 times a year

No. 5 *2017*

Editorial Board

International Editorial Board

Founders – National Academy of Sciences, Ukraine
Institute of Thermoelectricity of National Academy of Sciences and Ministry of Education and Science of Ukraine

Certificate of state registration № КВ 15496-4068 ПР

Approved for printing by the Academic Council of Institute of Thermoelectricity of the National Academy of Sciences and Ministry of Education and Science, Ukraine

Address of editorial office:
Ukraine, 58002, Chernivtsi, General Post Office, P.O. Box 86.
Phone: +(380-372) 90 31 65.
Fax: +(380-3722) 4 19 17.
E-mail: jt@inst.cv.ua
http://www.jt.inst.cv.ua

Signed for publication 27.11.17. Format 70×108/16. Offset paper №1. Offset printing.
Printer's sheet 11.5. Publisher's signature 9.2. Circulation 400 copies. Order 5.

Printed from the layout original made by "Journal of Thermoelectricity" editorial board in the printing house of "Bukrek" publishers,
10, Radischev Str., Chernivtsi, 58000, Ukraine

CONTENTS

P.V. Gorskiy

P.V. Gorskiy, *Doctor Phys.-math. science*

Institute of Thermoelectricity of the NAS and MES of Ukraine, 1, Nauky str, Chernivtsi, 58029, Ukraine; *e-mail: anatych@gmail.com*

OPTIMIZATION OF THERMOELECTRIC MATERIALS BASED ON *Zn-Cd-Sb* ALLOYS FOR ANISOTROPIC THERMOELEMENTS

Based on the calculation of the distribution of charge carriers and concentration dependences of the kinetic coefficients of $Zn_{0.2}Cd_{0.8}Sb$ alloy it was established that the highest anisotropic figure of merit of this alloy is achieved in plane "2,3", when it is in the intrinsic region.

The calculations were performed for the nondegenerate electron-hole gas of charge carriers in the approximation of effective mass. Approximation of two ellipsoidal valleys was considered: one electron and one hole. To determine the dependences of components of effective electron and hole mass tensors on the alloy composition, we used a linear approximation by zinc content which was based on the results of calculations of the band structure of CdSb and $Zn_{0.5}Cd_{0.5}Sb$. Moreover, it was considered that the dependence of the mobility of electrons and holes on the alloy composition is determined solely by the dependences of the corresponding components of effective mass tensors on the alloy composition. It was also considered that low zinc content does not affect the lattice thermal conductivity of an alloy that was considered to be inversely proportional to temperature.

The extreme values of anisotropic thermoelectric figures of merit of $Zn_{0.2}Cd_{0.8}Sb$ alloy, calculated at temperatures 300, 400 and 600K, made $2.45 \cdot 10^{-8}$, $2.30 \cdot 10^{-7}$ and $2.1 \cdot 10^{-6} K^{-1}$, respectively, which, at least in the order of magnitude, agrees with the experimental data. The optimal angle of crystal cut corresponding to these figures of merit is about 34^0. The reasons for the discrepancies between the results obtained with both the experiment and the theoretical calculations of the previous authors were also discussed.. Bibl. 11, Fig. 6.

Key words: anisotropic figure of merit, electrons, holes, effective mass tensor, doping level, intrinsic conduction, intrinsic concentration of charge carriers, charge carrier mobility, optimal angle of crystal cut, linear approximation by composition.

Introduction

Technologically, anisotropic thermoelements as compared to thermocouple thermoelements, have the advantage of being much easier to produce due to the absence of a complex interconnect system. However, their thermoelectric figure of merit is much lower than that of thermocouple thermoelements. Therefore, their efficiency as electric energy generators is also essentially lower. Nevertheless, they are of certain interest for use in various sensors and recording devices [1 – 3]. Therefore, there is still a certain interest in the study and search for ways to optimize the corresponding single-crystal materials in order to achieve the highest possible values of the difference the thermoEMF and anisotropic figure of merit. Exactly this research is the purpose of the present article.

Calculation of the anisotropic figure of merit of *Zn-Cd-Sb* alloys and discussion of the results.

Taking into account that in the case of materials with the parabolic band spectrum the most advantageous in terms of their use for creation of anisotropic thermoelements is participation in the

processes of heat and electricity transfer of both electrons and holes, we will first consider the statistics of charge carriers in material. In the single-valley approximation the number of electrons n_e in the conduction band and holes n_h in the valence band for the nondegenerate gas is determined by the expressions [4]:

$$n_e = \frac{4\sqrt{2\pi}\left(m_{e1}^* m_{e2}^* m_{e3}^*\right)^{1/2}\left(k_B T\right)^{3/2}}{h^3}\exp\left(\zeta/k_B T\right), \tag{1}$$

$$n_h = \frac{4\sqrt{2\pi}\left(m_{h1}^* m_{h2}^* m_{h3}^*\right)^{1/2}\left(k_B T\right)^{3/2}}{h^3}\exp\left(-\left(\zeta + E_g\right)/k_B T\right). \tag{2}$$

In these formulae, $m_{e1}^*, m_{e2}^*, m_{e3}^*$, are used to designate components of effective electron mass tensor, and $m_{h1}^*, m_{h2}^*, m_{h3}^*$ – of effective hole mass tensor, h is the Planck constant, k_B is the Boltzmann constant, ζ is the chemical potential of electron subsystem, E_g is the forbidden band width.

Therefore, the semiconductor neutrality equation becomes:

$$\frac{4\sqrt{2\pi}\left(m_{e1}^* m_{e2}^* m_{e3}^*\right)^{1/2}\left(k_B T\right)^{3/2}}{h^3}\exp\left(\zeta/k_B T\right) + N_a = \frac{4\sqrt{2\pi}\left(m_{h1}^* m_{h2}^* m_{h3}^*\right)^{1/2}\left(k_B T\right)^{3/2}}{h^3}\times \\ \times\exp\left(-\left(\zeta + E_g\right)/k_B T\right) + N_d \tag{3}$$

where N_a and N_d designate the concentrations of single-charge acceptor and donor impurities, respectively.

Hence, the reduced chemical potential of electron subsystem is equal to:

$$\eta = \ln\left[\frac{-0.5\left(N_a - N_d\right) + \sqrt{0.25\left(N_a - N_d\right)^2 + a_e a_h \exp\left(-E_g/k_B T\right)}}{a_e}\right], \tag{4}$$

and concentrations of electrons and holes, respectively, are equal to:

$$n_e = -0.5\left(N_a - N_d\right) + \sqrt{0.25\left(N_a - N_d\right)^2 + a_e a_h \exp\left(-E_g/k_B T\right)}, \tag{5}$$

$$n_h = \frac{a_e a_h \exp\left(-E_g/kT\right)}{n_e}. \tag{6}$$

In so doing, in the presence of several sorts of electrons and holes, the values of a_e and a_h can be represented as:

$$a_e = \frac{4\sqrt{2\pi}}{h^3}\left(k_B T\right)^{3/2}\sum_s\left(m_{e1s}^* m_{e2s}^* m_{e3s}^*\right)^{1/2}, \tag{7}$$

$$a_h = \frac{4\sqrt{2\pi}}{h^3}\left(k_B T\right)^{3/2}\sum_s\left(m_{h1r}^* m_{h2r}^* m_{h3r}^*\right)^{1/2}. \tag{8}$$

where summation is carried out for all sorts of electrons and holes.

However, by definition:

$$a_e a_h \exp\left(-E_g/kT\right) = n_i^2, \tag{9}$$

where n_i is intrinsic concentration of charge carriers in material. So, concentrations of electrons in the conduction band and holes in the valence band, respectively, are equal to:

$$n_e = n_i\left(\sqrt{0.25d^2 + 1} - 0.5d\right), \tag{10}$$

$$n_h = \frac{n_i}{\sqrt{0.25d^2 + 1} - 0.5d}, \tag{11}$$

where we introduced material doping level which is equal to:

$$d = \left(N_a - N_d\right)/n_i \ . \tag{12}$$

For the compensated materials, $d = 0$, for materials of n-type conductivity, d is a large in absolute value negative number, for materials of *p*-type conductivity, d is a large in absolute value positive number.

Now we turn to calculation of components of electric conductivity, thermoEMF and thermal conductivity tensors of material. In the approximation of the parabolic spectrum of electrons and holes, the hole and electron thermoEMF separately are isotropic and in the case of nondegenerate gas of free charge carriers are determined by the Schottky-Pisarenko formula [5]:

$$\alpha_e = -\frac{k}{e}\left(2 - \eta\right), \tag{13}$$

$$\alpha_h = \frac{k}{e}\left(2 + \eta + \frac{E_g}{kT}\right), \tag{14}$$

which is written for the case when scattering of charge carriers takes place with an energy-independent cross section, which occurs in the case, for example, of scattering on the deformation potential of acoustic phonons at high temperatures.

We now determine the components of electric conductivity tensor in three main directions. In the same way as in [6], for the components of the electric conductivity tensor we find the following expressions:

$$\sigma_{1e} = \frac{2n_e e^4}{3\pi S\varepsilon_1\varepsilon_0\sqrt{3\pi}\left(k_B T\right)^{3/2}} \sum_s \frac{\sqrt{m_{e1s} + m_{e2s} + m_{e3s}}}{m_{e1s}}, \tag{15}$$

$$\sigma_{1h} = \frac{2n_h e^4}{3\pi R\varepsilon_1\varepsilon_0\sqrt{3\pi}\left(k_B T\right)^{3/2}} \sum_r \frac{\sqrt{m_{h1r} + m_{h2r} + m_{h3r}}}{m_{h1r}}, \tag{16}$$

$$\sigma_{2e} = \frac{2n_e e^4}{3\pi S\varepsilon_2\varepsilon_0\sqrt{3\pi}\left(k_B T\right)^{3/2}} \sum_s \frac{\sqrt{m_{e1s} + m_{e2s} + m_{e3s}}}{m_{e2s}}, \tag{17}$$

$$\sigma_{2h} = \frac{2n_h e^4}{3\pi R\varepsilon_2\varepsilon_0\sqrt{3\pi}\left(k_B T\right)^{3/2}} \sum_r \frac{\sqrt{m_{h1r} + m_{h2r} + m_{h3r}}}{m_{h2r}}, \tag{18}$$

$$\sigma_{3e} = \frac{2n_e e^4}{3\pi S\varepsilon_3\varepsilon_0\sqrt{3\pi}\left(k_B T\right)^{3/2}} \sum_s \frac{\sqrt{m_{e1s} + m_{e2s} + m_{e3s}}}{m_{e3s}}, \tag{19}$$

$$\sigma_{3h} = \frac{2n_h e^4}{3\pi R\varepsilon_3\varepsilon_0\sqrt{3\pi}\left(k_B T\right)^{3/2}} \sum_r \frac{\sqrt{m_{h1r} + m_{h2r} + m_{h3r}}}{m_{h3r}}. \tag{20}$$

In these formulae, S and R are the number of sorts of electrons and holes.

In a completely analogous way, we determine the components of the thermal conductivity tensor associated with free charge carriers:

$$\kappa_{1e} = \frac{4n_e e^2 k_B^{1/2}}{3\pi S\varepsilon_1\varepsilon_0\sqrt{3\pi}T^{1/2}} \sum_s \frac{\sqrt{m_{e1s} + m_{e2s} + m_{e3s}}}{m_{e1s}}, \tag{21}$$

$$\kappa_{1h} = \frac{4n_h e^2 k_B^{1/2}}{3\pi R\varepsilon_1\varepsilon_0\sqrt{3\pi}T^{1/2}} \sum_r \frac{\sqrt{m_{h1r} + m_{h2r} + m_{h3r}}}{m_{h1r}}, \tag{22}$$

$$\kappa_{2e} = \frac{4n_e e^2 k_B^{1/2}}{3\pi S\varepsilon_2\varepsilon_0\sqrt{3\pi}T^{1/2}} \sum_s \frac{\sqrt{m_{e1s} + m_{e2s} + m_{e3s}}}{m_{e2s}}, \tag{23}$$

$$\kappa_{2h} = \frac{4n_h e^2 k_B^{1/2}}{3\pi R\varepsilon_2\varepsilon_0\sqrt{3\pi}T^{1/2}} \sum_r \frac{\sqrt{m_{h1r} + m_{h2r} + m_{h3r}}}{m_{h2r}}, \tag{24}$$

$$\kappa_{3e} = \frac{4n_e e^2 k_B^{1/2}}{3\pi S\varepsilon_3\varepsilon_0\sqrt{3\pi}T^{1/2}} \sum_s \frac{\sqrt{m_{e1s} + m_{e2s} + m_{e3s}}}{m_{e3s}}, \tag{25}$$

$$\kappa_{3h} = \frac{4n_h e^2 k_B^{1/2}}{3\pi R\varepsilon_3\varepsilon_0\sqrt{3\pi}T^{1/2}} \sum_r \frac{\sqrt{m_{h1r} + m_{h2r} + m_{h3r}}}{m_{h3r}}, \tag{26}$$

Where ε_0 is dielectric permittivity of vacuum, ε_1, ε_2 ε_3 are the components of crystal dielectric permittivity tensor.

Therefore, if "1" is considered to be the direction of current, and "2" is the direction of temperature gradient, then the anisotropic figure of merit of material is equal to [3]:

$$z_{12} = \left(\frac{\alpha_e\sigma_{1e} + \alpha_h\sigma_{1h}}{\sigma_{1e} + \sigma_{1h}} - \frac{\alpha_e\sigma_{2e} + \alpha_h\sigma_{2h}}{\sigma_{2e} + \sigma_{2h}}\right)^2 \frac{\sigma_{1e} + \sigma_{1h}}{\kappa_{2e} + \kappa_{2h} + \kappa_{2l}}, \tag{27}$$

and in the opposite case it is equal to:

$$z_{21} = \left(\frac{\alpha_e\sigma_{1e} + \alpha_h\sigma_{1h}}{\sigma_{1e} + \sigma_{1h}} - \frac{\alpha_e\sigma_{2e} + \alpha_h\sigma_{2h}}{\sigma_{2e} + \sigma_{2h}}\right)^2 \frac{\sigma_{2e} + \sigma_{2h}}{\kappa_{1e} + \kappa_{1h} + \kappa_{1l}}. \tag{28}$$

Quite similarly, one can also introduce the anisotropic figures of merit for other directions:

$$z_{13} = \left(\frac{\alpha_e\sigma_{1e} + \alpha_h\sigma_{1h}}{\sigma_{1e} + \sigma_{1h}} - \frac{\alpha_e\sigma_{3e} + \alpha_h\sigma_{3h}}{\sigma_{3e} + \sigma_{3h}}\right)^2 \frac{\sigma_{1e} + \sigma_{1h}}{\kappa_{3e} + \kappa_{3h} + \kappa_{3l}}, \tag{29}$$

$$z_{31} = \left(\frac{\alpha_e\sigma_{1e} + \alpha_h\sigma_{1h}}{\sigma_{1e} + \sigma_{1h}} - \frac{\alpha_e\sigma_{3e} + \alpha_h\sigma_{3h}}{\sigma_{3e} + \sigma_{3h}}\right)^2 \frac{\sigma_{3e} + \sigma_{3h}}{\kappa_{1e} + \kappa_{1h} + \kappa_{1l}}, \tag{30}$$

$$z_{23} = \left(\frac{\alpha_e\sigma_{2e} + \alpha_h\sigma_{2h}}{\sigma_{2e} + \sigma_{2h}} - \frac{\alpha_e\sigma_{3e} + \alpha_h\sigma_{3h}}{\sigma_{3e} + \sigma_{3h}}\right)^2 \frac{\sigma_{2e} + \sigma_{2h}}{\kappa_{3e} + \kappa_{3h} + \kappa_{3l}}, \tag{31}$$

$$z_{32} = \left(\frac{\alpha_e\sigma_{2e} + \alpha_h\sigma_{2h}}{\sigma_{2e} + \sigma_{2h}} - \frac{\alpha_e\sigma_{3e} + \alpha_h\sigma_{3h}}{\sigma_{3e} + \sigma_{3h}}\right)^2 \frac{\sigma_{3e} + \sigma_{3h}}{\kappa_{2e} + \kappa_{2h} + \kappa_{2l}}. \tag{32}$$

From the above formulae it is seen that optimization of materials for anisotropic thermoelements involves, first, the choice of such a plane in a crystal and such mutually perpendicular directions of current and temperature gradient in it which provide the maximum value of thermoelectric figure of merit. Second, it involves doping of crystal with donor and (or) acceptor impurities in the appropriate quantity. The above formulae allow such optimization using a computer.

However, for this purpose, we will consider a more general case when the crystal is cut at a certain optimal angle to crystallographic axes. If these axes are designated by *i* and *k*, then the anisotropic thermoelectric figure of merit for these directions will be [1]:

$$z_{ik} = \frac{(\alpha_i - \alpha_k)^2 \sigma_i \sigma_k \cos^2\varphi \sin^2\varphi}{(\sigma_i \sin^2\varphi + \sigma_k \cos^2\varphi)(\kappa_i \sin^2\varphi + \kappa_k \cos^2\varphi)}. \quad (33)$$

Optimal angle φ_{0ik} is found from equation:

$$8\cos 2\varphi(\sin^2\varphi + p\cos^2\varphi)(\sin^2\varphi + q\cos^2\varphi) - (1-\cos 4\varphi)[(1-p)(\sin^2\varphi + q\cos^2\varphi) + (1-q)(\sin^2\varphi + p\cos^2\varphi)] = 0, \quad (34)$$

where $p = \sigma_k/\sigma_i$, $q = \kappa_k/\kappa_i$.

Then, optimization was carried out in the following order. First, by linear approximation, the dependence of electron and hole effective masses on the alloy composition was determined, for which purpose the results of calculations of the band structure of *CdSb* and $Zn_{0.5}Cd_{0.5}Sb$ were employed [6]. Then, formulae (4 – 6) were used to determine at different temperatures and $N_a - N_d \equiv n_0$ values the chemical potential of electron subsystem and the number of holes in the valence band and electrons in the conduction band. Following that, using the experimental data for the mobilities of electrons and holes in *CdSb,* the dependence of these mobilities on the composition of ternary alloy was determined on the assumption that given dependence is entirely due to the dependence of electron and hole effective masses on this composition. This data is quite enough to determine the components of thermoEMF, electric conductivity and thermal conductivity tensors related to free charge carriers. As regards lattice thermal conductivity, the author of this article quite consciously believed that at low zinc concentrations the components of respective tensor are equal to those in *CdSb* and are inversely proportional to temperature [7], as long as research on the dependence of Umklapp coefficient tensor on the composition of ternary alloy is not the purpose of the present article. After calculating the components of the kinetic coefficient tensors, in conformity with Eq.(34) the optimal angle φ_{0ik} and the appropriate extreme anisotropic figure of merit z_{ik} were determined. The results of described calculations for $Zn_{0.2}Cd_{0.8}Sb$ alloy are given in Figs. 1 – 6.

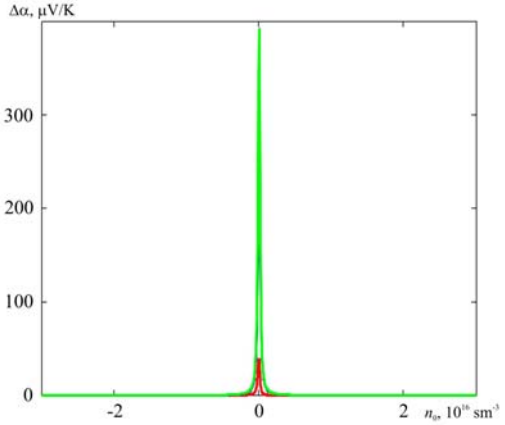

Fig.1. Dependence of the difference in components of thermoEMF tensor on doping level at a temperature of 300K. To the smallest difference corresponds plane "1, 2", to the greatest – plane "2, 3".

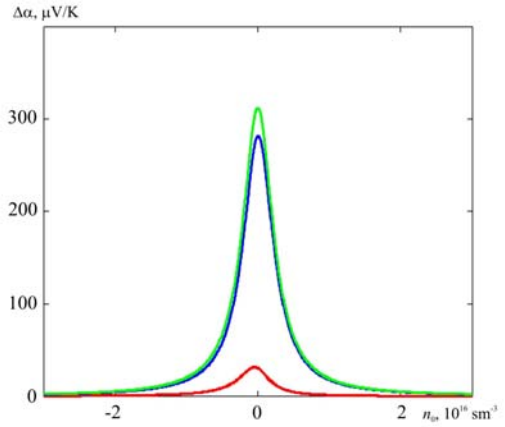

Fig.2. Dependence of the difference in components of thermoEMF tensor on doping level at a temperature of 400K. To the smallest difference corresponds plane "1, 2", to the greatest – plane "2, 3".

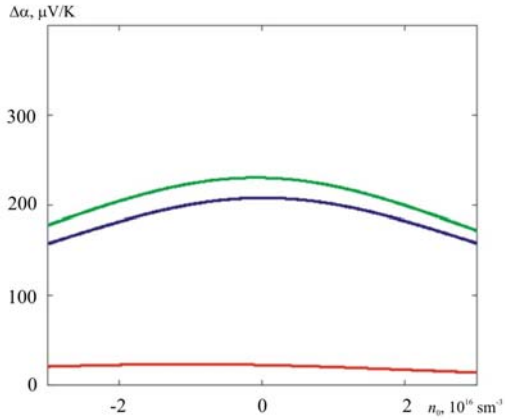

Fig.3. Dependence of the difference in components on doping level at a temperature of 600K. To the smallest difference corresponds plane "1, 2", to the greatest – plane "2, 3".

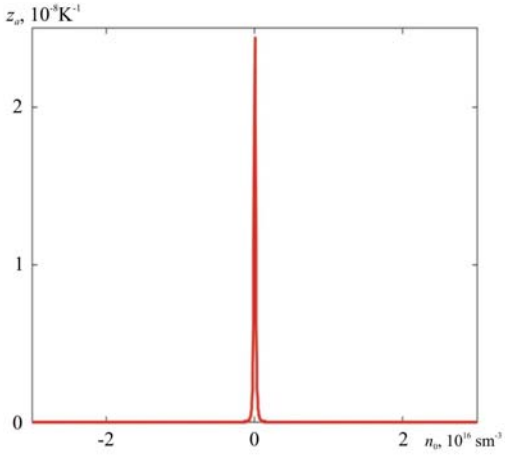

Fig.4. Dependence of extreme anisotropic figure of merit in plane "2,3" on doping level at a temperature of 300K.

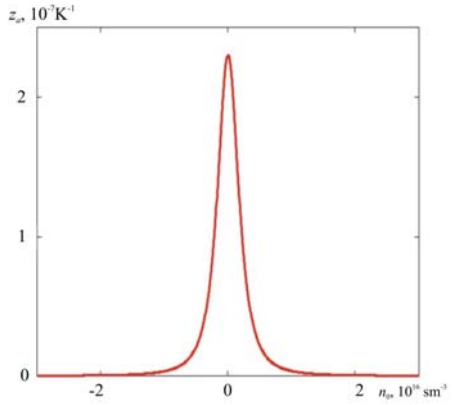

Fig.5. Dependence of extreme anisotropic figure of merit in plane "2,3" on doping level at a temperature of 400K

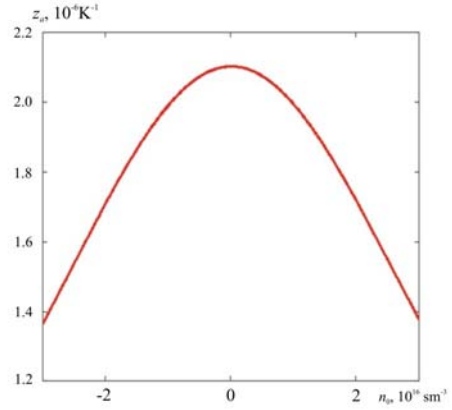

Fig.6. Dependence of extreme anisotropic figure of merit in plane "2,3" on doping level at a temperature of 600K

From the figures you can first see that plane "2, 3" is the best in terms of thermoEMF and anisotropic figure of merit, secondly, that the best from this standpoint is compensated material, as long as exactly in this case electrons and holes manifest themselves equally. However, the lower the temperature, the lower the intrinsic concentration of charge carriers, and, hence, the lower "decompensation" is required, so that the difference in components of thermoEMF tensor and anisotropic figure of merit of material decreased essentially as compared to the extreme values. And these extreme values at temperatures 300, 400 and 600 K for thermoEMF make 393, 311 and 230μV/K, respectively, and for the anisotropic figures of merit - $2.45\cdot10^{-8}$, $2.30\cdot10^{-7}$ and $2.10\cdot10^{-6}K^{-1}$, respectively. The angle corresponding to these figures of merit under which the crystal needs to be cut is $34^{0}05^{/}$.

It is interesting to compare the obtained results to the experimental data [8]. However, prior to passing to this comparison, the author of this paper should note that the tabulated data given in [8] contradict both the text and one another. Nevertheless, after eliminating these contradictions it turns out that at 300K the difference in components of thermoEMF tensor of $Zn_{0.2}Cd_{0.8}Sb$ alloy is 115μV/K instead of 393 at full compensation, and at 400 K – 135 μV/K instead of 311 at full compensation. In fact, at 300 K the alloy is weakly decompensated ($n_0 = 2.3\cdot10^{14}$ sm^{-3}), however, taking into account that at 400 K the intrinsic concentration of charge carriers is higher than at 300 K, it appears that at 400 K the level of "decompensation" essentially increases ($n_0 = 2.9\cdot10^{15}$ sm^{-3}). Such a statement, at first sight, may seem

absurd, if the material is the same. However, in [9 – 11] it is shown that zinc antimonide, and, hence, the alloys of *Zn-Cd-Sb* system due to chemical activity of zinc are capable of absorbing oxygen from the air with formation of vacancies of acceptor type, and the intensity of formation of these vacancies drastically grows with temperature, since the activation energy of this process is low [12]. And this, probably, is the reason for the growth of "decompensation" and, consequently, a decrease in the difference between the components of thermoEMF tensor. Such an explanation seems appropriate, since in [8] there is no indication that the measurement of physical characteristics of the investigated alloys was carried out in vacuum or in the atmosphere of inert gas. The same factor, most probably, accounts for the above mentioned "unexpected" electric conductivity increase by a factor of two when moving from $Zn_{0.15}Cd_{0.85}Sb$ composition to $Zn_{0.2}Cd_{0.8}Sb$ composition. This reasoning is confirmed by the fact that individual components of thermoEMF tensor of $Zn_{0.15}Cd_{0.85}Sb$ alloy preserve positive sign over the entire investigated temperature range, and the difference in components of thermoEMF tensor of $Zn_{0.15}Cd_{0.85}Sb$ alloy is essentially greater than the difference in components of thermoEMF tensor of $Zn_{0.2}Cd_{0.8}Sb$ alloy.

As regards the values of the anisotropic figure of merit, after eliminating the above contradictions it appears that maximum observed value of the anisotropic figure of merit of $Zn_{0.2}Cd_{0.8}Sb$ alloy at 400 K is equal to $1.32\cdot10^{-6}$ K^{-1}. The design anisotropic figure of merit of $Zn_{0.2}Cd_{0.8}Sb$ alloy at $n_0 = 2.9\cdot10^{15}$ sm^{-3} and temperature 400 K is $6.65\cdot10^{-8}$ K^{-1} and it is about half as large as that observed in [8]. It should be also borne in mind that when determining the anisotropic figure of merit in [8], the value of thermal conductivity was taken from the literary data, but its anisotropy was not taken into account. The difference of optimal angle from 45^0 and the anisotropy of electric conductivity were not taken into account either. However, if we consider, as it was done in [8], that the crystal was cut at an angle of 45^0, and, besides, that thermal conductivity is isotropic and equal to 1 W/(m·K), the design value of the anisotropic figure of merit at $n_0 = 2.9\cdot10^{15}$ cm^{-3} is equal to $5.85\cdot10^{-8}$K^{-1}. Thus, finally, we must assume that the difference between theory and experiment is explained, firstly, by the difference between true and model effective masses of electrons and holes, and, secondly, by the sharper than model dependence of charge carrier mobility in $Zn_xCd_{1-x}Sb$ alloys on zinc content.

Conclusion

1. It has been established that the greatest value of the difference in components of thermoEMF tensor and anisotropic figure of merit in the presence of two types of charge carriers with different signs is achieved when the material is in the intrinsic region, being fully compensated.
2. The most advantageous in terms of achieving maximum value of the anisotropic figure of merit of single-crystal alloy $Zn_{0.2}Cd_{0.8}Sb$ is plane "2,3", and crystal cut angle is $34^005^/$.
3. The experimentally observed values of the difference in components of thermoEMF tensor are lower than their extreme values, because alloys under study are not fully compensated, but have p-type conduction even at 400 K. In so doing, hole concentration in these alloys essentially depends on the intensity of absorption of oxygen from the air by zinc, which increases significantly with a rise in temperature.

The author considers it his pleasant duty to express gratitude to academician L.I.Anatychuk for the formulation of the problem and to chief research scientist L.M.Vikhor for the helpful and constructive discussion of the results of the work.

References

1. Anatychuk L.I. (1979). *Termoelementy i termoelektricheskiie usroistva. Spravochnik [Thermoelements and thermoelectric devices. Handbook]*. Kyiv: Naukova dumka [in Russian].

2. Anatychuk L.I. (1973). *Vikhrevyie termoelektricheskiie toki i vozmozhnosti ikh prakticheskogo ispolzovaniia [Eddy thermoelectric currents and possibilities of their practical use]. Extended abstract of Doctor's thesis]*. Lviv [in Russian].
3. Snarskii A.A., Palti A.M., Ashcheulov A.A. (1997). Anisotropnyie termoelementy. Obzor [Anisotropic thermoelements. Review]. *Fizika i tekhnika poluprovodnikov – Semiconductors*, 31(11), 1281 – 1297 [in Russian].
4. Kittel Ch. (1978). *Vvedeniie v fiziku tverdogo tela [Introduction to solid state physics*]. Moscow: Nauka [in Russian].
5. Goltsman B.M., Kudinov V.A., Smirnov I.A. (1972). *Poluprovodnikovyie termoelektricheskiie materialy na osnove Bi_2Te_3 [Semiconductor thermoelectric materials based on Bi_2Te_3]*. Moscow: Nauka [in Russian].
6. Glukhov K.E., Kharkhalis L.Yu., Shnaider M. (2010). Anisotropiia fizychnykh parametriv u tverdykh rozchynakh *CdSb-ZnSb* [Anisotropy of physical parameters in CdSb-ZnSb solid solutions]. *Termoelektryka – J.Thermoelectricity*, 2, 48 – 60 [in Ukrainian].
7. Gorskyi P.V. (2016). Hratkova teploprovidnist termoelektrychnykh materialiv na osnovi *Zn-Cd-Sb* [Lattice thermal conductivity of thermoelectric materials based on *Zn-Cd-Sb*]. *Termoelektryka – J.Thermoelectricity,* 2, 48 – 60 [in Ukrainian].
8. Buda I.S., Pilat I.M., Soliichuk K.D. (1973). Anisotropiia termoEDS monokristallov tverdykh rastvorov $Zn_xCd_{1-x}Sb$ [ThermoEMF anisotropy of single crystals of $Zn_xCd_{1-x}Sb$ solid solutions]. *Fizika i tekhnika poluprovodnikov – Semiconductors,* 7(10), 1281 – 1297 [in Russian].
9. Jund P., Viennois R., Tao X.et al. (2012). Physical properties of thermoelectric zinc antimonide using first-principle calculations. *Phys. Rev. B*, 85, 224105, 1 – 13.
10. Niedziołka K., Jund P. (2014). Influence of exchange correlation functional on the electronic properties of *ZnSb* as a promising thermoelectric material. *J. Electronic Materials*, 1 – 7.
11. Niedziołka K., Pothin R., Rouessac, F. et al. (2014). Theoretical and experimental search for *ZnSb*-based thermoelectric materials. *J. Phys.: Cond. Mat*., 26, 365401, 11.

Submitted 03.10.2017

Горський П.В. *докт. фіз.-мат. наук*

Інститут термоелектрики НАН і МОН України, вул. Науки, 1,
Чернівці, 58029, Україна*, e-mail: anatych@gmail.com*

ОПТИМІЗАЦІЯ ТЕРМОЕЛЕКТРИЧНИХ МАТЕРІАЛІВ НА ОСНОВІ СПЛАВІВ Zn-Cd-Sb ДЛЯ АНІЗОТРОПНИХ ТЕРМОЕЛЕМЕНТІВ

На основі розрахунку розподілу носіїв заряду та концентраційних залежностей кінетичних коефіцієнтів сплаву Zn0.2Cd0.8Sb встановлено, що найбільша анізотропна добротність цього сплаву досягається у площині «2-3», причому тоді, коли він знаходиться в області власної провідності.

Розрахунки виконувались для невиродженого електронно-діркового газу носіїв заряду у наближенні ефективної маси. Розглядалось наближення двох еліпсоїдальних долин: однієї електронної та однієї діркової. Для визначення залежностей компонент тензорів ефективних мас електронів та дірок від складу сплаву використовувалась лінійна апроксимація за вмістом цинку, яка робилась на основі результатів розрахунків зонної структури CdSb та Zn0.5Cd0.5Sb. Окрім того вважалось, що залежність рухливостей електронів та дірок від складу сплаву визначається виключно

залежностями відповідних компонент тензорів ефективних мас від складу сплаву. Також вважалось,що малий вміст цинку не впливає на граткову теплопровідність сплаву, яка вважалась обернено пропорційною до температури.

Розраховані екстремальні значення анізотропних термоелектричних добротностей сплаву Zn0.2Cd0.8Sb за температур 300, 400 та 600К склали 2.45·10-8, 2.30·10-7 та 2.1·10-6К-1 відповідно,що,принаймні за порядком величини,збігається з експериментальними даними. Відповідний до цих добротностей оптимальний кут вирізання кристалу складає близько 340. Тим не паче, обговорено також причини розбіжностей отриманих результатів як з експериментом, так і з теоретичними розрахунками попередніх авторів. Бібл. 11, Рис. 6.

Ключові слова: анізотропна добротність, електрони, дірки, тензор ефективної маси, ступінь легування, власна провідність, власна концентрація носіїв заряду, рухливість носіїв заряду, оптимальний кут вирізання кристалу, лінійна апроксимація за складом.

Горский П.В., *докт. физ.-мат. наук*

Институт термоэлектричества, ул. Науки, 1, Черновцы, 58029, Украина
e-mail: anatych@gmail.com

ОПТИМИЗАЦИЯ ТЕРМОЭЛЕКТРИЧЕСКИХ МАТЕРИАЛОВ НА ОСНОВЕ СПЛАВОВ *Zn-Cd-Sb* ДЛЯ АНИЗОТРОПНЫХ ТЕРМОЭЛЕМЕНТОВ

На основе расчетов распределения носителей заряда и концентрационных зависимостей кинетических коэффициентов сплава $Zn_{0.2}Cd_{0.8}Sb$ установлено, что наибольшая анизотропная добротность этого сплава достигается в плоскости «2-3», причем тогда, когда он находится в области собственной проводимости.

Расчеты выполнялись для невырожденного электронно-дырочного газа носителей заряда в приближении эффективной массы. Рассматривалось приближение двух эллипсоидальных долин: одной электронной и одной дырочной. Для определения зависимостей компонент тензоров эффективных масс электронов и дырок от содержания сплава использовалась линейная аппроксимация по содержанию цинка, которая делалась на основе результатов расчетов зонной структуры CdSb и $Zn_{0.5}Cd_{0.5}Sb$. Кроме того полагалось, что зависимость подвижностей электронов и дырок от состава сплава определяется исключительно зависимостями соответствующих компонент тензоров эффективных масс от состава сплава. Также полагалось, что малое содержание цинка не влияет на решеточную теплопроводность сплава, которая полагалась обратно пропорциональной температуре.

Рассчитанные экстремальные значения анизотропных термоэлектрических добротностей сплава $Zn_{0.2}Cd_{0.8}Sb$ при температурах 300, 400 и 600К составили $2.45\cdot10^{-8}$, $2.30\cdot10^{-7}$ и $2.1\cdot10^{-6}K^{-1}$ соответственно, что, по крайней мере, по порядку величины, совпадает с экспериментальными данными. Соответствующий этим добротностям оптимальный угол вырезания кристалла составляет около 34^0. Тем не менее, обсуждены также причины расхождения полученных результатов с экспериментом. Библ. 11, Рис. 6.

Ключевые слова: анизотропная добротность, электроны, дырки, тензор эффективной массы, степень легирования, собственная проводимость, собственная концентрация носителей заряда, подвижность носителей заряда, оптимальный угол вырезания кристалла, линейная аппроксимация по составу.

References

12. Anatychuk L.I. (1979). *Termoelementy i termoelektricheskiie usroistva. Spravochnik [Thermoelements and thermoelectric devices. Handbook]*. Kyiv: Naukova dumka [in Russian].
13. Anatychuk L.I. (1973). *Vikhrevyie termoelektricheskiie toki i vozmozhnosti ikh prakticheskogo ispolzovaniia [Eddy thermoelectric currents and possibilities of their practical use]. Extended abstract of Doctor's thesis]*. Lviv [in Russian].
14. Snarskii A.A., Palti A.M., Ashcheulov A.A. (1997). Anisotropnyie termoelementy. Obzor [Anisotropic thermoelements. Review]. *Fizika i tekhnika poluprovodnikov – Semiconductors*, 31(11), 1281 – 1297 [in Russian].
15. Kittel Ch. (1978). *Vvedeniie v fiziku tverdogo tela [Introduction to solid state physics*]. Moscow: Nauka [in Russian].
16. Goltsman B.M., Kudinov V.A., Smirnov I.A. (1972). *Poluprovodnikovyie termoelektricheskiie materialy na osnove Bi_2Te_3 [Semiconductor thermoelectric materials based on Bi_2Te_3]*. Moscow: Nauka [in Russian].
17. Glukhov K.E., Kharkhalis L.Yu., Shnaider M. (2010). Anisotropiia fizychnykh parametriv u tverdykh rozchynakh *CdSb-ZnSb* [Anisotropy of physical parameters in CdSb-ZnSb solid solutions]. *Termoelektryka – J.Thermoelectricity*, 2, 48 – 60 [in Ukrainian].
18. Gorskyi P.V. (2016). Hratkova teploprovidnist termoelektrychnykh materialiv na osnovi *Zn-Cd-Sb* [Lattice thermal conductivity of thermoelectric materials based on *Zn-Cd-Sb*]. *Termoelektryka – J.Thermoelectricity,* 2, 48 – 60 [in Ukrainian].
19. Buda I.S., Pilat I.M., Soliichuk K.D. (1973). Anisotropiia termoEDS monokristallov tverdykh rastvorov $Zn_xCd_{1-x}Sb$ [ThermoEMF anisotropy of single crystals of $Zn_xCd_{1-x}Sb$ solid solutions]. *Fizika i tekhnika poluprovodnikov – Semiconductors,* 7(10), 1281 – 1297 [in Russian].
20. Jund P., Viennois R., Tao X.et al. (2012). Physical properties of thermoelectric zinc antimonide using first-principle calculations. *Phys. Rev. B*, 85, 224105, 1 – 13.
21. Niedziołka K., Jund P. (2014). Influence of exchange correlation functional on the electronic properties of *ZnSb* as a promising thermoelectric material. *J. Electronic Materials*, 1 – 7.
22. Niedziołka K., Pothin R., Rouessac, F. et al. (2014). Theoretical and experimental search for *ZnSb*-based thermoelectric materials. *J. Phys.: Cond. Mat*., 26, 365401, 11.

Submitted 03.10.2017

O.M. Manik, *Candidate Phys.-math. Sciences,*
T.O. Manik, *Candidate Phys.-math. Sciences,*
V.R. Bilinsky-Slotylo, *Candidate Phys.-math. Sciences*

Institute of Thermoelectricity of the NAS and MES of Ukraine,
1, Nauky str, Chernivtsi, 58029, Ukraine; *e-mail: anatych@gmail.com*
Yurii Fedkovych Chenivtsi National University, 2, Kotsiubynskyi str.,
Chernivtsi, 58012, Ukraine*; e-mail: anatych@gmail.com*

CRYSTALLINE STRUCTURE AND CHEMICAL BOND OF *Cd-Sb-Zn*

A complex approach was developed for calculating the electronic structure of hybrid orbitals corresponding to nonequivalent interatomic distances in low-symmetry crystalline structures. Calculations of effective charges, effective radii, redistribution of the electron density, dissociation energy of nonequivalent hybrid orbitals (NHO) in Cd-Sb-Zn crystalline structures were carried out. The results can be used in the development of technology for obtaining new thermoelectric materials based on ternary systems of cadmium and zinc antimonides. Bibl. 9, Tables 2.
Key words: chemical bond, nonequivalent hybrid orbitals, crystalline structures, state diagrams, polymorphous transformations, phase transitions, dissociation energy.

Introduction

Ternary *Cd-Sb-Zn* systems are promising for use as thermoelectric materials [1]. However, to obtain materials with predicted properties, studies are needed the results of which allow controlling the technological modes of their production. At the present time, information in this direction is mostly experimental in nature [2]. Depending on the heat treatment conditions, cadmium-antimony alloys, as well as zinc-antimony alloys, crystallize in accordance with the stable and metastable state diagrams. In the study of solid-phase transformations, of particular interest are structural changes of these alloys when heated above the critical point and cooled to subcrystalline temperatures.

The state diagram of *Cd-Sb-Zn* system according to [3] consists of three partial diagrams of stable equilibrium *CdSb-ZnSb*-(*Cd, Sb, Zn*), three of metastable equilibrium (1): Cd_4Sb_3-Zn_4Sb_3-(*Cd, Sb, Zn*) and three of metastable equilibrium (2): Cd_3Sb_2-Zn_3Sb_2-(*Cd, Sb, Zn*). In this system, various structural states of the melts can be formed. The section of *CdSb-ZnSb* is quasi-binary.

The results of X-ray diffraction of alloys of three-component *Cd-Sb-Zn* system testify to formation of a continuous series of solid solutions $Sb_2Zn_{3x}Cdb_{3(1-x)}$, designated by γ-phase which is formed on the basis of two-component compounds ζ- Zn_3Sb_2 and Cd_3Sb_2, unstable at room temperature.

The state diagram of *CdSb-ZnSb* system, constructed by heating curves, is a system of a continuous series of solid solutions with the minimum on the liquidus curve in the area of 85 mol. % *CdSb*. Also, formation of a continuous series of solid solutions is noted under equilibrium conditions, while eutectics formation takes place under nonequilibrium conditions.

In [4], a stable diagram of the quasibinary section of *CdSb-ZnSb* is constructed. The phenomenon of thermal instability of the structure of melts is revealed, which manifests itself in the possibility of crystallization of phases varying in the degree of stability. In a particular case, the rapid cooling of the melts produces nonequilibrium crystallization along a stable diagram, regardless of the degree of overheating. The availability of such an amount of experimental information makes it possible to approach the solution of the problem of the theoretical description of melting and crystallization processes.

Theoretical concepts using classical approaches in the analysis of the molten state of substances [5] are based on fitting the selected interpretation model to the results of specific experimental studies. Difficulties arising from such an interpretation of the experimental material necessitated the development of a microscopic theory that combines classical schemes for the application of various methods to the solution of problems of materials science from the standpoint of chemical bonding [6].

With the help of these approaches, calculations of the elasticity coefficients of nonequivalent chemical bonds in crystals of *CdSb-ZnSb* solid solutions were carried out in [7]. The present work contributes to further studies started in [7] on the nature of chemical bond in crystalline structures of *Cd-Sb-Zn* system. The need for such work is due to the fact that a number of issues related to the technology for obtaining high-quality materials of *Cd-Sb-Zn* system remain open and contradictory; thermodynamic constants are almost not investigated. In connection with this, it is especially urgent to pursue research that makes it possible to quantitatively describe the interdependence between the macroscopic properties of the materials under study and their microscopic parameters from the position of the chemical bond. Taking into account the above arguments, the present paper set the task to generalize the calculation methods given in [8] to the case of crystal structures of *Cd-Sb-Zn* systems and on the basis of quantum-chemical approach to calculate effective charges, effective radii, electron density redistribution, dissociation energy of nonequivalent hybrid orbitals (NHO) corresponding to nonequivalent interatomic distances in the crystalline structures of *Cd-Sb-Zn* system, to compare the results obtained with those available in the literature and give recommendations on the development of technological approaches to obtaining high-quality thermoelectric materials based on the crystalline structures of *Cd-Sb-Zn* system.

Quantum chemical calculations of NHO parameters of *Cd-Sb-Zn* system

In [8], analysis of empirical information on the properties of elements and electronic structure of compounds formed by them was performed in terms of ionic radii R_u. The simplest relations were obtained by postulating the linear dependence of the number of electrons n in the outer shell on the logarithm of its Fermi radius. The relationship between the slope ratio of the rectilinear dependences $\mathrm{tg}\alpha = \Delta \log R_u / \Delta n$ and the electronegativities allowed us to write down a relation that gives a good agreement of the experimental data set in the form:

$$\log R_{UA}^{x} = \log R_{UA}^{0} - x\mathrm{tg}\alpha \qquad (1)$$

where R^0_{UA} is the radius of atom in the unexcited state, and x is valence.

As long as equation (1) describes changes in R_u of A and B atoms with a change in the number of electrons in the orbitals of each, it is necessary to analyze the dependence of interatomic distances d_i on the effective charges: $d_i = f(z_{ef})$. It turned out that at any point of this dependence, except for $d_i = d_{\min}$, the charge density on the ion boundary is different. Formation of (A-B) bond with $d_i \angle d_{\min}$ is accompanied by charge redistribution to other directions of atomic interaction, i.e. the bond becomes a

donor. In so doing, the reduction of charge ($+\Delta q$) or its localization ($-\Delta q$) in this bond direction equally changes the value of the charge that this pair has at $d_i = d_{min}$.

With regard to the above remarks, the dependence (1) takes on the form of a system of equations:

$$\log R_{UA}^{ZA} = \log R_{UA}^{0} - (Z_{\min A} + \frac{\Delta q}{2})\mathrm{tg}\alpha_A \quad (2)$$

$$\log R_{UA}^{ZA} = \log R_{UA}^{0} - (Z_{\min A} + \frac{\Delta q}{2})\mathrm{tg}\alpha_B \quad (3)$$

$$d_i = R_{UA}^{ZA} + R_{UB}^{ZB} \quad (4)$$

Function $d_i = f(z_{ef})$, calculated in crystal chemical approach with equal valences ($X_A = -X_B$), is correct from quantum mechanical standpoint only for $d_i = d_{min}$, but it is sufficient for system (2)-(4) to be solved at known d_i.

Therefore, to solve the problem, it was necessary to have lattice parameters, nonequivalent interatomic distances both in *CdSb* and in *ZnSb* sublattices. Thus, we have 5 NHO in *CdSb* sublattice, 5 NHO in *ZnSb* sublattice and one NHO, when in *CSb* lattice *Cd* atom will be substituted by *Zn* atoms, and vice versa – *Cd-Zn* bond. The numerical values of these interatomic distances were obtained by solving the inverse problem: from the known experimental data [9] giving the concentration dependences of lattice periods and densities of *CdSb-ZnSb*, we calculated the parameters of $Cd_xZn_{1-x}Sb$ crystalline structures of different composition ($0 \le x \le 1$) at interval $\Delta x = 0.1$; the lattice constants and interatomic distances were found in the approximation of Vegard's law according to the procedure developed in [6]. The results of calculations of interatomic distances in the *CdSb* and *ZnSb* sublattices are given in Table 1.

Table 1

Concentration dependences of interatomic distances d_i in $Zn_xCd_{1-x}Sb$ crystalline structures

% *Zn*	0	10	20	30	40	50	60	70	80	90	100
d_1(*Cd-Sb*) Å	2.80	2.784	2.768	2.752	2.736	2.72	2.704	2.688	2.672	2.656	-
d_2(*Cd-Sb*) Å	2.81	2.794	2.778	2.762	2.746	2.73	2.714	2.698	2.682	2.666	-
d_3(*Cd-Sb*) Å	2.91	2.895	2.88	2.865	2.85	2.835	2.82	2.805	2.79	2.771	-
CdSb d_4(*Sb-Sb*) Å	2.81	2.809	2.808	2.807	2.806	2.805	2.804	2.803	2.802	2.801	-
Cd-Sb d_5(*Cd - Cd*) Å	2.99	2.973	2.956	2.939	2.922	2.905	2.888	2.871	2.854	2.837	-
d_6(*Zn-Sb*) Å	-	2.789	2.773	2.757	2.741	2.725	2.709	2.693	2.677	2661.	2.645
d_7(*Zn-Sb*) Å	-	2.793	2.777	2.76	2.744	2.727	2.71	2.694	2.677	2.66	2.64

Continuation of Table 1

d_8(*Zn-Sb*) Å	-	2.895	2.88	2.865	2.85	2.835	2.82	2.805	2.79	2.775	2.76
ZnSb d_9(*Sb-Sb*) Å	-	2.809	2.808	2.807	2.806	2.805	2.804	2.803	2.802	2.801	2.80
ZnSb d_{10}(*Zn-Zn*)	-	2.973	2.956	2.939	2.922	2.905	2.888	2.871	2.854	2.837	2.82
d_{11}(*Cd-Zn*)	2.99	2.973	2.956	2.939	2.922	2.905	2.888	2.871	2.854	2.837	2.82

In the table, the following designations are accepted: φ_i is the *i-th* orbital with interatomic distance d_i ; φ_1, φ_2, φ_3 are orbitals of *Cd-Sb* bonds with interatomic distances d_1, d_2, d_3; φ_4 – *Sb-Sb* in *CdSb* sublattice with interatomic distance d_4; φ_5 corresponds to *Cd – Cd* bond with interatomic distance d_5. Then follow bonds φ_6, φ_7, φ_8 – (*Zn-Sb*) with interatomic distances d_6, d_7, d_8; φ_9 – (*Sb-Sb*) in *ZnSb* sublattice and φ_{10} – (*Zn- Zn*) with interatomic distances d_9 and d_{10}.

The interatomic distances for (*Cd-Zn*) bonds are also given, designated as φ_{11} – (*Cd-Zn*) and d_{11}, respectively.

To find the effective charges, the electron density redistribution, the system of equations (2) – (4) was written for each *i*-th orbital, and then by solving the inverse problem by known interatomic distances $d_i(1 \le x \le 11)$, the R_{UCd}, R_{UZn}, R_{USb} were found. The values of R^0_{Cd}, R^0_{Zn}, R^0_{Sb} and $\mathrm{tg}\alpha_{Cd}$, $\mathrm{tg}\alpha_{Zn}$, $\mathrm{tg}\alpha_{Sb}$ required for the calculations were found by the method [8]. As a result of the calculations, the following numerical values were obtained:

$$\begin{aligned} &R^0_{UCd} = 1.51\text{Å};\ R^0_{UZu} = 1.37\text{Å};\quad R^0_{USb} = 1.45\text{Å};\\ &\mathrm{tg}\alpha_{Cd} = 0.097;\ \mathrm{tg}\alpha_{Zn} = 0.135;\ \mathrm{tg}\alpha_{Sb} = 0.074. \end{aligned} \tag{5}$$

Later in this paper, as a result of taking into account the quantum-mechanical interpretation of the empirical material, a dependence of NHO bond energy on the interatomic distances, effective radii and electronic configurations of atoms in Cd_xSb-$Zn_{1-x}Sb$ crystals was obtained in the form:

$$D^{(j)}_{A-B} = \frac{c_1(R^0_{UA} + R^0_{UB})}{(\mathrm{tg}\alpha_A + \mathrm{tg}\alpha_B)} \cdot \left(\frac{c_2 d_j}{d_j^2 - R_{UA} - R_{UB}} - \frac{1}{d_j} \right), \tag{6}$$

where R^0_{UA} and $\mathrm{tg}\alpha_{A(B)}$ are coefficients of equations (2) – (4) for atoms *A* and *B*, R_{UA} and R_{UB} are effective radii of their ions in bond (*A – B*) of length $d_j(1 \le j \le 11)$; C_1 and C_2 are constants: C_1 is coefficient showing interrelation between dimensional and energy characteristics of atomic interaction, such as ionization potentials, screening effects, electronegativity, and the effective radii and interatomic distances. In the case of using non-system units, when the distance is measured in angstroms, C_1 has a dimension in electron-volts, C_2 is a coefficient depending on the type of crystalline structure, chemical bond. Taking into account the similarity theory, the coefficient C_2 is chosen to be dimensionless.

The results of calculations of the bond energies of individual NHO for the composition $Cd_{0.5}Zn_{0.5}Sb$ are given in Table 2. In so doing, the values of coefficients C_1 and C_2 first approximation were chosen equal to unity.

Table 2

Effective charges, effective radii and dissociation energies of NHO in $Cd_{0.5}Zn_{0.5}Sb$ crystalline structures

φ_j	φ_1 (*Cd-Sb*)	φ_2 (*Cd-Sb*)	φ_3 (*Cd-Sb*)	*CdSb* φ_4 (*Cd-Cd*)	*CdSb* φ_5 (*Cd-Cd*)	φ_6 (*Zn-Sb*)	φ_7 (*Zn-Sb*)	φ_8 (*Zn-Sb*)	*ZnSb* φ_9 (*Cd-Sb*)	*ZnSb* φ_{10} (*Cd-Sb*)	φ_{10} (*Cd-Zn*)
d_j (Å)	2.72	2.73	2.835	2.805	2.905	2.725	2.727	2.835	2.805	2.905	2.905
R_U^{Cd} (Å)	1.127	1.13	1.17	-	1.4525	-	-	-	-	-	1.515
R_U^{Zn} (Å)	-	-	-	-	-	1.015	1.012	1.05	-	1.4525	1.39
R_U^{Sb} (Å)	1.593	1.6	1.665	1.4025	-	1.71	1.715	1.785	1.4025	-	-
Δq_j %	8	8	3.2	18.5	3	3.2	2	2	3.3	18.8	4.7
D_j(eV)	2.04	2.031	1.953	2.328	1.768	1.51	1.506	1.447	2.329	1.165	1.421

Table 2 also lists the values of effective radii R_{UCd}, R_{UZn}, R_{USb}, redistribution of electronic densities Δq_i ($1 \le i \le 11$) and interatomic distances for which the values of D_i were calculated.

Discussion of the results

Analysis of the results shows that the dependences given in this paper can be used not only for calculating the bond energies of individual NHO in $Zn_xCd_{1-x}Sb$ crystals, but also for developing technological modes for production of new materials with a predicted set of physicochemical properties. The obtained results agree with the results given in [2], [3] of studying the state diagrams of stable and metastable equilibrium [2], [3], specify the opportunities of phase transitions and polymorphous transformations when forming physicochemical properties in new synthesized materials depending on the atomic dimensions of the initial components and their physicochemical parameters.

The results obtained in this paper also agree with the results of studying thermal rearrangement of atoms in the melts [4]. In this connection, of particular interest becomes information on the mechanism of transition from some cluster microassociations of atoms to the other when forming a structure of melts crystallizable in the stable or metastable modes. The results presented in this paper allow us to establish the methods of variation and elucidate potential opportunities of structural state of the melts of *Cd-Sb-Zn* system.

Conclusion

1. A methodology was developed for using NHO for the calculations of interatomic interaction in crystalline structures of *Cd-Sb-Zn* system.
2. A procedure was developed and calculations of the redistribution of charges on NHO characterizing the formation of a donor or acceptor bond were carried out.
3. The effective radii, interatomic distances and dissociation energies in $Cd_{0.5}Zn_{0.5}Sb$ crystals were calculated.
4. The results obtained in this paper agree with the results of calculation of chemical bond parameters by the methods of microscopic theory, the results of research on thermal

rearrangement of atoms in the melts and can be used in the development of technological modes of synthesis of new materials based on $Zn_xCd_{1-x}Sb$.

References

1. Anatychuk L.I. (1979). *Termoelementy i termoelektricheskiie ustroistva [Thermoelements and thermoelectric devices]*. Kyiv: Naukova dumka [in Russian].
2. Lazarev V.B., Shevchenko V.Ya., Grinberg Ya.Kh., Sobolev V.V. (1978). *Poluprovodnikovyie soiedineniia gruppy $A^{II}B^{V}$ [Semiconductor compounds of $A^{II}B^{V}$ group]*. Moscow: Nauka [in Russian].
3. Dremliuzhenko S.G. (2002). *Sistemy na osnove CdSb: diagramma sostoianiia, polucheniie i svoistva splavov. Spravochnik [Systems on the basis of CdSb: state diagram, manufacture and properties of alloys. Handbook]*. Chernivtsi: Ruta [in Russian].
4. Psarev V.I., Kirii V.G., Viktorov V.V. (1979). Osobennosti kristallizatsii tverdykh rastvorov kvazibinarnogo razreza *ZnSb-CdSb* [Crystallization features of solid solutions of *ZnSb-CdSb* quazi-binary section]. *Izvestiia Akademii Nauk SSSR. Neorganicheskiie materialy – Bulletin of the USSR Academy of Sciences. Inorganic Materials*, 15 (3), 395 – 399 [in Russian].
5. Ubbelohde A.R. (1982). *Rasplavlennoie sostoianiie veshchestva [The molten state of matter]*. Moscow: Metallurgiia [Russian transl].
6. Manik O.M. (1999). *Bahatofaktornyi pidhid v teoretychnomu materialoznavstvi [Multi-factor approach in theoretical materials research]*. Chernivtsi: Prut [in Ukrainian].
7. Yeremenko A.I., Lototskii V.B., Manik O.N., Raranskii N.D. (2007). Peculiarities of chemical bond in crystals of *CdSb-ZnSb* solid solutions. *J.Thermoelectricity*, 1, 53 – 65.
8. Manik O.N., Manik T.O., Bilinsky-Slotylo V.R. (2016). Peculiarities of electronic structure of hybrid orbitals and interatomic interaction in cadmium antimonide crystals. *J. Thermoelectricity*, 5, 57 – 64.
9. Balaziuk V.N., Hrytsiuk B.M., Drapak L.S., Lototskyi V.B., Novikov S.M., Rarenko A.I. (2001). Anizotropiia pruzhnosti i mikrotverdosti monokrystaliv tverdykh rozchyniv systemy *CdSb-ZnSb* [Elasticity and microhardness anisotropy of single crystals of solid solutions of *CdSb-ZnSb* system]. *Naukovyi visnyk Chernivetskoho* Universytetu. *Fizyka. Elektronika – Scientific Bulletin of Chernivtsi University. Physics. Electronics*, 112, 71 – 74 [in Ukrainian].

Submitted 10.10.2017

Маник О. М., *канд. фіз.-мат. наук*
Маник Т. О. *канд. фіз.-мат. наук.*,
Білинський-Слотило В. Р. *канд. фіз.-мат. наук*

Інститут термоелектрики НАН і МОН України, вул. Науки, 1,
Чернівці, 58029, Україна, *e-mail: anatych@gmail.com*;
Чернівецький національний університет імені Юрія Федьковича,
вул. Коцюбинського 2, Чернівці, 58012, Україна
e-mail: anatych@gmail.com

КРИСТАЛІЧНІ СТРУКТУРИ ТА ХІМІЧНИЙ ЗВ'ЯЗОК СИСТЕМИ *Cd-Sb-Zn*

Розроблено комплексний підхід для розрахунків параметрів електронної будови гібридних орбіталей, що відповідають нееквівалентним міжатомним відстаням у низькосимметричних кристалічних структурах. На основі квантовомеханічного підходу проведено розрахунки ефективних зарядів, ефективних радіусів, перерозподілу електронної щільності, енергії дисоціації нееквівалентних гібридних орбіталей (НГО) у кристалічних структурах системи Cd-Sb-Zn. Отримані результати можуть бути використані при розробці технології одержання нових термоелектричних матеріалів на їх основі. Бібл.9, Табл. 2.
Ключові слова: хімічний зв'язок, нееквівалентні гібридні орбіталі, кристалічні структури, діаграми станів поліморфні перетворення, фазові переходи, енергія дисоціації.

Маник О. Н. *канд. физ.-мат. наук*
Маник Т. О. *канд. фіз.-мат. наук,*
Билинский-Слотыло В. Р. *канд. физ.-мат. наук*

[1]Институт термоэлектричества НАН и МОН Украины, ул. Науки, 1,
Черновцы, 58029, Украина, *e-mail: anatych@gmail.com*;
[2]Черновицкий национальный университет имени Юрия Федьковича,
ул. Коцюбинского 2, Черновцы, 58012, Украина
e-mail: anatych@gmail.com

КРИСТАЛЛИЧЕСКАЯ СТРУКТУРА И ХИМИЧЕСКАЯ СВЯЗЬ *Cd-Sb-Zn*

Разработан комплексный подход для расчетов параметров электронного строения гибридных орбиталей, соответствующих неэквивалентным межатомным расстояниям в низкосимметричных кристаллических структурах. Проведены расчеты эффективных зарядов, эффективных радиусов, перераспределения электронной плотности, энергии диссоциации неэквивалентных гибридных орбиталей (НГО) в кристаллических структурах системы Cd-Sb-Zn. Полученные результаты могут быть использованы при разработке технологии получения новых термоэлектрических материалов на основе тройных систем антимонидов кадмия и цинка. Библ.9, Табл. 2.
Ключевые слова: химическая связь, неэквивалентные гибридные орбитали, кристаллические структуры, диаграммы состояний, полиморфные превращения, фазовые переходи, энергия диссоциации.

References

1. Anatychuk L.I. (1979). *Termoelementy i termoelektricheskiie ustroistva [Thermoelements and thermoelectric devices]*. Kyiv: Naukova dumka [in Russian].
2. Lazarev V.B., Shevchenko V.Ya., Grinberg Ya.Kh., Sobolev V.V. (1978). *Poluprovodnikovyie soiedineniia gruppy $A^{II}B^{V}$ [Semiconductor compounds of $A^{II}B^{V}$ group]*. Moscow: Nauka [in Russian].
3. Dremliuzhenko S.G. (2002). *Sistemy na osnove CdSb: diagramma sostoianiia, polucheniie i svoistva splavov. Spravochnik [Systems on the basis of CdSb: state diagram, manufacture and properties of alloys. Handbook]*. Chernivtsi: Ruta [in Russian].
4. Psarev V.I., Kirii V.G., Viktorov V.V. (1979). Osobennosti kristallizatsii tverdykh rastvorov kvazibinarnogo razreza *ZnSb-CdSb* [Crystallization features of solid solutions of *ZnSb-CdSb*

quazi-binary section]. *Izvestiia Akademii Nauk SSSR. Neorganicheskiie materialy – Bulletin of the USSR Academy of Sciences. Inorganic Materials*, 15 (3), 395 – 399 [in Russian].

5. Ubbelohde A.R. (1982). *Rasplavlennoie sostoianiie veshchestva [The molten state of matter]*. Moscow: Metallurgiia [Russian transl].
6. Manik O.M. (1999). *Bahatofaktornyi pidhid v teoretychnomu materialoznavstvi [Multi-factor approach in theoretical materials research]*. Chernivtsi: Prut [in Ukrainian].
7. Yeremenko A.I., Lototskii V.B., Manik O.N., Raranskii N.D. (2007). Peculiarities of chemical bond in crystals of *CdSb-ZnSb* solid solutions. *J.Thermoelectricity*, 1, 53 – 65.
8. Manik O.N., Manik T.O., Bilinsky-Slotylo V.R. (2016). Peculiarities of electronic structure of hybrid orbitals and interatomic interaction in cadmium antimonide crystals. *J. Thermoelectricity*, 5, 57 – 64.
9. Balaziuk V.N., Hrytsiuk B.M., Drapak L.S., Lototskyi V.B., Novikov S.M., Rarenko A.I. (2001). Anizotropiia pruzhnosti i mikrotverdosti monokrystaliv tverdykh rozchyniv systemy *CdSb-ZnSb* [Elasticity and microhardness anisotropy of single crystals of solid solutions of *CdSb-ZnSb* system]. *Naukovyi visnyk Chernivetskoho* Universytetu*. Fizyka. Elektronika – Scientific Bulletin of Chernivtsi University. Physics. Electronics*, 112, 71 – 74 [in Ukrainian].

Submitted 10.10.2017

V.A. Romaka *Doctor tech. sciences*[1,2], **L.P. Romaka** *Candidate chem. sciences*[3],
P.-F.Rogl *Doctor physics*[4], **V.V. Romaka** *Doctor tech. sciences* [2,4],
Yu.V.Stadnyk *Candidate chem. sciences* , **A.M.Horyn** *Candidate chem. sciences* ,
I.R.Opirskyy *Candidate tech. science* [2]

[1]Ya. Pidstryhach Institute for Applied Problems of Mechanics and Mathematics
National Academy of Sciences of Ukraine, 3-b, Naukova Str., Lviv, 79060, Ukraine;
[2]National University "Lvivska Politechnika", 12, S. Bandera Str., Lviv, 79013, Ukraine;
[3]Ivan Franko National University of Lviv, 6, Kyryla and Mefodiya Str., Lviv, 79005, Ukraine;
[4]Universität Wien, 42, Währinger Str., Wien, A-1090, Österreich

FEATURES OF ELECTRICAL CONDUCTIVITY MECHANISMS OF $ZrNi_{1-x}Rh_xSn$ THERMOELECTRIC MATERIAL

The crystalline and electronic structures, the kinetic, magnetic and thermodynamic characteristics of $ZrNi_{1-x}Rh_xSn$ thermoelectric material in the ranges T=80–400 K, x=0.005–0.10 were studied. The mechanisms of simultaneous generation of structural defects of acceptor and donor nature which determine the electrical conductivity of material, as well as the dependence of the bandgap ε_g on the concentration of Rh were established. It is shown that it is energetically favourable to substitute Ni atoms ($3d^84s^2$) at 4c crystallographic site by Rh atoms ($4d^85s^1$), which generates structural defects of acceptor nature (more s-electrons in Ni) with accumulation of part of Ni atoms at the tetrahedral vacant sites (generation of donors). It is concluded that the experimentally established donor nature of the defects of ZrNiSn compound ("a priori doping") is due to filling of the tetrahedral vacant sites by donor-generating Ni atoms. Bibl. 16, Fig. 10.
Key words: electronic structure, resistivity, the Seebeck coefficient.

Introduction

In continuation of the program of search for new thermoelectric materials with high efficiency of thermal into electric energy conversion [1], the features of electric conductivity mechanisms of semiconductor thermoelectric material $ZrNi_{1-x}Rh_xSn$ were studied. Materials based on *n-ZrNiSn*, *n-HfNiSn* and *n-TiNiSn* semiconductors possess high values of thermoelectric figure of merit *Z*, stable characteristics in a wide temperature range [2,3], and their *ZT* values correspond to the best figures of tellurides, clathrates and scutterudites [4 – 6]. Performance optimization of materials based on the above semiconductors is done by heavy doping with donor and/or acceptor impurities, and materials themselves are heavily doped and strongly compensated semiconductors (HDSC) [7]. Understanding electric conductivity mechanisms in $ZrNi_{1-x}Rh_xSn$ will allow more comprehensive determination of synthesis conditions to obtain maximum efficiency of thermal into electric energy conversion.

The nature of electronic conductivity type of *n-ZrNiSn* in [8] is related to crystalline structure disorder (structural type *MgAgAs*, spatial group $F\bar{4}3m$ [9]), the essence of which is partial, up to ~1%, occupancy by *Ni* ($3d^84s^2$) atoms of 4*a* site of *Zr* ($4d^25s^2$) atoms, generating structural defects of donor nature (*Ni* has more *d*-electrons). Doping of *n-ZrNiSn*, in particular, with atoms of rare-earth and 3*d*- and/or 4*p*-metals, puts in order the structure (*Ni* leaves the site of *Zr*) and donors generated by "a priori doping" disappear [2,8].

On the other hand, the structure of *ZrNiSn* compound comprises essential tetrahedral vacant sites (Fig. 1, *a,b*) [9]. The authors of [10] revealed the effect of accumulation of *Ni* atoms at these vacant sites, including excess Ni_{1+x} atoms up to concentrations $x \leq 0.30$, which generate defects of donor nature. It was also revealed that the bandgap ε_g essentially depends on the concentration of Ni_{1+x} atoms at such vacant sites. It was concluded that in semiconductors of cubic symmetry with covalent bonds and tetrahedral vacant sites the latter play the role of vacancies Vac (traps) both for intrinsic and impurity atoms, generating in this case structural defects which determine its properties. The studies of thermodynamic processes in *Zr-Ni-Sn* system [11] proved the results of [10] with respect to accumulation of $Ni(Ni_{1+x})$ atoms at tetrahedral vacant sites of *ZrNiSn* compound.

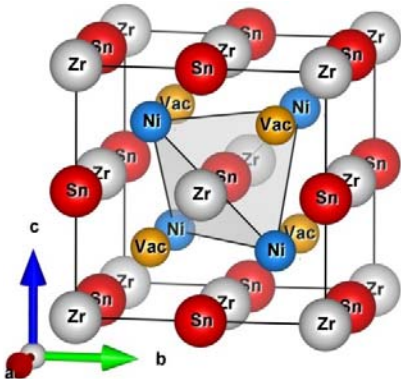

a)

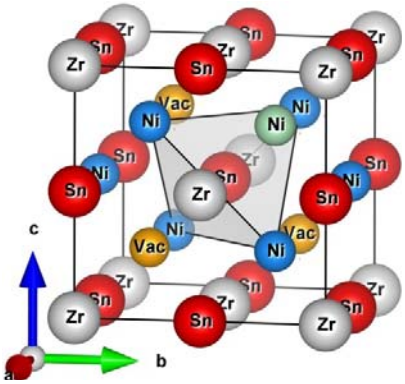

b)

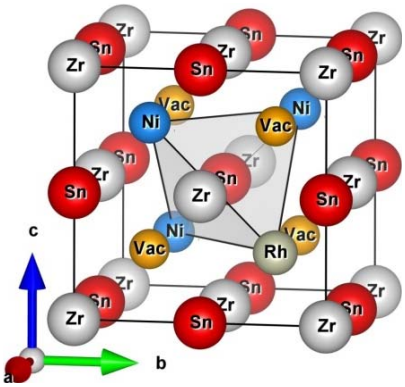

c)

*Fig. 1. Models of crystalline structures ZrNiSn (**a**), $(Zr_{1-y}Ni_y)Ni_{1+x}Sn$ (b) and $ZrNi_{1-x}Rh_xSn$ (c).*

Investigations of the kinetic characteristics of $ZrNi_{1-x}M_xSn$, where $M = Cr, Mn, Fe, Co$, revealed that even at gigantic concentrations of impurity ($N_A^M \approx 3.8 \cdot 10^{21}$ sm^{-3} ($x \approx 0.20$)) all generated acceptors are ionized (trap electrons), and the Fermi level ε_F is located near the midgap ε_g [2]. A similar result was also obtained in the investigation of $HfNi_{1-x}Rh_xSn$ [12]. That is, when doping *n*-type conductivity semiconductor with acceptor impurity, donors of unknown origin manifest themselves simultaneously with acceptors. At the same time, in [2,12] it was assumed that only acceptors will be generated (*Ni* has more *d*- and *s*-electrons than *M* and *Rh* ($4d^8 5s^1$), respectively).

The question arises as to the nature of these donors in $ZrNi_{1-x}M_xSn$ and $HfNi_{1-x}Rh_xSn$. It is important to find an answer, since the object of study is a similar semiconductor $ZrNi_{1-x}Rh_xSn$.

If we take into account the results of [10,11], then in the base compound *ZrNiSn* part of *Ni* atoms is arranged at vacant sites, generating defects of donor nature ("a priori doping") [2]. In other words, it can be assumed that the experimentally established donor nature of defects of *n-ZrNiSn* [2] is due not so much to structural disorder [8], as to occupation by *Ni* atoms of tetrahedral vacant sites, generating donors. On the other hand, we can also assume that in $ZrNi_{1-x}Rh_xSn$, part of *Ni* atoms and *Rh* impurities in different ratios can occupy both (4*c*) *Ni* site and the vacancy, generating structural defects of acceptor and donor nature, respectively.

Below, based on the results of calculations and experimental investigations it is shown that defects of acceptor and donor nature are generated in $ZrNi_{1-x}Rh_xSn$ simultaneously. Thermodynamic calculations have established that it is energetically favourable to substitute *Ni* atoms at *4c* crystallographic site by *Rh* atoms, which generates structural defects of acceptor nature, with accumulation of part of *Ni* atoms at tetrahedral vacant sites, which generates structural defects of donor nature.

Investigation procedures

The object to be investigated included crystalline structure, electronic density distribution (DOS), the kinetic, energy and magnetic characteristics of $ZrNi_{1-x}Rh_xSn$. The samples were synthesized in the laboratory of Institute for Physical Chemistry, Vienna University. The X-ray structural analysis (powder method) was used to obtain the data arrays (diffractometer Guinier-Huber image plate system, $CuK\alpha_1$), and Fullprof program [13] was employed for the calculation of structural characteristics. The chemical and phase compositions of the samples were controlled by microprobe analyzer (EPMA, energy-dispersive X-ray analyzer). The electronic structure calculations were performed by the Korringa-Kohn-Rostoker (KKR) method in coherent potential approximation (CPA) and local density approximation (LDA) [14] with the use of Moruzzi-Janak-Williams exchange-correlation potential [15]. The accuracy of calculating the position of the Fermi level ε_F is ± 8 meV. The temperature and concentration dependences of the electrical resistivity (ρ) and the Seebeck coefficient (α) were measured with respect to copper and magnetic susceptibility (χ) (Faraday's method) of $ZrNi_{1-x}Rh_xSn$ samples in the ranges: $T = 80 - 400$ K, $N_A^{Rh} \approx 9.5 \cdot 10^{19}$ sm^{-3} – $1.9 \cdot 10^{21} \cdot$sm^{-3} ($x = 0.005 - 0.10$) and magnetic field strength $H \leq 10$ kE.

Research on the crystalline and electronic structures of $ZrNi_{1-x}Rh_xSn$

A microprobe analysis of the concentration of atoms on the surface of $ZrNi_{1-x}Rh_xSn$ samples has established their conformity to the initial batch compositions, and X-ray phase and structural analyses have shown that X-ray diffraction patterns of samples have no traces of other phases. It was expected that substitution of *Ni* atoms ($r_{Ni} = 0.124$ nm) by larger size *Rh* atoms ($r_{Rh} = 0.136$ nm) will lead to increase of unit cell period $a(x)$. However, the behavior of $a(x)$ is of rather complex nature (Fig. 2*a*),

showing the processes of structural changes. Thus, the maximum on the dependence $a(x)$ is the specific feature of materials based on *ZrNiSn* [2] and serves one of the arguments concerning the disordered structural model proposed in [8].

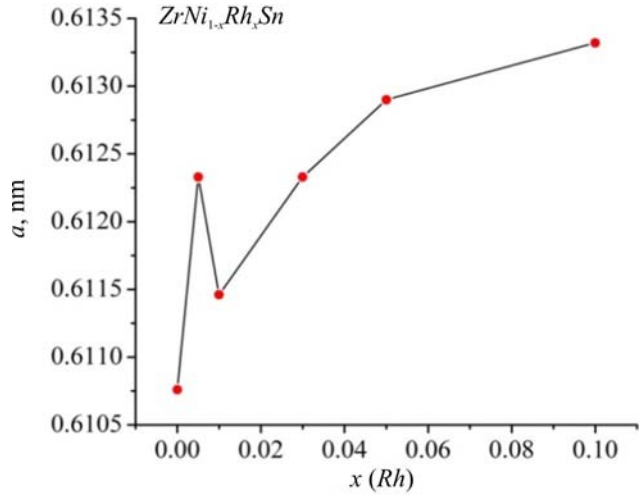

a)

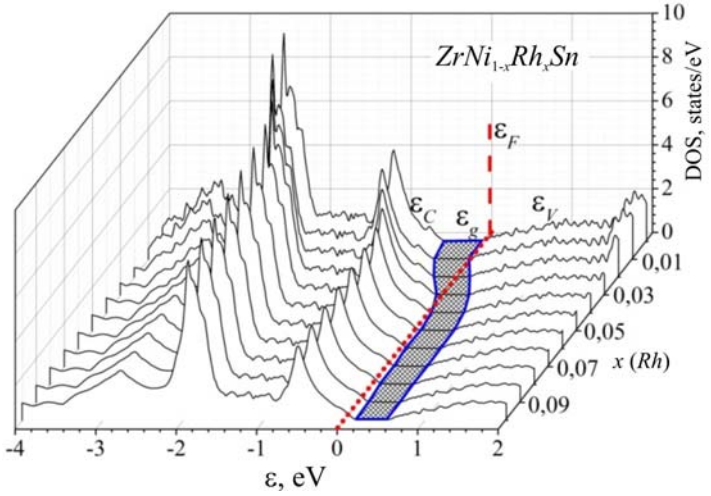

b)

*Fig. 2. Change in the values of unit cell period a(x) (**a**) and the electronic density of states DOS (**b**) of $ZrNi_{1-x}Rh_xSn$.*

The refinement of $ZrNi_{1-x}Rh_xSn$ structure has shown that at Rh $x \geq 0.01$ the structure is ordered, that is, the occupancy of *Zr* site is 100 %, and defects of donor nature are "healed" by displacement of small *Ni* atoms ($r_{Ni} = 0.124$ nm) from 4*a* site by larger-size *Zr* atoms ($r_{Zr} = 0.160$ nm). Simultaneously, there is substitution at 4*c* site of small *Ni* atoms by *Rh* (Fig. 1*c*). As long as the difference in atomic radii of *Zr* and *Ni* $(r_{Zr} - r_{Ni}) = 0.036$ nm is larger than that for *Rh* and *Ni* $(r_{Rh} - r_{Ni}) = 0.011$ nm, the nature of the maximum on $a(x)$ becomes clear. Thus, the amplitude of change in the values of $a(x)$ in the regions of $0 \leq x \leq 0.01$ and $0.01 < x \leq 0.10$ is different. In the former case, these changes are greater because of displacement of *Ni* atoms from 4*a* site by *Zr* atoms (growth of dependence $a(x)$). After displacement of *Ni* from *Zr* site (structure ordering), the growth of the values of $a(x)$ in the region of $0.01 \leq x \leq 0.10$ arises due to occupancy of (4*c*) *Ni* site by *Rh* atoms.

Apart from the structural features, increase in concentration of *Rh* in $ZrNi_{1-x}Rh_xSn$, introduces essential changes to electron density redistribution that are caused by two processes:

– liquidation of defects of donor nature at displacement of ~ 1 % of *Ni* atoms from *Zr* site (4*a*);

– generation of defects of acceptor nature at substitution of *Ni* (4*c*) atoms by *Rh*.

Thus, on the basis of *structural* investigations of $ZrNi_{1-x}Rh_xSn$ we can state that increase in the concentration of *Rh* changes the ratio of donors and acceptors – compensation ratio, and the majority carriers at $x \geq 0.02$ will be holes. The presence of acceptors and donors will affect the band structure and become apparent at the investigation of electronic structure and kinetic characteristics.

To predict the behavior of the Fermi level ε_F, the bandgap ε_g and the kinetic characteristics of $ZrNi_{1-x}Rh_xSn$, the electronic density of states (DOS) was calculated (Fig. 2*b*). As long as crystalline structure of $ZrNi_{1-x}Rh_xSn$, $x \geq 0.01$ is ordered, calculation of DOS was performed for such structural variant. As is seen from Fig. 2*b*, at the lowest concentrations of *Rh* impurity, the Fermi level ε_F $ZrNi_{1-x}Rh_xSn$ starts drifting from conduction band ε_C, at a distance of ~ 97.6 meV from which it was in *n-ZrNiSn* [2], to the midgap ε_g and further to valence band ε_V, to intersect it at $x \approx 0.04$. When the Fermi level ε_F intersects the midgap ($x \approx 0.02$) and further moves to valence band ε_V, the type of conductivity will change and holes will become the majority carriers. Apart from drift ε_F caused by change in material compensation, the bandgap ε_g will decrease (Fig. 2*b*).

Thus, the results of calculation of the electronic density of states DOS of $ZrNi_{1-x}Rh_xSn$, based on structural investigations, confirm the predicted acceptor nature of generated defects, the linear dependence of the Fermi level ε_F drift velocity, a change in the type of majority carriers and realization of dielectric-metal transition, which is the Anderson transition [16]. The results of kinetic and magnetic studies will show the correspondence of these calculations to the real processes in the thermoelectric material.

Research on the electrokinetic, energy and magnetic characteristics of $ZrNi_{1-x}Rh_xSn$

The temperature and concentration dependences of the electrical resistivity ρ and the Seebeck coefficient α of $ZrNi_{1-x}Rh_xSn$ are presented in Figs. 3, 4. The dependences $\ln\rho(1/T)$ and $\alpha(1/T)$ of $ZrNi_{1-x}Rh_xSn$ (Fig. 3) are typical for HGSC semiconductors, and the available activation areas point to several mechanisms of charge carrier transport [2,7,16]. The dependences $\ln\rho(1/T)$ are approximated using the known relationship [7]:

$$\rho^{-1}(T) = \rho_1^{-1} \exp\left(-\frac{\varepsilon_1^{\rho}}{k_B T}\right) + \rho_3^{-1}\left(-\frac{\varepsilon_3^{\rho}}{k_B T}\right), \quad (1)$$

where the first, high-temperature, summand describes activation of current carriers ε_1^{ρ} from the Fermi level ε_F to percolation level of continuous energy bands, and the second, low-temperature, summand – hopping conductivity ε_3^{ρ}. In turn, the temperature dependences of the Seebeck coefficient $\alpha(1/T)$ of $ZrNi_{1-x}Rh_xSn$ can be approximated using the following relationship [16]:

$$\alpha = \frac{k_B}{e}\left(\frac{\varepsilon_i^{\alpha}}{k_B T} - \gamma + 1\right), \quad (2)$$

where γ is parameter that depends on the nature of scattering. From the high-temperature area of the dependence $\alpha(1/T)$ the values of activation energy ε_1^{α} were calculated which, as shown in [2], are proportional to the amplitude of large-scale fluctuation of continuous energy bands (Fig. 1), and from the low-temperature area – the value of activation energy ε_3^{α} proportional to modulation amplitude of small-scale fluctuation of HDSC semiconductors [2, 7].

For *n-ZrNiSn* calculated was the value of electron activation energy from the Fermi level ε_F to percolation level of conduction band $\varepsilon_1^{\rho} = 97.6$ meV. This activation is indicated by the negative values of the Seebeck coefficient over the entire temperature range. The presence of low-temperature activation on the dependence $\ln\rho(1/T)$ testifies to hopping conductivity on impurity donor states with activation energy $\varepsilon_3^{\rho} = 11.9$ meV. From the high- and low-temperature areas of the dependences $\alpha(1/T)$ the values of activation energy were calculated: $\varepsilon_1^{\alpha} = 83.8$ меV and $\varepsilon_3^{\alpha} = 11.5$ meV. As long as the value of ε_1^{α} reflects the amplitude of large-scale fluctuation of continuous energy bands of HDSC semiconductors, the proximity of values ε_1^{α} and ε_1^{ρ} is a sign of strong compensation of *n-ZrNiSn* [2,7].

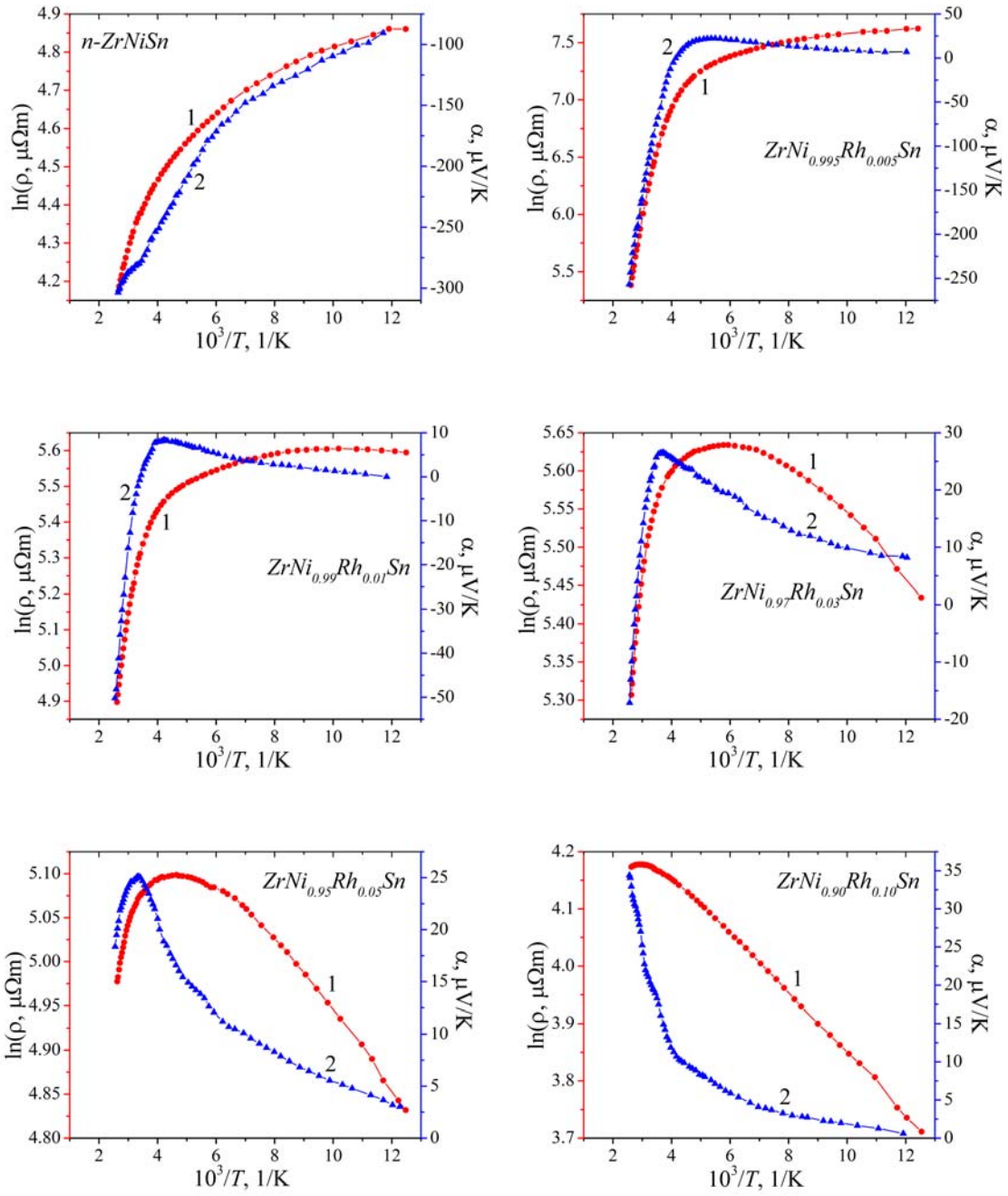

Fig. 3. Temperature dependences of electrical resistivity lnρ(1/T) (1) and the Seebeck coefficient α(1/T) (2) of $ZrNi_{1-x}Rh_xSn$.

Doping of *n-ZrNiSn* with *Rh* impurity changes both the type of dependences lnρ(1/*T*) and α(1/*T*), and the values of ρ(*x*) and α(*x*) (Figs. 3,4). Introduction of the lowest concentration of *Rh* (*x* = 0.005) drastically increases the values of electrical resistivity, for instance, at a temperature of 80 K from ρ(*x* = 0) = 129.1 μOhm·m to ρ(*x*=0.005)=2042.6 μOhm·m. In this case, the sign of the Seebeck coefficient a(*x*) of $ZrNi_{1-x}Rh_xSn$ changes from negative to positive: α(*x* = 0) = -88.6 μV/K and α(*x* = 0.005) = 7.0 μV/K. A change in the sign of α(*x*) followed from the results of structural studies and calculations of electronic structure, since it turned out that at *4c* site of *Ni*(*Rh*) atoms structural defects of acceptor nature are generated.

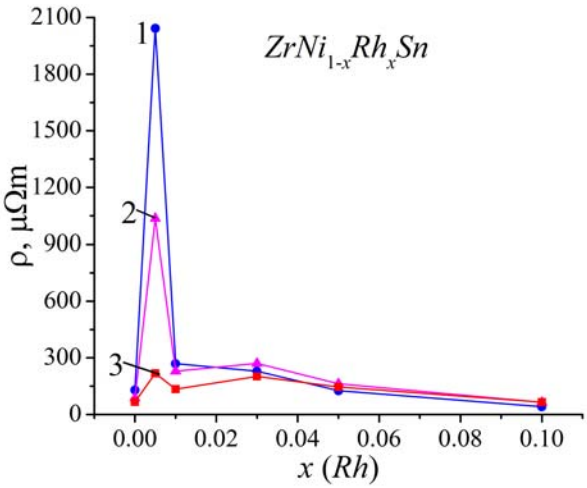

a)

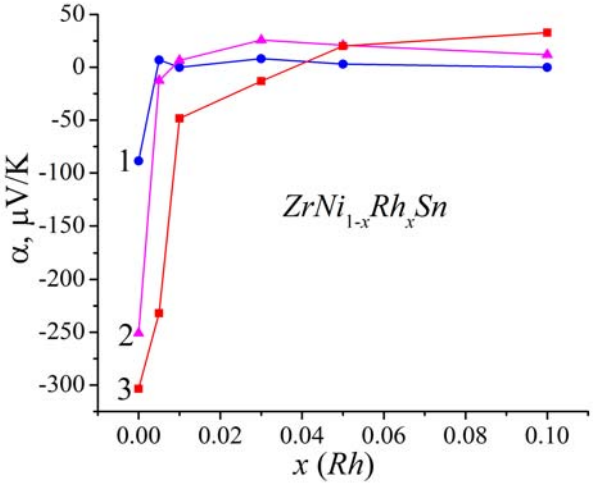

b)

*Fig. 4. Change in the values of electrical resistivity ρ(x) (**a**) and the Seebeck coefficient α(x) (b) of $ZrNi_{1-x}Rh_xSn$ at different temperatures: 1 – 80 K, 2 – 250 K, 3 – 380 K.*

On the other hand, a change in the sign of the Seebeck coefficient α(*x*) of $ZrNi_{1-x}Rh_xSn$, *x* = 0.005, at low temperatures testifies that the number of ionized acceptors exceeds the number of ionized donors, holes are the majority carriers, and the Fermi level ε_F is closer to the level of valence

band. Such a behavior of ε_F is a natural reaction to doping of *n*-semiconductor with acceptors, which increases compensation ratio (the ratio between ionized acceptors and donors) of HDSC semiconductors [2,7]. However, with a rise in temperature ($T_{inv} \geq 254$ K), the sign of the Seebeck coefficient unexpectedly becomes negative, showing that electrons again, like in *n-ZrNiSn*, are majority carriers.

It turns out that in $ZrNi_{1-x}Rh_xSn$, $x = 0.005$, the Fermi level ε_F with a rise in temperature drifts from the valence band (low temperatures) to conduction band (high temperatures), intersecting in this case the midgap ε_g at $T_{inv} \approx 254$ K. At this temperature, there is a state of full compensation to which correspond equal concentrations of ionized acceptors and donors.

From the high-temperature area of the dependence $\ln\rho(1/T)$ of $ZrNi_{1-x}Rh_xSn$, $x = 0.005$, calculated were the values of activation energy $\varepsilon_1^{\rho}(x = 0.005) = 127.2$ meV (Fig. 5*a*). As long as the sign of the Seebeck coefficient at these temperatures is negative, we see a departure of the Fermi level ε_F from conduction band as compared to *n-ZrNiSn*, where $\varepsilon_1^{\rho} = 97.6$ meV. Moreover, the appearance of the maximum on the dependence $\alpha(1/T)$ at a temperature of $T_{ext} \approx 190$ K (Fig. 3) shows that the conductivity of thermoelectric material involves electrons and holes simultaneously, and the concentrations and relations between them vary with temperature.

Increase in the compensation ratio of $ZrNi_{1-x}Rh_xSn$, $x = 0.005$, is indicated by increase in the values of activation energy $\varepsilon_1^{\alpha}(x = 0.005) = 186$ meV (Fig. 5*b*). Thus, if in *n-ZrNiSn* the amplitude of large-scale fluctuation of continuous energy bands was $\varepsilon_1^{\alpha} = 83.8$ mV, then in $ZrNi_{1-x}Rh_xSn$, $x = 0.005$, it increased by a factor of ~ 2.2, due to which the Fermi level ε_F was arranged near the midgap ε_g at a temperature of $T_{inv} \approx 254$ K, and semiconductor became fully compensated (in fully compensated semiconductor $\varepsilon_1^{\alpha} = \varepsilon_g/2$ [6]. We believe that at low temperatures and the smallest concentrations of *Rh* ($x = 0.005$) the energy of electron is insufficient for overshoot to conduction band (for ionization of donor), and impurity acceptor states are shallow, the temperature of 80 K is sufficient for their ionization and holes become the majority carriers. With a rise in temperature, when ionization of donors is possible, the concentration of electrons and their contribution to conductivity increase. Under these conditions, the Seebeck coefficient changes its sign from positive to negative, and the Fermi level ε_F at a temperature of $T_{inv} \approx 254$ K intersects the midgap ε_g. Using the temperature dependence of compensation ratio, as well as the fact that at full compensation the amplitude of large-scale fluctuation of continuous energy bands is equal to $\varepsilon_g/2$ [6], for $ZrNi_{1-x}Rh_xSn$, $x = 0.005$, the bandgap was estimated as $\varepsilon_g \approx 372$ meV (Fig. 5*b*, inset).

Assuming that hole concentration in $ZrNi_{1-x}Rh_xSn$ is related to generation of defects of acceptor nature at substitution of *Rh* atoms for *Ni,* the concentration of free electrons present in *n-ZrNiSn* should decrease by the same law at their "freezing out" to acceptors. Ideally, the number of electrons should decrease by the number of generated acceptors.

On the other hand, if we proceed from the disordered model of *n-ZrNiSn* [8], the behavior of $\ln\rho(1/T)$ and $\alpha(1/T)$ $ZrNi_{1-x}Rh_xSn$, $x = 0.005$, is caused not only by decrease of the concentration of electrons at their "freezing out", but also by the decrease of the number of electrons at displacement by *Ni* of *Zr* atoms from 4*a* site and liquidation of donor nature defects at $x \approx 0.01$. That is, in $ZrNi_{1-x}Rh_xSn$, at concentrations $0 < x \leq 0.01$, the velocity of decreasing the number of electrons due to liquidation of donors exceeds the velocity of increasing hole concentration, and conductivity at all temperatures should be determined by holes. At the same time, the experimental results record a considerable number of electrons of unknown origin and do not agree with the conclusions made on the basis of the disordered model of *ZrNiSn* structure [8].

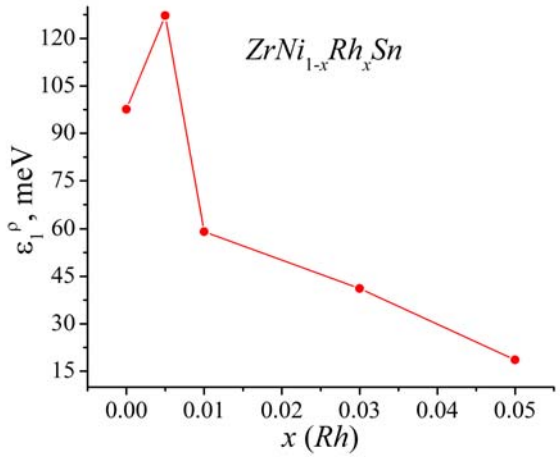

a)

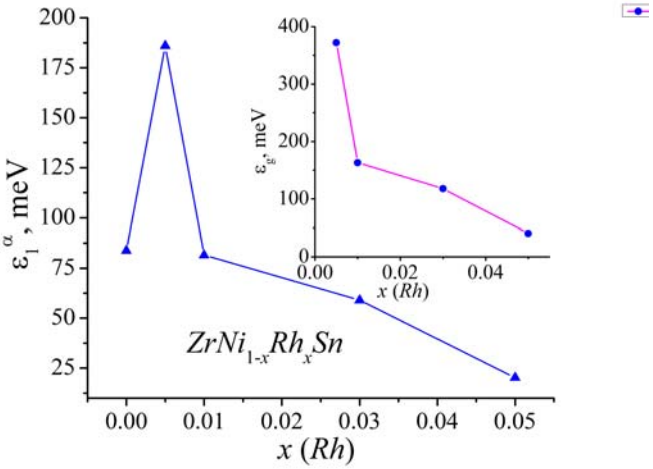

b)

*Fig. 5. Change in the values of activation energy $\varepsilon_1^{\rho}(x)$ (**a**) and ε_1^{α} (b) for $ZrNi_{1-x}Rh_xSn$. Inset (b): change in the values of the bandgap ε_g of $ZrNi_{1-x}Rh_xSn$.*

To check the correctness of the disordered model of *n-ZrNiSn* structure [8], we will study the behavior of the kinetic and energy characteristics of $ZrNi_{1-x}Rh_xSn$, $x \geq 0.01$, when the number of introduced acceptors corresponds to or exceeds the number of donors, created with partial ($x \approx 0.01$) occupancy by *Ni* of *Zr* atoms at 4*a* site. Thus, with increasing concentration of *Rh* ($x > 0.005$) and at a temperature of 80 K, the values of resistivity of $ZrNi_{1-x}Rh_xSn$ drastically reduce from $\rho(x = 0.01) = 269.0$ μΩ·m to $\rho(x = 0.05) = 125.4$ μOhm·m and $\rho(x = 0.10) = 40.9$ μΩ·m. The positive values of the Seebeck coefficient at low temperatures testify that the number of ionized acceptors exceeds the number of such donors, and the Fermi level ε_F is located closer to valence band. This contributes to the growth of the hole concentration, and metallization of conductivity (absence of hopping conductivity) (Fig. 3) shows that the entire small-scale relief of the valence band is filled with holes [6]. We can note that the $\rho(x)$ behavior of $ZrNi_{1-x}Rh_xSn$ *at low temperatures* is consistent with

the results of structural investigations, in particular, with respect to the model of disordered *ZrNiSn* structure [8] and the distribution of the electronic density of states (Fig. 2).

However, with a rise in temperature in the samples of $ZrNi_{1-x}Rh_xSn$, $x = 0.01$ and $x = 0.03$, at $T_{inv} \geq 295$ K anda $T_{inv.} \geq 362$ K, respectively, the sign of the Seebeck coefficient, just as at $x = 0.005$, changes from positive to negative (Fig. 6), and electrons become the majority carriers. And this is despite the fact that the concentration of acceptors is much in excess of the concentration of donors in the model of disordered structure of *n-ZrNiSn*. Such a behavior of the Seebeck coefficient is possible on condition that in material, simultaneously with acceptors, donors of unknown origin are either generated or had been present in the base compound *ZrNiSn* with larger ionization energy than that in acceptors. Moreover, the compensation ratio and position of the Fermi level ε_F in $ZrNi_{1-x}Rh_xSn$ depend both on impurity concentration and on temperature. Taking into account that defects of donor nature become apparent at much higher concentrations than if they were generated by the disorder in *ZrNiSn* ($x \approx 0.01$) structure, the model of defects of crystalline structure of *ZrNiSn* compound proposed in [8] needs to be corrected.

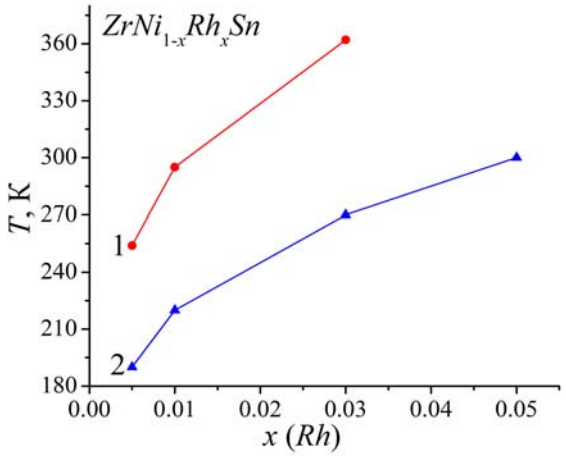

Fig. 6. Change in the values of inversion temperature $T_{inv.}$ of the Seebeck coefficient sign (1) and maximum $T_{ext.}$ on the dependence α(1/T) (2) of $ZrNi_{1-x}Rh_xSn$

The conclusion that acceptors and donors become simultaneously apparent in $ZrNi_{1-x}Rh_xSn$ follows from the analysis of behavior of the Fermi level ε_F for samples with concentrations $x = 0.01$ and $x = 0.03$. Thus, if the drift of the Fermi level ε_F from the conduction band deep into the bandgap of $ZrNi_{1-x}Rh_xSn$ at the lowest concentration of *Rh* is understandable, its reverse motion again to conduction band at $x \geq 0.01$ is impossible to be explained in the framework of the model that substitution of *Rh* for *Ni* generates only acceptors. The decrease in the activation values of ε_1^{ρ} from $\varepsilon_1^{\rho}(x = 0.005) = 127.2$ meV to $\varepsilon_1^{\rho}(x = 0.01) = 59.1$ meV and $\varepsilon_1^{\rho}(x = 0.03) = 41.2$ meV, as well as the negative values of the Seebeck coefficient in the areas of $\ln\rho(1/T)$, from which the values of these energies were calculated, testifies that there is activation toward conduction band. But this is possible only if there are donors in $ZrNi_{1-x}Rh_xSn$ whose origin is unknown to us.

Taking into account that in the samples of $ZrNi_{1-x}Rh_xSn$ with $x = 0.01$ and $x = 0.03$ at temperatures $T_{inv.} \approx 295$ K and $T_{inv.} \approx 362$ K (Fig. 6), the Fermi level ε_F intersects the midgap ε_g and the state of full compensation is realized, the bandgap width was estimated on the basis of the dependence $\varepsilon_1^{\alpha 0} \approx \varepsilon_g/2$ [6]. It appeared that in $ZrNi_{1-x}Rh_xSn$ the value of ε_g drastically decreases with increasing concentration of *Rh* with $\varepsilon_g(x = 0.01) \approx 163$ meV to $\varepsilon_g(x = 0.03) \approx 118$ meV (inset in Fig. 5*b*).

In the samples of $ZrNi_{1-x}Rh_xSn$, $x \geq 0.05$, the sign of the Seebeck coefficient at all temperatures remains positive (Fig. 3,4). The presence of high-temperature activation on the dependence $\ln\rho(1/T)$ points to arrangement of the Fermi level ε_F close to valence band at a distance of $\varepsilon_1^{\rho}(x = 0.05) = 18.2$ meV. On the other hand, the extreme on the dependence $\alpha(1/T)$ $ZrNi_{1-x}Rh_xSn$, $x = 0.05$, at $T_{ext.} \approx 300$ K (Fig. 3) points to participation in conduction of electrons and holes, but at a temperature of $T \leq 400$ K the number of ionized acceptors exceeds the number of such donors. As long as we have not reached the state of full compensation, we cannot estimate correctly the values of bandgap ε_g for $ZrNi_{1-x}Rh_xSn$, $x = 0.05$.

In the samples of $ZrNi_{1-x}Rh_xSn$, $x = 0.10$, when in the temperature range of $T = 80 – 400$ K on the dependence $\ln\rho(1/T)$ there are no activation areas whatsoever (Fig. 3), we can state that the Fermi level ε_F has intersected the percolation level of valence band: the dielectric-metal conductivity transition, i.e. the Anderson transition, took place [6,16]. However, the presence of maximum on the dependence $\ln\rho(1/T)$ and the onset of formation of high-temperature activation can testify that at higher temperatures the Fermi level ε_F will leave the valence band and enter the bandgap: the upset of metallic conduction will occur [6]. In a p-type semiconductor this is possible only on the condition of appearance of free electrons of unknown origin which ionize acceptors, increasing compensation ratio and forcing the Fermi level ε_F to leave the valence band.

The results of research on magnetic susceptibility of χ $ZrNi_{1-x}Rh_xSn$ (Fig. 7) also point to simultaneous generation of defects of acceptor and donor nature. The samples of $ZrNi_{1-x}Rh_xSn$, $x > 0.01$, are Pauli paramagnetics, the magnetic susceptibility χ of which is determined by electron gas and is proportional to density of states on the Fermi level $g(\varepsilon_F)$. At the concentrations of $x > 0.03$, the dependence $\chi(x)$ drastically changes the slope, achieves plateau and scarcely changes up to $x = 0.10$. Taking into account that $\chi \sim g(\varepsilon_F)$ [6], the slight change in the values of $\chi(x)$ in $ZrNi_{1-x}Rh_xSn$ means that the density of states at the Fermi level $g(\varepsilon_F)$ also changes only slightly, which is possible only on condition of simultaneous appearance of carriers opposite in sign as a result of simultaneous generation of donors and acceptors. Note that *n-ZrNiSn* is a weak diamagnetic, as indicated by the negative values of magnetic susceptibility $\chi(x = 0) = -0.07$ sm^3/g, and the growth of the values of $\chi(x)$ in the area $x = 0 – 0.01$ is not related to the growth of $g(\varepsilon_F)$.

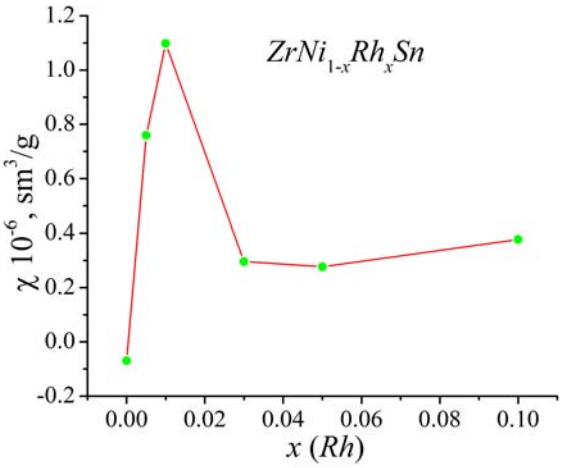

Fig. 7. Change in the values of magnetic susceptibility χ of $ZrNi_{1-x}Rh_xSn$ at T=300 K.

Thus, the results of research on semiconductor thermoelectric material $ZrNi_{1-x}Rh_xSn$ testify to complicated processes of electronic structure reconstruction, caused both by generation of structural defects of donor and acceptor nature, and by the change in temperature, varying the bandgap and

compensation ratio (the ratio between ionized donors and acceptors). However, this research is not enough to understand the mechanism of donor appearance in a semiconductor doped with an acceptor impurity. On the other hand, the accuracy of X-ray methods for studying the structure of $ZrNi_{1-x}Rh_xSn$ did not determine whether *Ni* and/or *Rh* atoms are accumulated at tetrahedral vacant sites, generating structural defects of donor nature. For practical solution of the problem with respect to the method for generation of donors in $ZrNi_{1-x}Rh_xSn$ it is necessary to use more sensitive research methods, in particular, thermodynamic calculations.

Research on the thermodynamic characteristics of $ZrNi_{1-x}Rh_xSn$

Thermodynamic characteristics were calculated for the following models of $ZrNi_{1-x}Rh_xSn$:

a) an ideal model of $ZrNi_{1-x}Rh_xSn$, where *Ni* atoms are substituted by *Rh* atoms at 4*c* crystallographic site, generating acceptors, none of the atoms in this case occupies tetrahedral vacant sites (Vac) (Fig. 8). For this model, there is a decrease in the values of the enthalpy of formation, indicating a lack of solubility at a temperature of T = 0 K. However, with a rise in temperature, the contribution of configuration entropy, in the equation of which the total number of atoms in the cell remains constant, becomes more significant, and on the temperature curve $\Delta G(T)$ there appears a minimum which, with a rise in temperature, shifts toward higher concentrations of *Rh*. Thus, in this model, the entropy component of the thermodynamic potential is decisive in the formation of a semiconducting solid solution.

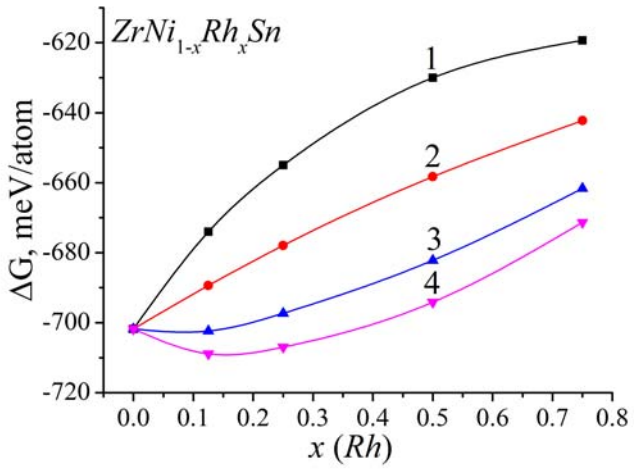

Fig. 8. Change in the values of thermodynamic potential ΔG(x) of $ZrNi_{1-x}Rh_xSn$ for the case of substitution of Ni atoms by Rh at 4c site at different temperatures: 1 – 0 K, 2 – 473 K, 3 – 873 K, 4 – 1273 K.

b) model $Zr(Ni_{1-x}Rh_x)Ni_ySn$, in which *Rh* atoms are substituted for *Ni* at 4*c* crystallographic site, and *Ni* atoms partially occupy tetrahedral vacant sites (Vac) (Fig. 9). This model, taking into account the results of research [10,11], considers the cases when *Ni* atoms, on the one hand, are displaced from 4*c* crystallographic site by *Rh* atoms, generating acceptors, and, on the other hand, partially occupy tetrahedral vacant sites (Vac), generating structural defects of donor nature. The substitution of *Rh* atoms for *Ni* at 4c site in the presence of *Ni* atoms at tetrahedral vacant sites increases the enthalpy of formation of alloys, however, because of the increase in the number of atoms in the cell, the maximum of configuration entropy shifts towards lower concentrations of *Rh*.

This leads to a significant reduction in the thermodynamic potential at a temperature of 1273 K compared to an ordered solid solution. Consequently, the presence of *Ni* atoms at tetrahedral vacant sites (Vac) makes the process of *Rh* substitution for *Ni* energetically favourable at high temperatures

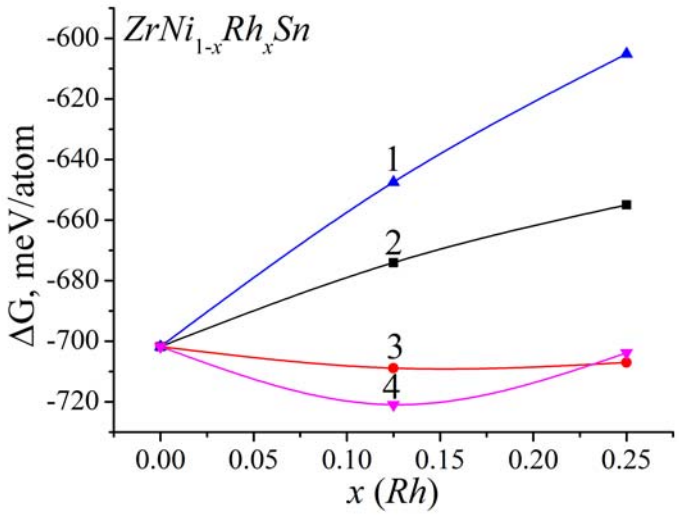

Fig. 9. Change in the values of thermodynamic potential ΔG(x) of $ZrNi_{1-x}Rh_xSn$ at different temperatures for the cases:
1 – substitution of Ni by Rh at 4c position and Ni occupies Vac at 0 K;
2 – substitution of Ni by Rh at 4c position at 0 K (fragment of Fig. 8);
3 – substitution of Ni atoms by Rh at 4c position at 1273 K (fragment of Fig. 8);
4 – substitution of Ni atoms by Rh at 4c position and Ni occupies Vac at 1273 K.

c) model $ZrNi_{1-x}Rh_xSn$, in which *Ni* atoms fully occupy 4*c* crystallographic site, and *Rh* atoms partially occupy tetrahedral vacant sites (Vac), replacing *Ni* atoms and generating structural defects of donor nature (Fig. 10). From the results of calculations it follows that substitution of *Rh* atoms for *Ni* atoms in Vac is energetically unfavourable even at high temperatures. From the results of thermodynamic calculations it definitely follows that in $ZrNi_{1-x}Rh_xSn$ it is energetically favourable when *Rh* atoms occupy 4c crystallographic site of *Ni* atoms, generating structural defects of acceptor nature, with a simultaneous generation of donors by accumulation of part of *Ni* atoms at the tetrahedral vacant sites (Vac) of the structure.

Conclusion

Thus, as a result of comprehensive research on the crystalline and electronic structures, the kinetic, magnetic and thermodynamic characteristics of $ZrNi_{1-x}Rh_xSn$ thermoelectric material, the methods for simultaneous generation of structural defects of acceptor and donor nature were established, as well as the dependence of the bandgap ε_g on the concentration of *Rh*. It is shown that it is energetically favourable to substitute *Ni* atoms *($3d^8 4s^2$)* at 4*c* crystallographic site by *Rh* atoms *($4d^8 5s^1$),* which generates structural defects of acceptor nature *(*more *s*-electrons in *Ni)* with accumulation of part of *Ni* atoms at the tetrahedral vacant sites *(*generation of donors*)*. It is concluded that the experimentally established donor nature of the defects of *ZrNiSn* basic compound ("a priori doping") is due to filling of the tetrahedral vacant sites by donor-generating *Ni* atoms.

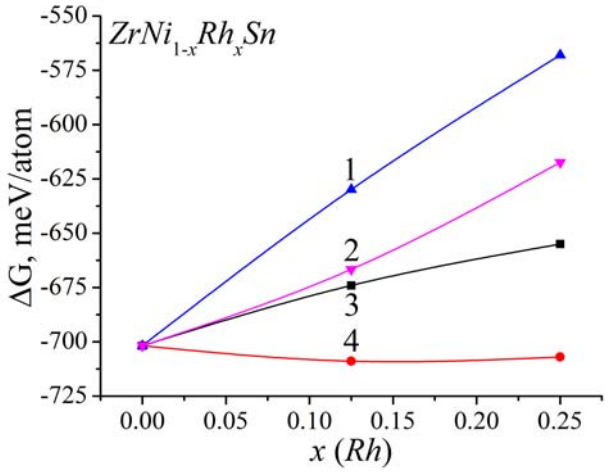

Fig. 10. Change in the values of thermodynamic potential ΔG(x) of $ZrNi_{1-x}Rh_xSn$ at different temperatures for the cases:
1 – Ni at 4c position and Rh occupies Vac at 0 K;
2 – Ni at 4c position and Rh occupies Vac at 1273 K;
3 – substitution of Ni by Rh at 4c position at 0 K (fragment of Fig. 8);
4 – substitution of Ni by Rh at 4c position at 1273 K (fragment of Fig. 8).

The work was performed in the framework of Austrian BMWFW Ernst Mach grant (ICM-2017-06580).

References

1. Anatychuk L.I. (1979). *Termoelementy i termoelektricheskiie ustroistva. Spravochnik [Thermoelements and thermoelectric devices. Handbook]*. Kyiv: Naukova dumka [in Russian].
2. Romaka V.A., Romaka V.V., Stadnyk Yu.V. (2011). *Intermetalichni napivprovidnyky: vlastyvosti ta zastosuvannia [Intermetallic semiconductors]*. Lviv: Lvivska Politechnica [in Ukrainian].
3. Romaka V.V., Rogl P.-F., Carlini R. and Fanciulli C. (2017). Prediction of the thermoelectric properties of Half-Heusler phases from the density functional theory. In *Alloys and Intermetallic Compounds.* C.Artini (Ed.). London-NY: Taylor & Francis Group.
4. Gurth M., Rogl G., Romaka V.V., Bauer E., Rogl P. (2016). Thermoelectric high *ZT* half-Heusler alloys $Ti_{1-x-y}Zr_xHf_yNiSn$ ($0 \le x \le 1$; $0 \le y \le 1$). *Materialia*, 104, 210 – 222.
5. Romaka L., Stadnyk Yu.V., Romaka V.A., Horyn A.M. (2017). Features of structural, electrokinetic and energy state characteristics of $V_{x+y}Co_{1-y}Sb_3$. *Phys. and Chem. of Solid State*, 15(3), 328 – 332.
6. Carlini R., Fanciulli C., Boulet P., Record M.C., Romaka V.V. and Rogl P.-F. Skutterudites for Thermoelectric Applications: Properties, Synthesis and Modeling (2017). In *Alloys and Intermetallic Compounds.* C. Artini (Ed.). London-NY: Taylor & Francis Group.

7. Shklovskii B.I., Efros A.L. (1979). *Elektronnyie svoistva legirovannykh poluprovodnikov [Electronic properties of doped semiconductors]*. Moscow: Nauka [in Russian].
8. Romaka V.A., Fruchart D., Hlil E.K., Gladyshevskii R.E., Gignoux D., Romaka V.V., Kuzhel B.S. and Krayjvskii R.V. (2010). Features of an intermetallic *n-ZrNiSn* semiconductor heavily doped with atoms of rare-earth metals. *Semiconductors*, 44(3), 293 – 302.
9. Romaka V.V., Romaka L.P., Krayovskyy V.Ya., Stadnyk Yu.V. (2015). *Stanidy ridkisnozemelnykh ta perekhidnykh metaliv [Stannides of rare-earth and transient metals]*. Lviv: Lvivska politechnica [in Ukrainian].
10. Romaka V.A., Rogl P., Stadnyk Yu.V., Romaka V.V, Hlil E.K., Krajovskii V.Ya., A.M. Goryn (2010). Features of conduction mechanisms in *n-HfNiSn* semiconductor heavily doped with a *Rh* acceptor impurity. *Semiconductors*, 47(9), 2245 – 1152.
11. Sauerschnig P., Grytsiv A., Vrestal J., Romaka V.V., Smetana B., Giesterg G., Bauer E., Rogl P. On the constitution and thermodynamic modelling of the system *Zr-Ni-Sn*. *Journal of Alloys and Compounds*.
12. Romaka V.A., Rogl P., Romaka V.V., Stadnyk Yu.V., Hlil E.K., Kraiovskii V.Ya., and Goryn' A.M. (2010). Effect of the accumulation of excess *Ni* atoms in the crystal structure of the intermetallic semiconductor *n-ZrNiSn. Semiconductors*, 47(7), 892 – 898.
13. Roisnel T., Rodriguez-Carvajal J. (2001). WinPLOTR: a windows tool for powder diffraction patterns analysis. *Mater. Sci. Forum, Proc. EPDIC7* 378 – 381, 118 – 123.
14. Schruter M., Ebert H., Akai H., Entel P., Hoffmann E., Reddy G.G. (1995). First-principles investigations of atomic disorder effects on magnetic and structural instabilities in transition-metal alloys. *Phys. Rev. B 52*, 188 – 209.
15. Moruzzi V.L., Janak J.F., Williams A.R. (1978). *Calculated electronic properties of metals*. NY.
16. Mott H., Davis T. (1982). *Elektronnyiie processy v nekristallicheskikh veshchestvakh [Electronic processes in noncrystalline substances]*. Moscow: Mir [Russian transl].

Submitted 18.10.2017

Ромака В.А. *док. техн. наук.*[1,2]**, Ромака Л.П.** *канд. хім. наук.*[3]**,**
Рогль П.-Ф. *док. фізики*[4]**, Ромака В.В.** *док. техн. наук.*[2,4]**,**
Стадник Ю.В. *канд. хім. наук.*[3]**, Горинь А.М.** *канд. хім. наук.*[3]**,**
Опірський І.Р. *канд. техн. наук.*[2]

[1]Інститут прикладних проблем механіки і математики ім. Я.С. Підстригача
НАН України, вул. Наукова, 3-б, Львів, 79060, Україна;
[2]Національний університет "Львівська політехніка", вул. С. Бандери, 12, Львів, 79013, Україна;
[3]Львівський національний університет ім. І. Франка, вул. Кирила і Мефодія, 6,
Львів, 79005, Україна;
[4]Віденський університет, вул. Верінгерштрасе, 42, Відень, А-1090, Австрія

ОСОБЛИВОСТІ МЕХАНІЗМІВ ЕЛЕКТРОПРОВІДНОСТІ ТЕРМОЕЛЕКТРИЧНОГО МАТЕРІАЛУ $ZrNi_{1-x}Rh_xSn$

Досліджено кристалічну та електронну структури, кінетичні, магнітні і термодинамічні характеристики термоелектричного матеріалу $ZrNi_{1-x}Rh_xSn$ у діапазонах: T=80–400 K, x=0.005–0.10. Встановлено механізми одночасного генерування структурних дефектів акцепторної та донорної природи, які визначають електропровідність матеріалу, а також залежність ширини забороненої зони ε_g від концентрації Rh. Показано, що енергетично доцільним є зайняття атомами Rh ($4d^85s^1$) кристалографічної позиції 4c атомів Ni ($3d^84s^2$), що генерує структурні дефекти акцепторної природи (у Ni більше s-електронів) та акумулювання частини атомів Ni у тетраедричних пустотах структури (генерування донорів). Зроблено висновок, що експериментально встановлена донорна природа дефектів сполуки ZrNiSn («апріорне легування») спричинена заповненням атомами Ni тетраедричних пустот, що генерує донори. Бібл. 16, Рис. 10.

Ключові слова: електронна структура, електроопір, коефіцієнт термо-ерс.

Ромака В.А. *док. техн. наук.*[1,2], **Ромака Л.П.** *канд. хим. наук.*[3],
Рогль П.-Ф. *док. физики*[4], **Ромака В.В.** *док. техн. наук.*[2,4],
Стадник Ю.В. *канд. хим. наук.*[3], **Горинь А.М.** *канд. хим. наук.*[3],
Опирский И.Р. *канд. техн. наук.*[2]

[1]Институт прикладных проблем механики и математики им. Я.С. Підстригача НАН Украины, ул. Научная, 3-бы, Львов, 79060, Украина;
[2]Национальный университет “Львовская политехника”, ул. С. Бандеры, 12, Львов, 79013, Украина;
[3]Львовский национальный университет им. І. Франко, ул. Кирилла и Мефодия, 6, Львов, 79005, Украина;
[4]Венский университет, ул. Верінгерштрасе, 42, Вена, А-1090, Австрия

ОСОБЕННОСТИ МЕХАНИЗМОВ ЭЛЕКТРОПРОВОДНОСТИ ТЕРМОЭЛЕКТРИЧЕСКОГО МАТЕРИАЛА $ZrNi_{1-x}Rh_xSn$

Исследовано кристаллическую и электронную структуры, кинетические, магнитные и термодинамические характеристики термоэлектрического материала $Zrni_{1-xrhxsn}$ в диапазонах: T=80–400 K, x=0.005-0.10. Установлены механизмы одновременного генерирования структурных дефектов акцепторной и донорної природы, которые определяют электропроводность материала, а также зависимость ширины запрещенной зоны εg от концентрации Rh. Показаниный, что энергетически целесообразным есть занятия атомами Rh ($4d^{85}s^1$) кристаллографической позиции 4c атомов Ni ($3d^{84}s^2$), что генерирует структурные дефекты акцепторной природы (в Ni больше s-электронов) и аккумулирование части атомов Ni в тетраедричних пустотах структуры (генерирование доноров). Сделан вывод, которая экспериментально установлена донорна природа дефектов соединения Zrnisn («априорное легирование») вызванная заполнениям атомами Ni тетраедричних пустот, которое генерирует доноры. Библ. 16, Рис. 10.

Ключевые слова: электронная структура, электросопротивление, коэффициент термо-ерс.

References

17. Anatychuk L.I. (1979). *Termoelementy i termoelektricheskiie ustroistva. Spravochnik [Thermoelements and thermoelectric devices. Handbook]*. Kyiv: Naukova dumka [in Russian].
18. Romaka V.A., Romaka V.V., Stadnyk Yu.V. (2011). *Intermetalichni napivprovidnyky: vlastyvosti ta zastosuvannia [Intermetallic semiconductors]*. Lviv: Lvivska Politechnica [in Ukrainian].
19. Romaka V.V., Rogl P.-F., Carlini R. and Fanciulli C. (2017). Prediction of the thermoelectric properties of Half-Heusler phases from the density functional theory. In *Alloys and Intermetallic Compounds.* C.Artini (Ed.). London-NY: Taylor & Francis Group.
20. Gurth M., Rogl G., Romaka V.V., Bauer E., Rogl P. (2016). Thermoelectric high *ZT* half-Heusler alloys $Ti_{1-x-y}Zr_xHf_yNiSn$ ($0 \le x \le 1$; $0 \le y \le 1$). *Materialia*, 104, 210 – 222.
21. Romaka L., Stadnyk Yu.V., Romaka V.A., Horyn A.M. (2017). Features of structural, electrokinetic and energy state characteristics of $V_{x+y}Co_{1-y}Sb_3$. *Phys. and Chem. of Solid State*, 15(3), 328 – 332.
22. Carlini R., Fanciulli C., Boulet P., Record M.C., Romaka V.V. and Rogl P.-F. Skutterudites for Thermoelectric Applications: Properties, Synthesis and Modeling (2017). In *Alloys and Intermetallic Compounds.* C. Artini (Ed.). London-NY: Taylor & Francis Group.
23. Shklovskii B.I., Efros A.L. (1979). *Elektronnyie svoistva legirovannykh poluprovodnikov [Electronic properties of doped semiconductors]*. Moscow: Nauka [in Russian].
24. Romaka V.A., Fruchart D., Hlil E.K., Gladyshevskii R.E., Gignoux D., Romaka V.V., Kuzhel B.S. and Krayjvskii R.V. (2010). Features of an intermetallic *n-ZrNiSn* semiconductor heavily doped with atoms of rare-earth metals. *Semiconductors*, 44(3), 293 – 302.
25. Romaka V.V., Romaka L.P., Krayovskyy V.Ya., Stadnyk Yu.V. (2015). *Stanidy ridkisnozemelnykh ta perekhidnykh metaliv [Stannides of rare-earth and transient metals]*. Lviv: Lvivska politechnica [in Ukrainian].
26. Romaka V.A., Rogl P., Stadnyk Yu.V., Romaka V.V, Hlil E.K., Krajovskii V.Ya., A.M. Goryn (2010). Features of conduction mechanisms in *n-HfNiSn* semiconductor heavily doped with a *Rh* acceptor impurity. *Semiconductors*, 47(9), 2245 – 1152.
27. Sauerschnig P., Grytsiv A., Vrestal J., Romaka V.V., Smetana B., Giesterg G., Bauer E., Rogl P. On the constitution and thermodynamic modelling of the system *Zr-Ni-Sn*. *Journal of Alloys and Compounds*.
28. Romaka V.A., Rogl P., Romaka V.V., Stadnyk Yu.V., Hlil E.K., Kraiovskii V.Ya., and Goryn' A.M. (2010). Effect of the accumulation of excess *Ni* atoms in the crystal structure of the intermetallic semiconductor *n-ZrNiSn. Semiconductors*, 47(7), 892 – 898.
29. Roisnel T., Rodriguez-Carvajal J. (2001). WinPLOTR: a windows tool for powder diffraction patterns analysis. *Mater. Sci. Forum, Proc. EPDIC7* 378 – 381, 118 – 123.

30. Schruter M., Ebert H., Akai H., Entel P., Hoffmann E., Reddy G.G. (1995). First-principles investigations of atomic disorder effects on magnetic and structural instabilities in transition-metal alloys. *Phys. Rev. B 52*, 188 – 209.
31. Moruzzi V.L., Janak J.F., Williams A.R. (1978). *Calculated electronic properties of metals*. NY.
32. Mott H., Davis T. (1982). *Elektronnyiie processy v nekristallicheskikh veshchestvakh [Electronic processes in noncrystalline substances]*. Moscow: Mir [Russian transl].

Submitted 18.10.2017

L.I.Anatychuk *acad. National Academy of Sciences of Ukraine*[1,2],
N.V.Pasechnikova *Doctor med. sciences, National Academy of medical sciences of Ukraine*[3],
R.R. Kobylianskyi *Candidate Phys.-math. sciences*[1,2],
A.V. Prybyla *Candidate Phys.-math. Sciences*[1,2],
V.O. Naumenko *Doctor med. sciences*[3],
O.S. Zadorozhnyi *Candidate med. sciences*[3],
R.E. Nazaretian[3], V.V. Myrnenko[3]

[1] Institute of Thermoelectricity of the NAS and MES of Ukraine,
1, Nauky str, Chernivtsi, 58029, Ukraine; *e-mail: anatych@gmail.com*
[2]Yu.Fedkovych Chernivtsi National University,
2, Kotsiubynskyi str., Chernivtsi, 58012, Ukraine
e-mail: anatych@gmail.com
[3]State Institution "The Filatov Institute of Eye Diseases and Tissue Therapy of the NAMS of Ukraine", Odesa, Ukraine

COMPUTER SIMULATION OF THERMAL PROCESSES IN HUMAN EYE

The paper presents the results of computer simulation of thermal processes in human eye. The schematic, mathematical and computer models of human eye were built with regard to its thermophysical features, blood circulation, metabolic and heat exchange processes. The patterns of temperature distribution in different segments of human eye at controlled local hypothermia of corneal surface were determined. It was established that the required temperature decrease of eye retina by 2°C is achieved by cooling corneal surface to +18°C. Bibl. 38, Fig. 6, Table 2.
Key words: human eye, computer simulation, diagnosis and treatment of ophthalmologic diseases.

Introduction

General characterization of the problem. Currently, therapeutic hypothermia is widely used to protect biological tissues and organs from ischemia in various fields of medicine, in particular in cardiac surgery, neurosurgery and resuscitation [1 - 3]. Therapeutic hypothermia is considered as the most efficient physical method for the protection of nerve cells (brain, retina, etc), since from the point of view of evidence-based medicine there is no efficient pharmacological neuroprotection method in neuro-reanimation practice. In ophthalmic practice, there is also information that local hypothermia leads to a decrease in intraocular pressure, a reduction in pain syndrome, a decrease in the inflammatory response, stops bleeding, in conditions of acute ischemia reduces damage to retinal nerve cells, reduces edema and traumatization of the cornea at chemical burns of eyes and has other useful properties [4, 5].

In the world literature, there are data on the dynamics of biochemical processes, as well as hemo- and hydrodynamic parameters in the eye of animals and humans under the influence of low temperatures on the eye [6 - 11], as well as on the methods for measuring the intraocular temperature [12 - 20]. However, until now, the question of the distribution of intraocular temperature under the influence of various physical factors remains poorly understood [21 - 25].

Understanding the patterns of intraocular temperature distribution, as well as evaluating the relationship between the temperature parameters of the external and internal segments of the eye under various environmental conditions, in norm and pathology, under the influence of physical factors on the eye, will allow the development of a computer model for intraocular temperature distribution. Thus, in biological systems that are not susceptible to direct investigation, such as human eye, computer simulation can be used as an alternative method for assessing the intraocular temperature and is the best tool for predicting intraocular thermal processes. If such a computer model is available, it will be possible to more accurately imagine the dynamics of thermal processes in the eye under the influence of various external thermal factors (hypothermia and hyperthermia), which are used in clinical ophthalmology. Consequently, there will be an additional opportunity to improve the efficiency and safety of some methods of treatment of ophthalmic diseases.

It should be noted that the study of the dynamics of intraocular temperature under hypothermia will allow the development of a technology for controlled hypothermia of the eye, more efficient use of advantageous low-temperature effects for the treatment of eye diseases and reduce the risk of a number of complications in ophthalmic surgery. Prospects for neuroprotection with the use of moderate local hypothermia in ophthalmosurgery also require the creation of a computer model for the evaluation of thermal processes in the eye under the influence of one or several external factors [26, 27]. To create an adequate computer model of thermal processes, it is not enough to have temperature data recorded on the outer corneal surface [28]. It is necessary to understand the general patterns of temperature distribution in different segments of the eye, as well as the interrelation between the temperature parameters of the external and internal segments of the eye under various environmental conditions and when the physical factors affect the eye.

The development of thermoelectric devices for controlled local hypothermia of the eyes looks promising for the purpose of using such devices in patients with acute (eye injury) and chronic (diabetes) pathology of the eye. It is also advisable to use such devices in patients with traumatic eye injuries, retinal detachment and other acute pathology of the organ of vision at the prehospital stage (including in combat conditions), which will reduce the risk of complications and preserve the viability of eye structures until the patient is delivered to a specialized a medical institution for the provision of highly qualified care. Thus, the development and introduction of such thermoelectric equipment into medical practice is relevant, as it will provide physicians with a simple and effective method of diagnosis and treatment of various ophthalmic diseases. However, to develop the design and select the optimal dynamic modes of operation of thermoelectric devices for controlled local eye hypothermia, it is also necessary to develop computer methods for modeling thermal processes and to determine the patterns of the distribution of temperature and heat fluxes of the human eye.

Therefore, *the purpose of this work* is to develop a computer model and computer simulation methods of human eye processes in order to determine the patterns of temperature distribution in different segments of the eye with controlled local hypothermia of corneal surface.

Schematic model of human eye

A schematic model of human eye was developed with due regard to its anatomic structure, thermophysical features, blood circulation, metabolic and heat exchange processes (Figs.1*a,b*, 2*a,b*).

Human eyeball is composed of three tunics (external (cornea and sclera), middle (vascular tunic), inner (nervous tunic of eyeball)) and internal content (vitreous body, lens, watery moisture of the anterior and posterior chambers of the eye) [29].

The external (fibrous) tunic of the eye is represented by cornea and sclera. Cornea is a transparent nonvascular part of the external tunic of the eye. The cornea performs the function of conducting and refracting rays of light, as well as protecting the content of the eyeball from adverse external influences. The diameter of the cornea is, on the average, 11.0 mm, the thickness in the centre is about 0.5 mm, the refractive power is 43.0 diopters (dpt). Normally, the cornea is smooth, transparent, shiny, spherical. Nutrition of the cornea occurs due to the pericorneal network of vessels, the moisture of the anterior chamber of the eye and tears. Transparency of the cornea is ensured by its homogeneous structure, lack of vessels and strictly defined water content. Sclera is an opaque part of the external fibrous tunic of the eye. Its thickness is 1 mm. The sclera performs protective and shape-forming functions.

The middle (vascular) tunic of the eye, or uveal tract, consists of three parts: iris, ciliary body and choroid. Iris is a diagram of the eye. The thickness of the iris is merely 0.4-0.6 mm. The iris consists of connective-tissue stroma, vessels, epithelium, covering iris at the front and two layers of pigment epithelium at the back, providing its opacity. Pupil is a round hole in the centre of the iris. Due to a change in its diameter, the pupil controls the flow of light incident on the retina. The ciliary body is a part of the choroid of the eye, which in the form of a ring passes between the root of the iris and the choroid. The boundary between the ciliary body and the choroid lies along cogged line. The ciliary body produces intraocular fluid and participates in the act of accommodation (provides a clear vision at various distances due to a change in the lens curvature). The choroid is a part of the uveal tract, separated from the ciliary body by cogged line. The choroid is composed of several layers of vessels. The layer of wide chorio capillaries adjoins the retina and is separated from it by a thin Bruch's membrane. Located externally is a layer of middle vessels (mostly arterioles), behind which there is a layer of larger vessels (venules). Between the sclera and the choroid there is a suprachoroidal space where vessels and nerves transit. The choroid assures nutrition to the external layers of the retina (visual receptor cells).

The inner tunic of the eyeball (nervous tunic) is a highly nervous tissue that provides the perception of light stimuli. From the optic nerve disk to the cogged line there is the optically active part of the retina. In front of the cogged line located 6 – 7 mm from the limb it is reduced to the epithelium that covers the internal parts of ciliary body and iris. This part of the retina does not participate in the act of vision. The nutrition of the retina is due to the choroid and vessels of the central retinal artery system. The most photosensitive part of the yellow spot is the central fossa, or foveola. In the retina there are neurons of visual analyzer: photoreceptors (first neuron) - rods and cones, bipolar cells (second neuron) and ganglion cells (third neuron). Rods and cones are a receptor part of visual analyzer and are in the outer layers of the retina, directly in its pigment epithelium. Rods located on the periphery are responsible for peripheral vision – a field of view and light perception. Cones that are largely concentrated in the field of yellow spot provide central vision (visual acuity) and color perception. Axons of ganglion cells converge, forming the optic nerve. The disk of the optic nerve corresponds to the point of exit of the nerve fibers from the eyeball and does not contain photosensitive elements.

The internal content of the eyeball includes vitreous body, lens and watery moisture of the anterior and posterior chambers of the eye.

The vitreous body by weight and volume is about 2/3 of the eyeball. This is a transparent non-vascular gelatinous structure that fills the space between the retina, the ciliary body, the fibers of Zinn's zonule and the lens.

The vitreous body is covered with a thin membrane, inside which there is a skeleton of fine fibrils and a gel-like substance. The vitreous humor is more than 99 % water, in which a small amount of protein, hyaluronic acid and electrolytes are dissolved.

The lens is a transparent, non-vascular elastic formation which has the shape of a double-convex lens of 3.5 – 4 mm in thickness and 9 – 10 mm in diameter. The substance of the lens of dense consistency is enclosed in a thin capsule. The lens performs the functions of conduction and refraction of light, as well as participation in accommodation. The refractive power of the lens is about 18-19 dpt. The lens is located directly behind the iris and suspended on the fibers of Zinn's zonule which are woven into a lens capsule at its equator. The equator divides the capsule of the lens into the anterior and posterior. Under the anterior capsule of the lens there is the subcapsular epithelium, which produces fibers throughout life. The lens becomes flatter and denser, losing its elasticity. Gradually, the ability to accommodation is lost, since the condensed matter of the lens cannot change its shape. The lens almost 65 % consists of water, and the protein content reaches 35 % – more than in any other tissue of our body.

Intraocular fluid is produced in the ciliary body, fills the anterior and posterior chambers of the eye. The anterior camera of the eye is the space between the cornea, iris and lens. The posterior chamber of the eye is a narrow gap between the iris and lens with Zinn's zonule. Watery moisture takes part in the nutrition of non-vascular media of the eye, and its exchange largely determines the value of intraocular pressure. The main way of the outflow of intraocular fluid is the angle of the anterior chamber of the eye, formed by the root of the iris and the cornea. Through the system of trabeculae and a layer of cells of the inner epithelium, fluid enters Schlemm's canal (venous sinus), from where it flows into the veins of the sclera.

All arterial blood enters the eyeball by the ophthalmic artery, a branch of internal carotid artery. Ophthalmic artery forms the following branches which run to the eyeball: central retinal artery assuring blood supply to internal retinal layers; posterior short ciliary which dichotomously branch out in the choroid and supply it with blood; posterior long ciliary arteries which pass to suprachoroidal space to ciliary body; anterior ciliary arteries extend away from the muscular branches of the ophthalmic artery. Posterior long and anterior ciliary arteries, anastomosing with each other, form a large arterial circle of iris. Away from it, in the radial direction, extend vessels that form around the pupil a small arterial circuit of iris. Due to posterior long and anterior ciliary arteries, the iris and ciliary body are provided with blood, a pericorneal vessel network is formed, which is involved in the nutrition of the cornea. The outflow of blood from the eyeball is via vorticose veins, anterior ciliary veins and the central retinal vein. Vorticose veins collect blood from the uveal tract and leave the eyeball, obliquely piercing the sclera near the equator of the eye. The anterior ciliary veins and the central vein of the retina divert blood from the territory of homonymous arteries [29].

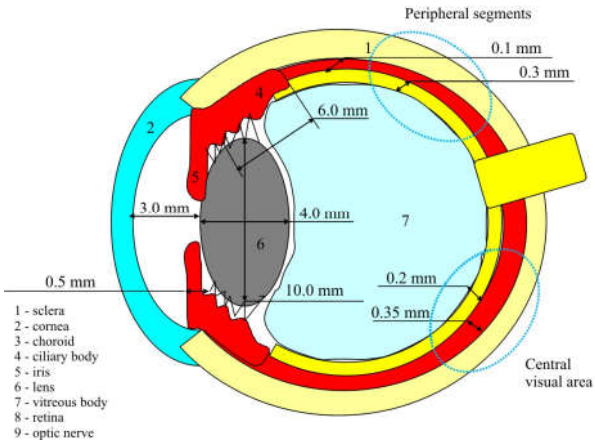

a)

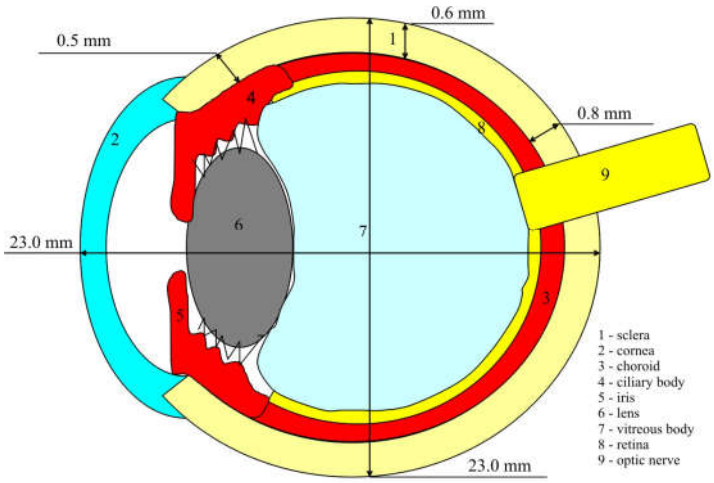

b)

Fig.1 a,b. Schematic model of eye (side view)
1 – sclera; 2 – cornea; 3 – choroid; 4 – ciliary body;
5 – iris; 6 – lens; 7 – vitreous body; 8 – retina; 9 – optic nerve

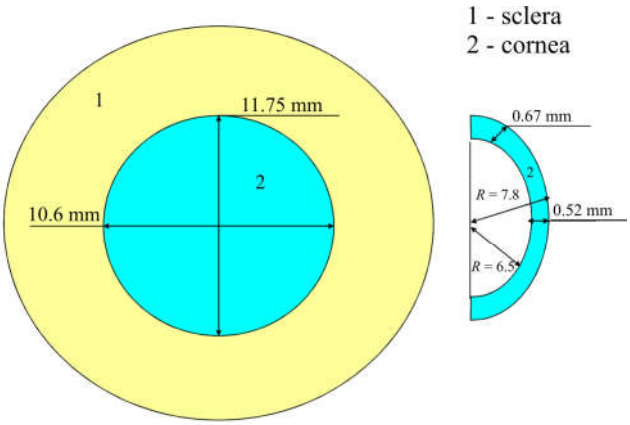

a)

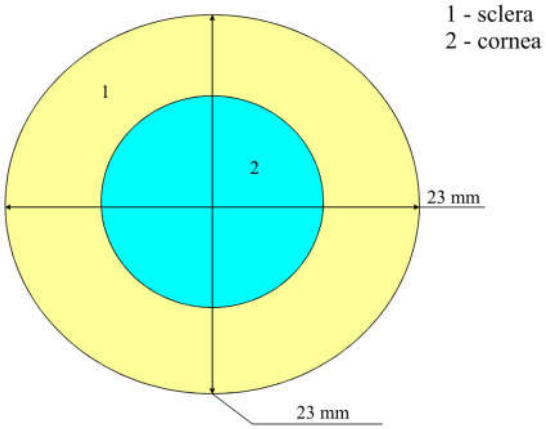

b)

Fig.2 a,b. Schematic model of eye (front view). склера - sclera ; рогівка - cornea

Blood circulation in the choroid is the main source of heat in the eye of animals and humans. Blood coming to the eye at a temperature practically equal to body temperature, forms thermal gradient which induces transfer of heat from the blood to eye tissues. The more intensive blood circulation, the greater amount of heat is passed to eye tissues. Blood circulation in the iris and ciliary body is also the source of heat. However, to a lesser degree, since blood circulation in the iris and ciliary body is relatively small as compared to blood circulation in the choroid. Heat distributed in the eye tissues passes to the environment through corneal surface due to convection and radiation [30].

The above Figs. 1a, b – 2a, b show the schematic layout of human eye structures and their dimensions.

The thermophysical properties of human eye structures (cornea, anterior chamber humidity, lens, vitreous body and retina), namely the values of thermal conductivity, density and specific heat that are taken as control values, are listed in Table 1. The values of thermal conductivity, density and specific heat of iris and ciliary body were considered to be equal to indicators of anterior chamber humidity. For the cornea and vitreous body the physical constants are close to the values of water, but the values of thermal conductivity and specific heat for the lens are considerably lower [31].

Table 1.

Thermophysical properties of human eye [31]

Eye structures	Thermal conductivity W/(m·K)	Density kg/m^3	Specific heat J/(kg·K)
Cornea (external surface temperature 32.0 – 34.0 ºC)	0.580	1050	4178
Humidity of anterior eye (volume 0.25 – 0.3 ml)	0.580	1000	3997
Lens	0.400	1050	3000
Vitreous body (volume 3.5 – 4 ml, temperature 34.0 – 36.0 ºC)	0.603	1000	4178
Retina	0.628	1000	4190
Blood Plasma (36.85 ºC)	0.53 – 0.55 0.599	1050 1025	4050 3820
Water (20 ºC)	0.6	993.4	4184
Retinal blood perfusion 0.012 s^{-1}.			

Mathematical description

To describe the process of heat exchange in "living" biological tissues, use is made of the Pennes equation (1) [32]. The generation of metabolic heat is considered to be uniformly distributed along the entire biological tissue, blood perfusion is also considered to be uniform and isotropic. According to the Pennes model, thermal equilibrium is created directly in the capillary circle of the microcirculatory bed (blood at temperature T_b comes to capillaries where heat exchange takes place, and blood temperature drops to temperature of biological tissue T).

Pennes simulated the effect of blood as isotropic heat source proportional to blood flow velocity and the difference between body temperature and local temperature of tissue in the form of the following equation [33 – 37]:

$$k\nabla^2 T + \rho_b c_b \omega_b (T_b - T) + Q_m + Q_i = \rho c \frac{\partial T}{\partial t}, \quad (1)$$

where k is thermal conductivity of biological tissue;
T is temperature of biological tissue;
ρ_b is blood density;
c_b is blood specific heat;
ω_b is blood perfusion;
T_b is arterial blood temperature (T_b = 37 °C);
Q_m is heat released due to metabolism;
Q_i is internal source of heat;
ρ is biological tissue density;
c is biological tissue specific heat;
t is time variable.

In Eq.(1), ∇^2 is a Laplacian operator which for the three-dimensional model is as follows:

$$\nabla^2 = \frac{\partial^2}{\partial x^2} + \frac{\partial^2}{\partial y^2} + \frac{\partial^2}{\partial z^2}. \quad (2)$$

The summand in the left side of Eq.(1) is the rate of change in thermal energy located in the unit volume of biological tissue. Three summands in the right side of this equation are, accordingly, the rate of change in thermal energy due to thermal conductivity under temperature gradient, blood perfusion and metabolic heat.

For the steady-state case $\partial T/\partial t = 0$, so Eq.(1) is simplified to:

$$k\nabla^2 T + \rho_b c_b \omega_b (T_b - T) + Q_m + Q_i = 0. \quad (3)$$

Eq.(3) should be solved with the following boundary conditions:

1. Blood temperature is approximately equal to biological tissue temperature $T_b = T$ =37°C.

2. Heat flux density (convection) from the surface of biological tissue q_0 is determined by means of the Newton-Richman equation (4):

$$q_0 = \alpha(T_{ext} - T), \quad (4)$$

where α = 12 is heat exchange coefficient; T_{ext} = 20°C is ambient temperature.

3. Heat flux density (radiation) from the surface of biological tissue q is determined by means of the Stephan-Boltzmann equation (5):

$$q = \sigma \cdot S \cdot \varepsilon_{1,2} \cdot (T_{ext}^4 - T^4), \quad (5)$$

where σ is the Stephan-Boltzmann constant, S is the area of the surface from which radiation occurs, ε_{12} is emissivity.

4. Total heat flux Q from the surface of biological tissue is determined by the expression:

$$Q = q_0 + q. \quad (6)$$

The analytical solution of Eq.(3) with the boundary conditions (4 – 6) is rather complex, so COMSOL Multiphysics applied software package was used [38], which allows simulation of thermophysical processes in biological tissue.

Computer model of human eye and simulation results

In order to determine temperature distribution in human eye, a three-dimensional computer model of human eye was created with regard to its thermophysical features, blood circulation,

metabolic and heat exchange processes. For this purpose, Comsol Multiphysics applied software package was used [38], allowing simulation of thermophysical processes in biological tissue with consideration of blood circulation and metabolism.

The distribution of temperature and heat flux density in human eye was calculated by the finite element method. According to this method, an object under study is split into a large number of finite elements, and in each of them the value of function is sought which satisfies given differential equations of second kind with the respective boundary conditions. The accuracy of solving the formulated problem depends on the level of splitting and is ensured by using a large number of finite elements [38].

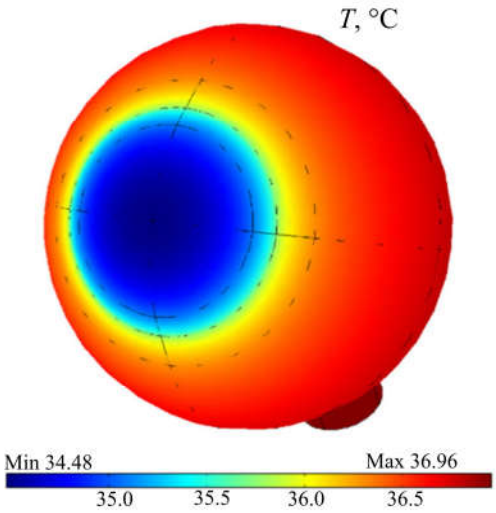

Fig.3. Computer model of human eye in Comsol Multiphysics program

With the aid of object-oriented computer simulation, the distributions of temperature and thermal flows in different structures of human eye were obtained that are shown in in Figs.3 - 4 *a, b*.

It is known that the basis for the neuroprotective effect of hypothermia is a reduction in the induction of apoptosis of neurons by decreasing the rate of metabolic processes therein. Thus, a reduction of brain temperature by 1°C assures a reduction of oxygen consumption by neurons and glucose metabolism by 5% [39]. Thus, according to medical requirements for the development of technology of controlled local hypothermia of the eye, it is necessary to predict what temperature of corneal surface should be reached in order to lower the temperature of the retina by 2 – 5°C.

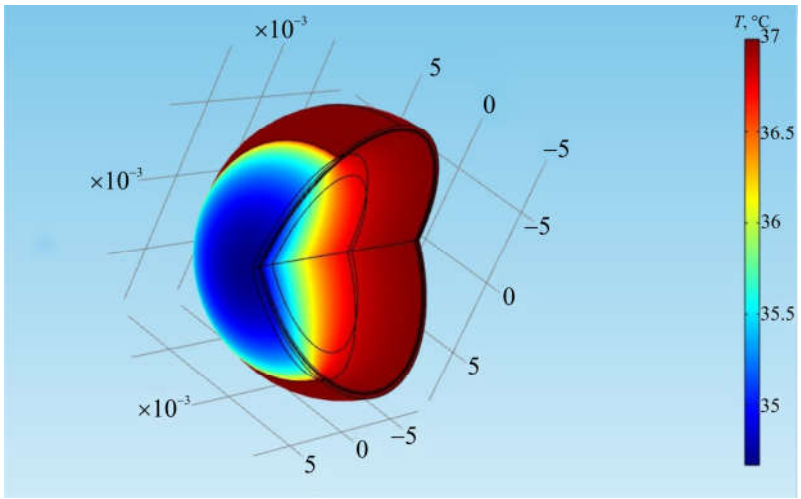

a)

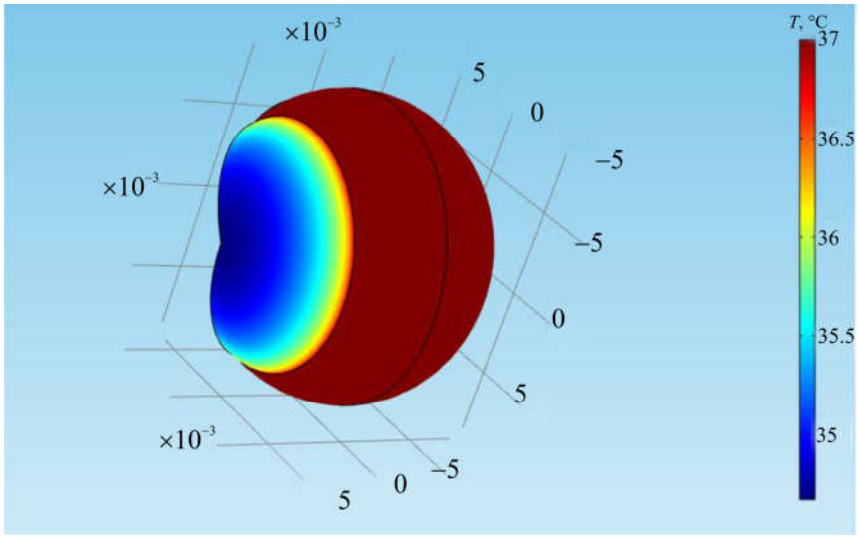

b)

Fig.4 a, b. Temperature distribution in human eye at ambient temperature T = 22°C

Also, computer simulation was made of temperature distributions in different structures of human eye at cooling of cornea to the required temperatures. As an example, Figs. 5 - 6 show temperature distributions in human eye at corneal surface temperatures T = 18°C and T = -5°C.

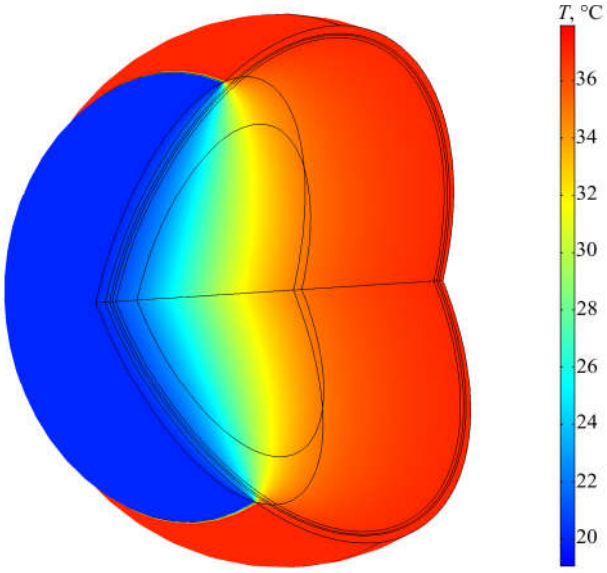

Fig. 5. Temperature distribution in human eye at corneal surface temperature T = 18°C

By means of computer simulation it was established that the required decrease of temperature of vitreous body and, accordingly, eye retina by 2 °C is achieved by cooling corneal surface to +18 °C, and to decrease eye retina temperature by 5 °C, corneal surface should be cooled to -5 °C. The results obtained enable one to develop the technology of controlled local therapeutic hypothermia in ophthalmology.

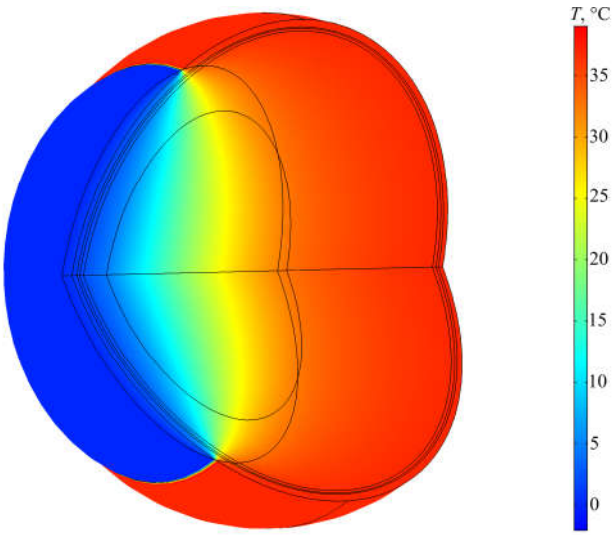

Fig.6. Temperature distribution in human eye at corneal surface temperature T = -5°C

Computer simulation results are listed in Table 2.

Table 2

Computer simulation results

Eye structures	Ambient temperature T = +22°C	Temperature at cooling of corneal surface to T = +18°C	Temperature at cooling of corneal surface to T = -5°C
Cornea	+34	+18	-5
Vitreous body (and, accordingly, eye retina)	+37	+35	+32

Conclusion

1. Schematic, mathematical and computer models of human eye were built with regard to its thermophysical features, blood circulation, metabolic and heat exchange processes.
2. Computer methods for simulation of thermal processes in human eye were developed. The distributions of temperature and thermal flows in human eye were determined. It was established that the required decrease of temperature of eye retina by 2 °C is achieved by cooling corneal surface to +18 °C.
3. The results obtained will be used for creation of up-to-date thermoelectric medical apparatus for the diagnosis and treatment of ophthalmologic diseases, which will improve the efficiency of diagnosis of pathology of visual organs, make it possible to observe in dynamics the development of pathological process in eye structures, improve the efficiency of treatment of acute and chronic eye diseases, develop and introduce the technology of controlled local therapeutic hypothermia in ophthalmology.

References

1. Usenko L.V., Tsarev A.V. (2009). Iskusstvennaia hipotermia v sovremennoi reanimatologii [Artificial hypothermia in modern resuscitation]. *Obshchaia reanimatologiia – General Resuscitation*, 1, 21-23 [in

Russian].

2. Tiainen, H. Parikka, M. Makijarvi, O. Takkunen, S. Sarna, R. Roine. (2009). Arrhythmias and heart rate variability during and after therapeutic hypothermia for cardiac arrest. *Critical Care Medicine*, 37(2), 403-409.
3. Deakin C.D., Nolan J.P., Soar J., Sunde K., Koster R.W., Smith G.B., Perkins G.D. (2010). European Resuscitation Council Guidelines for Resuscitation 2010. Section 4. Adult advanced life support. *Resuscitation*, 81, 1305-1352.
4. Abramov V.G., Artamonov V.P. (1973). *Primeneniie kholoda v oftalmologii [Use of cold in ophthalmology]*. Yaroslavl [in Russian].
5. K. Tamai, E.Toumoto, A. Majima. (1997). Local hypothermia protects the retina from ischaemic injury in vitrectomy. *Brit. J. Ophthalmol*, 81(9), 789-794.
6. Alzaga A.G., Cerdan M., Varon J. (2006). Therapeutic hypothermia. *Resuscitation*, 70(3), 369-380.
7. Iguchi Y., Asami T., Ueno S., et al. (2014). Changes in vitreous temperature during intravitreal surgery. *Invest. Ophthalmol. Vis. Sci*., 55, 2344-2349.
8. Oosterhuis J.A., Journee-de Korver H.G., Kakebeeke-Kemme H.M., Bleeker J.C. (1995). Transpupillary thermotherapy in choroidal melanomas. *Arch Ophthalmol*, 113, 15-321.
9. Rem A.I., Oosterhuis J.A., Journee-de Korver H.G., de Wolff-Rouendaal D., Keunen J.E. (2003). Transscleral thermotherapy: short- and long-term effects of transscleral conductive heating in rabbit eyes. *Arch Ophthalmol*. 121, 510-6.
10. Machemer R., Parel J.M., Norton E.W. (1972). Vitrectomy: a pars plana approach. Technical improvements and further results. *Trans. Am. Acad. Ophthalmol. Otolaryngol*, 76, 462-466.
11. Tan J.H., Ng E.Y.K, Acharya U.R., Chee C. (2009). Infrared thermography on ocular surface temperature: A review. *Infrared Physics & Technology*, 52, 97–108.
12. Schwartz B., Feller M.R. (1962). Temperature gradients in the rabbit eye. *Investigative Ophthalmology*, 1(4), 513-521.
13. May D.R., Freedland R.J. (1983). Ocular hypothermia: anterior chamber perfusion. *British Journal of Ophthalmology*, 67, 808-813.
14. Fatt I., Forester J.F. (1972). Errors in eye tissue temperature measurements when using a metallic probe. *Exp. Eye Res.*, 14, 270-276.
15. Buiko A.S., Yelagina V.A., Mazokhin S.I., Logai I.M., Shitova I.Ya. (1988). Lokalnaia SVCH-hypertermiia v kompleksnom lechenii zlokachestvennykh opukholei vek i orbity [Local UHF-hyperthermia in combined therapy of malignant tumors of eyelids and orbital cavity]. *Meditsinskaia radiologiia - Medical Radiology*, 8, 7-11.
16. Purslow C., Wolffsohn J. (2005). Ocular surface temperature: a review. *Eye and Contact Lens*, 31, 117–123.
17. Anatychuk L.I., Pasechnikova N.V., Zadorozhnyi O.S., Kobylianskyi R.R., Havryliuk M.V., Nazaretian R.E., Myrnenko V.V. (2015). Thermoelectric device for measurement of intraocular temperature. *J.Thermoelectricity*, 3, 31-40.
18. Anatychuk L.I., Pasechnikova N.V., Kobylianskyi R.R., Havryliuk M.V., Naumenko V.A., Myrnenko V.V., Nazaretian R.E., Zadorozhnyi O.S. (2016). Termoelektricheskiie datchiki dlia registratsii vnutriglaznoi temperatury [Thermoelectric sensors of recording of intraocular temperature]. *Sensorna elektronika i mikrosystemni tekhnologii - Sensor Electronics and Microsystem Technologies*, 13(3), 30-38 [in Russian].
19. *Patent of Ukraine № 117677*. (2017). Anatychuk L.I., Pasechnikova N.V., Kobylianskyi R.R., Naumenko V.O., Zadorozhnyi O.S., Havryliuk M.V., Nazaretian R.E., Myrnenko V.V. Thermoelectric device for measurement and recording of intraocular temperature [in Ukrainian].
20. Anatychuk L.I., Pasechnikova N.V., Zadorozhnyi O.S., Nazaretian R.E., Myrnenko V.V., Kobyliankyi R.R., Havryliuk M.V. (2015). Raspredeleniie temperatury v razlichnykh otdelakh glaza krolika v zavisimosti ot temperatury okruzhaiushchei sredy [Temperature distribution in different segments of rabbit eye depending on ambient temperature]. *Oftalmologiia. Vostochnaia Yevropa – Ophthalmology. Eastern Europe*, 4, 60-68 [in Russian].

21. Anatychuk L.I., Pasechnikova N.V., Zadorozhnyi O.S., Nazaretian R.E., Myrnenko V.V., Kobyliankyi R.R., Havryliuk M.V. (2015). Osobennosti raspredeleniia temperatury v glazu krolika [Peculiarities of temperature distribution in rabbit eye]. *OFTALMOLOGİYA: Elmi-Praktik Jurnal*, 19, 44-51 [in Russian].
22. Anatychuk L.I., Pasechnikova N.V., Zadorozhnyi O.S., Nazaretian R.E., Myrnenko V.V., Kobyliankyi R.R., Havryliuk M.V. (2015). Originalnoie ustroistvo i podkhody k izucheniiu raspredeleniia temperatury v razlichnykh otdelakh glaza [Original device and approaches to the study of temperature distribution in different eye segments]. *Oftalmologicheskii Zhurnal - J. Ophthalmology*, 6, 50-53 [in Russian].
23. Anatychuk L., Pasechnikova N., Zadorozhnyy O., Kobylianskyi R., Nazaretyan R., Myrnenko V. (2016). Experimental study of intraocular temperature distribution in the rabbit under various environmental conditions. *Acta Ophthalmologica (Abstracts from the 2016 European Association for Vision and Eye Research Conference),* 94, S 256. – October 2016 (DOI: 10.1111/j.1755-3768.2016.0267).
24. Anatychuk L.I., Pasechnikova N.V., Zadorozhnyi O.S., Kobylyanskyi R.R., Nazaretian R.E., Myrnenko V.V., Havryliuk M.V. (2016). Ustroistvo dlia intraokuliarnoi termometrii i osobennosti raspredeleniia temperatury v razlichnykh otdelakh glaza krolika [Intraocular thermometry device and peculiarities of temperature distribution in different segments of rabbit eye]. *Zhurnal Natsionalnoi Akademii meditsinskikh nauk Ukrainy – J. of the National Academy of Medical Sciences of Ukraine*, 22(1), 103-108 [in Russian].
25. Peksayar G., Altan-Yaycioglu R., Onal S. (2003). Excision and cryosurgery in the treatment of conjunctival malignant epithelial tumours. *Eye (Lond).* 2003 Mar;17(2):228-32.
26. Ooi E.H. and Ng E.Y.K. (2009). Ocular temperature distribution: a mathematical perspective. *Journal of Mechanics in Medicine and Biology*, 9(2), 199–227.
27. Vit V.V. (2003). *Stroieniie zritelnoi sistemy cheloveka [Structure of human visual system]*. Odessa: Astroprint [in Russian].
28. Mapstone R. (1968). Determinants of ocular temperature. *British Journal of Ophthalmology*, 52, 729-741.
29. Scott J.A. (1988). A finite element model of heat transport in the human eye. *Phys Med Biol*., 33(2), 227-241.
30. Pennes H.H. (1948). Analysis of tissue and arterial blood temperatures in the resting forearm *J. Appl. Physiol*., 1(2), 93 – 122.
31. Jiang S.C., Ma N., Li H.J., Zhang X.X. (2002). Effects of thermal properties and geometrical dimensions on skin burn injuries. *Burns*, 28, 713-717.
32. Cetingul M.P., Herman C. (2008). Identification of skin lesions from the transient thermal response using infrared imaging technique. *IEEE*, 1219-1222.
33. Ciesielski M., Mochnacki B., Szopa R. (2011). Numerical modeling of biological tissue heating. Admissible thermal dose. *Scientific Research of the Institute of Mathematics and Computer Science*, 1(10), 11-20.
34. Florin Filipoiu, Andrei Ioan Bogdan, Iulia Maria Carstea. (2010). Computer-aided analysis of the heat transfer in skin tissue. *Proc. of the 3rd WSEAS Int. Conference on Finite Differences - Finite Elements - Finite Volumes - Boundary Elements.* (Bucharest, Romania, 2010) (pp. 53-59).
35. Daniela Carstea, Ion Carstea, Iulia Maria Carstea. (2011). Interdisciplinarity in computer-aided analysis of thermal therapies. *WSEAS Transactions on Systems and Control*, 6(4), 115-124.
36. *COMSOL Multiphysics User's Guide*. COMSOLAB, 2010.
37. Yenari M.A., Han H.S. (2012). Neuroprotective mechanisms of hypothermia in brain ischaemia. *Nat. Rev. Neurosci.*, 13, 267-278.

Submitted 08.11.2017

Анатичук Л.І. *ак. НАН України*,[1,2]
Пасєчнікова Н.В. *доктор мед. наук, НАМН України*,[3]

Кобилянський Р.Р. *канд. фіз.-мат. наук*[1,2],
Прибила А.В. *канд. фіз.-мат. наук*[1,2],
Науменко В.О.[3], **Задорожний О.С.** *канд. мед. наук*[3],
Назаретян Р.Е.[3], **Мирненко В.В.**[3]

[1]Інститут термоелектрики НАН і МОН України, вул. Науки, 1,
Чернівці, 58029, Україна, *e-mail: anatych@gmail.com*;
[2]Чернівецький національний університет імені Юрія Федьковича,
вул. Коцюбинського 2, Чернівці, 58012, Україна
e-mail: anatych@gmail.com
[3]*ДУ «Інститут очних хвороб і тканинної терапії імені В.П. Філатова НАМН України», Одеса, Україна*

КОМП'ЮТЕРНЕ МОДЕЛЮВАННЯ ТЕПЛОВИХ ПРОЦЕСІВ ОКА ЛЮДИНИ

У роботі наведено результати комп'ютерного моделювання теплових процесів ока людини. Побудовано схематичну, математичну та комп'ютерну моделі ока людини з врахуванням його теплофізичних особливостей, кровообігу, процесів метаболізму і теплообміну. Визначено закономірності розподілів температури в різних відділах ока людини при контрольованій локальній гіпотермії поверхні рогівки. Встановлено, що необхідне зниження температури сітківки ока на 2°С досягається шляхом охолодження поверхні рогівки до температури +20°С. Бібл. 38, рис. 6, табл. 2.

Ключові слова: око людини, комп'ютерне моделювання, діагностика та лікування офтальмологічних захворювань.

Анатычук Л.И. *ак. НАН Украины*,[1,2]
Пасечникова Н.В. *доктор мед. наук, НАМН Украины*,[3]
Кобылянский Р.Р. *канд. физ.-мат. наук,*[1,2]
Прибила А.В. канд. *канд. физ.-мат. наук,*[1,2]
Науменко В.О.[3], **Задорожный А.С.** *канд. мед. наук*,[3]
Назаретян Р.Е.,[3] **Мирненко В.В.**[3]

[1] Институт термоэлектричества НАН и МОН Украины,
ул. Науки, 1, Черновцы, 58029, Украина, *e-mail: anatych@gmail.com*;
[2] Черновицкий национальный университет, им. Юрия Федьковича,
ул. Коцюбинського, 2, Черновцы, 58012, Украина,
e-mail: anatych@gmail.com,
[3]*ДУ «Институт глазных болезней и тканевой терапии им. В.П. Филатова НАМН Украины», Одесса, Украина*

КОМПЬЮТЕРНОЕ МОДЕЛИРОВАНИЕ ТЕПЛОВЫХ ПРОЦЕССОВ ГЛАЗА ЧЕЛОВЕКА

В работе приведены результаты компьютерного моделирования тепловых процессов глаза

человека. Построены схематическая, математическая и компьютерная модели глаза человека с учетом его теплофизических особенностей, кровообращения, процессов метаболизма и теплообмена. Определены закономерности распределения температуры в разных отделах глаза человека при контролируемой локальной гипотермии поверхности роговицы. Установлено, что необходимое снижение температуры сетчатки глаза на 2°С достигается путем охлаждения поверхности роговицы до температуры +20°С. Библ. 38, рис. 6, табл. 2.

Ключевые слова: глаз человека, компьютерное моделирование, диагностика и лечение офтальмологических заболеваний.

References

1. Usenko L.V., Tsarev A.V. (2009). Iskusstvennaia hipotermia v sovremennoi reanimatologii [Artificial hypothermia in modern resuscitation]. *Obshchaia reanimatologiia – General Resuscitation*, 1, 21-23 [in Russian].
2. Tiainen, H. Parikka, M. Makijarvi, O. Takkunen, S. Sarna, R. Roine. (2009). Arrhythmias and heart rate variability during and after therapeutic hypothermia for cardiac arrest. *Critical Care Medicine*, 37(2), 403-409.
3. Deakin C.D., Nolan J.P., Soar J., Sunde K., Koster R.W., Smith G.B., Perkins G.D. (2010). European Resuscitation Council Guidelines for Resuscitation 2010. Section 4. Adult advanced life support. *Resuscitation*, 81, 1305-1352.
4. Abramov V.G., Artamonov V.P. (1973). *Primeneniie kholoda v oftalmologii [Use of cold in ophthalmology]*. Yaroslavl [in Russian].
5. K. Tamai, E.Toumoto, A. Majima. (1997). Local hypothermia protects the retina from ischaemic injury in vitrectomy. *Brit. J. Ophthalmol*, 81(9), 789-794.
6. Alzaga A.G., Cerdan M., Varon J. (2006). Therapeutic hypothermia. *Resuscitation*, 70(3), 369-380.
7. Iguchi Y., Asami T., Ueno S., et al. (2014). Changes in vitreous temperature during intravitreal surgery. *Invest. Ophthalmol. Vis. Sci*., 55, 2344-2349.
8. Oosterhuis J.A., Journee-de Korver H.G., Kakebeeke-Kemme H.M., Bleeker J.C. (1995). Transpupillary thermotherapy in choroidal melanomas. *Arch Ophthalmol*, 113, 15-321.
9. Rem A.I., Oosterhuis J.A., Journee-de Korver H.G., de Wolff-Rouendaal D., Keunen J.E. (2003). Transscleral thermotherapy: short- and long-term effects of transscleral conductive heating in rabbit eyes. *Arch Ophthalmol*. 121, 510-6.
10. Machemer R., Parel J.M., Norton E.W. (1972). Vitrectomy: a pars plana approach. Technical improvements and further results. *Trans. Am. Acad. Ophthalmol. Otolaryngol*, 76, 462-466.
11. Tan J.H., Ng E.Y.K, Acharya U.R., Chee C. (2009). Infrared thermography on ocular surface temperature: A review. *Infrared Physics & Technology*, 52, 97–108.
12. Schwartz B., Feller M.R. (1962). Temperature gradients in the rabbit eye. *Investigative Ophthalmology*, 1(4), 513-521.
13. May D.R., Freedland R.J. (1983). Ocular hypothermia: anterior chamber perfusion. *British Journal of Ophthalmology*, 67, 808-813.
14. Fatt I., Forester J.F. (1972). Errors in eye tissue temperature measurements when using a metallic probe. *Exp. Eye Res.*, 14, 270-276.
15. Buiko A.S., Yelagina V.A., Mazokhin S.I., Logai I.M., Shitova I.Ya. (1988). Lokalnaia SVCH-hypertermiia v kompleksnom lechenii zlokachestvennykh opukholei vek i orbity [Local UHF-hyperthermia in combined therapy of malignant tumors of eyelids and orbital cavity]. *Meditsinskaia radiologiia - Medical Radiology*, 8, 7-11.
16. Purslow C., Wolffsohn J. (2005). Ocular surface temperature: a review. *Eye and Contact Lens*, 31, 117–123.
17. Anatychuk L.I., Pasechnikova N.V., Zadorozhnyi O.S., Kobylianskyi R.R., Havryliuk M.V., Nazaretian

R.E., Myrnenko V.V. (2015). Thermoelectric device for measurement of intraocular temperature. *J.Thermoelectricity*, 3, 31-40.

18. Anatychuk L.I., Pasechnikova N.V., Kobylianskyi R.R., Havryliuk M.V., Naumenko V.A., Myrnenko V.V., Nazaretian R.E., Zadorozhnyi O.S. (2016). Termoelektricheskiie datchiki dlia registratsii vnutriglaznoi temperatury [Thermoelectric sensors of recording of intraocular temperature]. *Sensorna elektronika i mikrosystemni tekhnologii - Sensor Electronics and Microsystem Technologies*, 13(3), 30-38 [in Russian].
19. *Patent of Ukraine № 117677*. (2017). Anatychuk L.I., Pasechnikova N.V., Kobylianskyi R.R., Naumenko V.O., Zadorozhnyi O.S., Havryliuk M.V., Nazaretian R.E., Myrnenko V.V. Thermoelectric device for measurement and recording of intraocular temperature [in Ukrainian].
20. Anatychuk L.I., Pasechnikova N.V., Zadorozhnyi O.S., Nazaretian R.E., Myrnenko V.V., Kobyliankyi R.R., Havryliuk M.V. (2015). Raspredeleniie temperatury v razlichnykh otdelakh glaza krolika v zavisimosti ot temperatury okruzhaiushchei sredy [Temperature distribution in different segments of rabbit eye depending on ambient temperature]. *Oftalmologiia. Vostochnaia Yevropa – Ophthalmology. Eastern Europe*, 4, 60-68 [in Russian].
21. Anatychuk L.I., Pasechnikova N.V., Zadorozhnyi O.S., Nazaretian R.E., Myrnenko V.V., Kobyliankyi R.R., Havryliuk M.V. (2015). Osobennosti raspredeleniia temperatury v glazu krolika [Peculiarities of temperature distribution in rabbit eye]. *OFTALMOLOGİYA: Elmi-Praktik Jurnal*, 19, 44-51 [in Russian].
22. Anatychuk L.I., Pasechnikova N.V., Zadorozhnyi O.S., Nazaretian R.E., Myrnenko V.V., Kobyliankyi R.R., Havryliuk M.V. (2015). Originalnoie ustroistvo i podkhody k izucheniiu raspredeleniia temperatury v razlichnykh otdelakh glaza [Original device and approaches to the study of temperature distribution in different eye segments]. *Oftalmologicheskii Zhurnal - J. Ophthalmology*, 6, 50-53 [in Russian].
23. Anatychuk L., Pasechnikova N., Zadorozhnyy O., Kobylianskyi R., Nazaretyan R., Myrnenko V. (2016). Experimental study of intraocular temperature distribution in the rabbit under various environmental conditions. *Acta Ophthalmologica (Abstracts from the 2016 European Association for Vision and Eye Research Conference),* 94, S 256. – October 2016 (DOI: 10.1111/j.1755-3768.2016.0267).
24. Anatychuk L.I., Pasechnikova N.V., Zadorozhnyi O.S., Kobylyanskyi R.R., Nazaretian R.E., Myrnenko V.V., Havryliuk M.V. (2016). Ustroistvo dlia intraokuliarnoi termometrii i osobennosti raspredeleniia temperatury v razlichnykh otdelakh glaza krolika [Intraocular thermometry device and peculiarities of temperature distribution in different segments of rabbit eye]. *Zhurnal Natsionalnoi Akademii meditsinskikh nauk Ukrainy – J. of the National Academy of Medical Sciences of Ukraine*, 22(1), 103-108 [in Russian].
25. Peksayar G., Altan-Yaycioglu R., Onal S. (2003). Excision and cryosurgery in the treatment of conjunctival malignant epithelial tumours. *Eye (Lond).* 2003 Mar;17(2):228-32.
26. Ooi E.H. and Ng E.Y.K. (2009). Ocular temperature distribution: a mathematical perspective. *Journal of Mechanics in Medicine and Biology*, 9(2), 199–227.
27. Vit V.V. (2003). *Stroieniie zritelnoi sistemy cheloveka [Structure of human visual system]*. Odessa: Astroprint [in Russian].
28. Mapstone R. (1968). Determinants of ocular temperature. *British Journal of Ophthalmology*, 52, 729-741.
29. Scott J.A. (1988). A finite element model of heat transport in the human eye. *Phys Med Biol*., 33(2), 227-241.
30. Pennes H.H. (1948). Analysis of tissue and arterial blood temperatures in the resting forearm *J. Appl. Physiol*., 1(2), 93 – 122.
31. Jiang S.C., Ma N., Li H.J., Zhang X.X. (2002). Effects of thermal properties and geometrical dimensions on skin burn injuries. *Burns*, 28, 713-717.
32. Cetingul M.P., Herman C. (2008). Identification of skin lesions from the transient thermal response using infrared imaging technique. *IEEE*, 1219-1222.
33. Ciesielski M., Mochnacki B., Szopa R. (2011). Numerical modeling of biological tissue heating. Admissible thermal dose. *Scientific Research of the Institute of Mathematics and Computer Science*,

1(10), 11-20.

34. Florin Filipoiu, Andrei Ioan Bogdan, Iulia Maria Carstea. (2010). Computer-aided analysis of the heat transfer in skin tissue. *Proc. of the 3rd WSEAS Int. Conference on Finite Differences - Finite Elements - Finite Volumes - Boundary Elements.* (Bucharest, Romania, 2010) (pp. 53-59).
35. Daniela Carstea, Ion Carstea, Iulia Maria Carstea. (2011). Interdisciplinarity in computer-aided analysis of thermal therapies. *WSEAS Transactions on Systems and Control*, 6(4), 115-124.
36. *COMSOL Multiphysics User's Guide*. COMSOLAB, 2010.
37. Yenari M.A., Han H.S. (2012). Neuroprotective mechanisms of hypothermia in brain ischaemia. *Nat. Rev. Neurosci.*, 13, 267-278.

Submitted 08.11.2017

L. I. Anatychuk

L. I. Anatychuk[1,2] *acad. National Academy of Sciences of Ukraine*,
A. V. Prybyla[1,2] *Candidate Phys.-math. Sciences*

[1]Institute of Thermoelectricity of the NAS and MES of Ukraine, 1, Nauky str, Chernivtsi, 58029, Ukraine;
[2]Yu.Fedkovych Chernivtsi National University, 2, Kotsiubynskyi str., Chernivtsi, 58000, Ukraine
e-mail: anatych@gmail.com

A. V. Prybyla

THE INFLUENCE OF QUALITY OF HEAT EXCHANGERS ON THE PROPERTIES OF THERMOELECTRIC LIQUID-LIQUID HEAT PUMPS

The paper presents the results of calculations of the influence of quality of heat exchange system on the properties of thermoelectric liquid-liquid heat pumps, in particular, for their use as a high-performance heater for a space-purpose water purifying device. Bibl. 7, Fig. 2.
Key words: thermoelectric heat pump, efficiency, distiller, heat exchanger.

Introduction

General characterization of the problem. Increasing the efficiency of thermoelectric heat pumps (THP) that have found their application in air conditioning systems of various applications [1 – 5] is an important and difficult task that can be solved using modern computer design methods [6, 7]. Its peculiarity is also that the achieved values of THP efficiency are close to the limit, which requires their research taking into account the most accurate and complete physical models.

A study [8] was carried out to establish the limiting possibilities of thermoelectric liquid-liquid heat pump. However, the data obtained are approximate, because in the calculations a simplified physical model of the THP was used that does not take into account the quality of the heat exchange system, which provides the transfer of heat flow to and from thermoelectric modules.

The purpose of our work is to determine the influence of quality of heat exchange system on the properties of thermoelectric liquid-liquid heat pump.

Physical model of THP

Physical model of thermoelectric liquid-liquid heat pump is shown in Fig. 1. It comprises a system of heat exchangers 1 assuring passage of heat flux Q_h through the hot side of thermoelectric modules, thermoelectric modules 3, heat exchangers 2 assuring passage of heat flux Q_c through the cold side of thermoelectric modules and a system of hydraulically bound channels 4 providing for circulation of liquid in the thermoelectric heat pump.

The model takes into account the losses in the temperature difference between the heat carrier and the surface of thermoelectric modules, leading in general to the reduction in the efficiency of thermoelectric heat pump.

To assure optimal operation of thermoelectric modules, each of them has individual power supply.

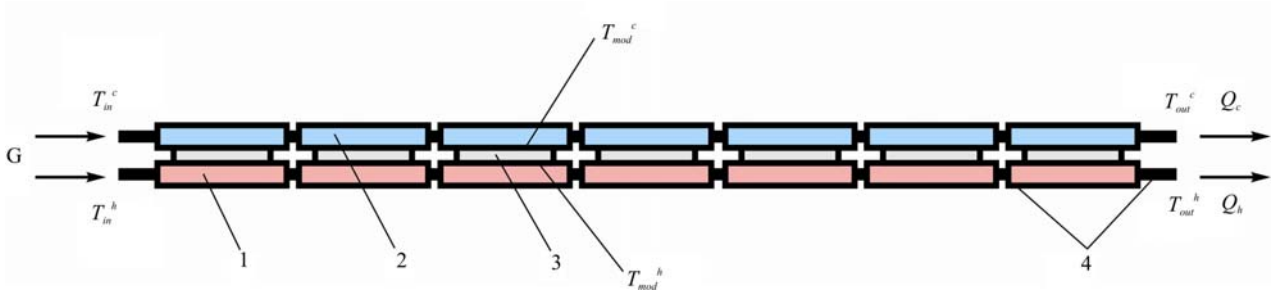

Fig. 1. Physical model of thermoelectric heat pump.

Mathematical and computer description of the model

To describe heat and electric current fluxes, we will use the laws of conservation of energy

$$div\vec{E} = 0 \tag{1}$$

and electric charge

$$div\vec{j} = 0, \tag{2}$$

where

$$\vec{E} = \vec{q} + U\vec{j}, \tag{3}$$

$$\vec{q} = \kappa\nabla T + \alpha T\vec{j}, \tag{4}$$

$$\vec{j} = -\sigma\nabla U - \sigma\alpha\nabla T. \tag{5}$$

Here, $\vec{E}$ is energy flux density, $\vec{q}$ is thermal flux density, $\vec{j}$ is electric current density, U is electric potential, T is temperature, α, σ, κ are the Seebeck coefficient, electric conductivity and thermal conductivity.

With regard to (3) – (5), one can obtain

$$\vec{E} = -(\kappa + \alpha^2\sigma T + \alpha U\sigma)\nabla T - (\alpha\sigma T + U\sigma)\nabla U. \tag{6}$$

Then the laws of conservation (1), (2) will acquire the form:

$$-\nabla\left[(\kappa + \alpha^2\sigma T + \alpha U\sigma)\nabla T\right] - \nabla\left[(\alpha\sigma T + U\sigma)\nabla U\right] = 0, \tag{7}$$

$$-\nabla(\sigma\alpha\nabla T) - \nabla(\sigma\nabla U) = 0. \tag{8}$$

$$\vec{E} = \vec{q} + U\vec{j}, \tag{3}$$

$$\vec{q} = \kappa\nabla T + \alpha T\vec{j}, \tag{4}$$

$$\vec{j} = -\sigma\nabla U - \sigma\alpha\nabla T. \tag{5}$$

Nonlinear differential equations of second order in partial derivatives (7) and (8) determine the distribution of temperature T and potential U in thermoelements.

An equation describing the process of heat transport in the walls of heat exchangers in the steady-state case is written as follows:

$$\nabla(-k_1 \cdot \nabla T_1) = Q_1, \tag{9}$$

where k_1 is thermal conductivity of heat exchanger walls, ∇T_1 is temperature gradient, Q_1 is heat flux.

Solving Eqs.(7) – (9), we obtain the distributions of temperatures, electric potential in the thermoelectric heat pump.

The above differential equations with the respective limiting conditions were solved using Comsol Multiphysics package of applied programs.

Computer simulation results

Below are given the results of calculations of the parameters of thermoelectric pump with respect to physical model shown in Fig.1. The optimal number of thermoelectric modules N was determined to assure the required cooling capacity Q_0, as well as the optimal supply current I_{opt} of each module to assure the highest integral coefficient of performance ε^{int} with regard to real losses of temperature difference in the heat exchange system ΔT^{loss} (from ΔT^{loss} = 0 to 2 K).

The initial data for calculations:

cooling capacity – 600 W;

heat carrier temperature at inlet to hot heat transfer loop – 36 ºC;

heat carrier temperature at inlet to cold heat transfer loop – 31 ºC;

heat carrier flow rate in each loop – 22 ml/s.

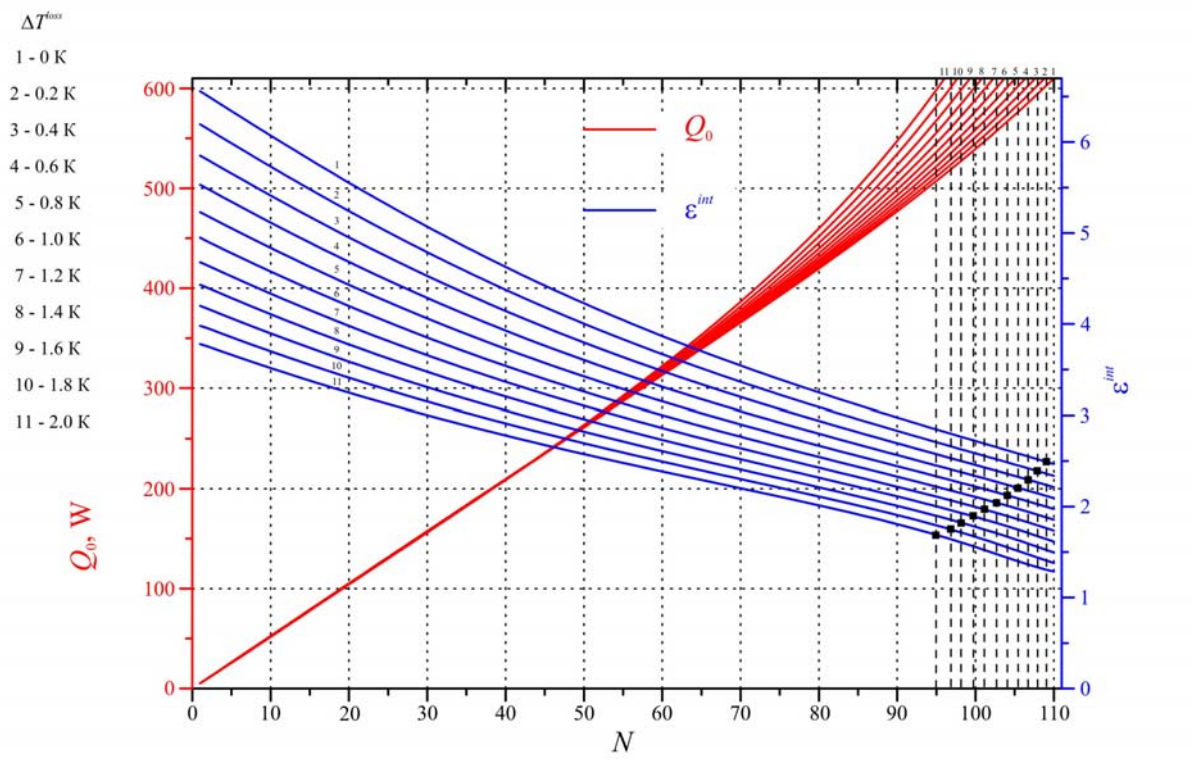

Fig. 2. Dependence of cumulative cooling capacity and integral coefficient of performance of thermoelectric heat pump on the number of thermoelectric modules for the cases of different losses of temperature difference in heat exchangers.

Thus, as a result of simulation it has been established with the deterioration in the quality of heat exchange system (increase of losses in temperature difference from ΔT^{loss} = 0 to 2 K), the coefficient of performance of thermoelectric heat pump decreases. Thus, while assuring the necessary cooling capacity of THP Q_0=600 W, the

coefficient of performance decreases from ε = 2.5 (ΔT^{loss} = 0 K) to ε = 1.7 (ΔT^{loss} = 2 K). In so doing, the total number of thermoelectric modules necessary to assure cooling capacity Q_0=600 Wт, decreases from 110 pcs (ΔT^{loss} = 0 K) to 95 pcs (ΔT^{loss} = 2 K). Such decrease in the number of modules is related to increase of their supply current with increasing temperature difference on them.

Comparison of the results obtained to the results of experimental research on thermoelectric heat pump [7] shows that the achieved value of coefficient of performance of THP ε = 1.85 corresponds to the level of the worst of considered variants of losses in the heat exchange system. This allows us to conclude that further research is required on optimizing the heat transfer system of THP in order to bring its efficiency closer to the maximum possible values.

Conclusion

1. It has been established that with the deterioration in the quality of heat exchange system, the coefficient of performance of thermoelectric heat pump decreases from ε = 2.5 (for ΔT^{loss} = 0 K) to ε = 1.7 (for ΔT^{loss} = 2 K) (with assuring the necessary cooling capacity of THP Q_0 = 600 W).
2. The total number of thermoelectric modules necessary to assure cooling capacity Q_0=600 W, is reduced from 110 pcs (ΔT^{loss} = 0 K) to 95 pcs (ΔT^{loss} = 2 K).
3. Comparison of the results obtained to the results of experimental research on THP shows that the achieved value of coefficient of performance of THP ε = 1.85 ε = 1.85 corresponds to the level of the worst of considered variants of losses in the heat exchange system.

References

1. Rozver Yu.Yu. (2003). Termoelektrychnyi kondytsioner dlia transportnykh zasobiv [Thermoelectric air-conditioner for vehicles]. *Termoelektryka – J.Thermoelectricity*, 2, 52 – 56 [in Ukrainian].
2. Anatychuk L. I., Vikhor L. N., Rozver Yu. Yu. (2004). Issledonaniie kharakteristik termoelektricheskogo okhladitelia potokov zhidkosti ili gaza [Investigation on performance of thermoelectric cooler of liquid or gas flows*]. Termoelektrichestvo - J. Thermoelectricity*, 1, 73-80 [in Russian].
3. Anatychuk L. I., Sudzuki N., Rozver Yu. Yu. (2005). Termoelektrychnyi kondytsioner dlia prymishchen [Indoor thermoelectric air-conditioner]. *Termoelektryka – J.Thermoelectricity,* 3, 53 – 56 [in Ukrainian].
4. Rifert V. G., Usenko V. I., Barabash P. A., et al. (2011). Razrabotka i ispytaniie sistemy regeneratsii vody iz zhidkikh othodov zhiznedeiatelnosti na bortu pilotiruemykh kosmicheskikh apparatov s ispolzovaniiem termoelektricheskogo teplovogo nasosa [Development and test of water regeneration system from liquid biowaste on board of manned spacecrafts with the use of thermoelectric heat pump]. *Termoelektrichestvo – J.Thermoelectricity*, 2, 63 – 74 [in Russian].
5. Anatychuk L. I., Barabash P. A., Rifert V. G., Rozver Yu. Yu., Usenko V. I., Cherkez R. G. (2013). Termoelektricheskii teplovoi nasos kak sredstvo povysheniia effektivnosti sistem ochistki vody pri kosmicheskikh polyotakh [Thermoelectric heat pump as a means of improving efficiency of water purification systems on space missions]. *Termoelektrichestvo – J.Thermoelectricity*, 6, 78 – 83 [in Russian].
6. Anatychuk L. I., Prybyla A. V. (2017). Pro hranychni mozhlyvosti termoelektrychnoho teplovoho nasosa ridyna-ridyna [Limiting possibilities of thermoelectric heat pump liquid-liquid]. *Termoelektryka – J.Thermoelectricity,* 4. 33 – 39 [in Ukrainian].
7. Anatychuk L. I., Rozver Yu. Yu., Prybyla A. V. (2017). Elsperymentalne doslidzhennia

termoelektrychnoho teplovoho nasosa ridyna-ridyna [Experimental study of thermoelectric liquid-liquid heat pump]. *Termoelektryka – J.Thermoelectricity,* 3, 33 – 39 [in Ukrainian].

Submitted 15.11.2017

Анатичук Л.І. *ак. НАН України*,[1,2]
Прибила А.В. *кандидат фіз.-мат. наук*[1,2]

Інститут термоелектрики НАН і МОН України, вул. Науки, 1,
Чернівці, 58029, Україна*, e-mail: anatych@gmail.com*
Чернівецький національний університетім. Юрія Федьковича,
вул. Коцюбинського 2, Чернівці, 58000, Україна,
e-mail: anatych@gmail.com

ПРО ВПЛИВ ЯКОСТІ ТЕПЛООБМІННИКІВ НА ВЛАСТИВОСТІ ТЕРМОЕЛЕКТРИЧНИХ ТЕПЛОВИХ НАСОСІВ РІДИНА-РІДИНА

У роботі наводяться результати розрахунків впливу якості системи теплообміну на властивості термоелектричного теплового насоса рідина-рідина., зокрема для їх використання у якості високоефективного нагрівника для приладу очистки води космічного призначення. Бібл. 7, Рис. 2.
Ключові слова: термоелектричний тепловий насос, ефективність, дистилятор, теплообмінник.

Анатычук Л.И.[1,2] *ак. НАН Украины*,
Прибыла А.В.[1,2] *канд.физ.-мат. наук*

Институт термоэлектричества, ул. Науки, 1, Черновцы, 58029, Украина
e-mail: anatych@gmail.com
Черновицкий национальный университет им. Юрия Федьковича,
ул. Коцюбинського 2, Черновцы, 58000, Украина
e-mail: anatych@gmail.com

В *работе приводятся результаты расчетов влияния качества системы теплообмена на свойстве термоэлектрического теплового насоса жидкость-жидкость., в частности для них использование в качестве высокоэффективного нагревателя для прибора очистки воды космического назначения. Библ. 7, Рис. 2.*
Ключевые слова: термоэлектрический тепловой насос, эффективность, дистиллятор, теплообменник.

References

1. Rozver Yu.Yu. (2003). Termoelektrychnyi kondytsioner dlia transportnykh zasobiv [Thermoelectric air-conditioner for vehicles]. *Termoelektryka – J.Thermoelectricity*, 2, 52 – 56 [in Ukrainian].
2. Anatychuk L. I., Vikhor L. N., Rozver Yu. Yu. (2004). Issledonaniie kharakteristik termoelektricheskogo okhladitelia potokov zhidkosti ili gaza [Investigation on performance of thermoelectric cooler of liquid or gas flows*]. Termoelektrichestvo - J. Thermoelectricity*, 1, 73-80 [in Russian].

3. Anatychuk L. I., Sudzuki N., Rozver Yu. Yu. (2005). Termoelektrychnyi kondytsioner dlia prymishchen [Indoor thermoelectric air-conditioner]. *Termoelektryka – J.Thermoelectricity,* 3, 53 – 56 [in Ukrainian].
4. Rifert V. G., Usenko V. I., Barabash P. A., et al. (2011). Razrabotka i ispytaniie sistemy regeneratsii vody iz zhidkikh othodov zhiznedeiatelnosti na bortu pilotiruemykh kosmicheskikh apparatov s ispolzovaniiem termoelektricheskogo teplovogo nasosa [Development and test of water regeneration system from liquid biowaste on board of manned spacecrafts with the use of thermoelectric heat pump]. *Termoelektrichestvo – J.Thermoelectricity*, 2, 63 – 74 [in Russian].
5. Anatychuk L. I., Barabash P. A., Rifert V. G., Rozver Yu. Yu., Usenko V. I., Cherkez R. G. (2013). Termoelektricheskii teplovoi nasos kak sredstvo povysheniia effektivnosti sistem ochistki vody pri kosmicheskikh polyotakh [Thermoelectric heat pump as a means of improving efficiency of water purification systems on space missions]. *Termoelektrichestvo – J.Thermoelectricity*, 6, 78 – 83 [in Russian].
6. Anatychuk L. I., Prybyla A. V. (2017). Pro hranychni mozhlyvosti termoelektrychnoho teplovoho nasosa ridyna-ridyna [Limiting possibilities of thermoelectric heat pump liquid-liquid]. *Termoelektryka – J.Thermoelectricity,* 4. 33 – 39 [in Ukrainian].
7. Anatychuk L. I., Rozver Yu. Yu., Prybyla A. V. (2017). Elsperymentalne doslidzhennia termoelektrychnoho teplovoho nasosa ridyna-ridyna [Experimental study of thermoelectric liquid-liquid heat pump]. *Termoelektryka – J.Thermoelectricity,* 3, 33 – 39 [in Ukrainian].

Submitted 15.11.2017

V.Ya. Mykhailovsky, *Doctor Phys.-math. Sciences*
V.V.Razinkov, M.V.Maksimuk, M.V.Havryliuk

Institute of Thermoelectricity of the NAS and MES of Ukraine,
1, Nauky str, Chernivtsi, 58029, Ukraine; *e-mail: anatych@gmail.com*

EXPERIMENTAL RESEARCH ON A THERMOELECTRIC GENERATOR CASCADE MODULE FOR SOLID FUEL TEG

This paper presents the results of experimental research on a thermoelectric generator cascade module of Bi_2Te_3-PbTe-TAGS-based materials to be used in solid fuel thermoelectric generators. The technological aspects of manufacturing the low-temperature and high-temperature stages are described, the general module design is represented, and the results of measuring energy characteristics of a cascade module at the cold side temperature of 30°C and the hot side temperatures of 200-500°C are given.. Bibl. 2, Fig. 9.
Key words: cascade module, thermoelectric generator, thermoelement, efficiency.

Introduction

Thermoelectric generator modules of cascade type are mainly used in industrial production for the recovery of waste heat of various energy equipment of high thermal power (500 – 800 °C): internal combustion engines, gas turbines, cement and steel furnaces, etc. [1 – 4]. At the same time, thermoelectric generators (TEGs) destined for household purposes traditionally employ single-stage bismuth telluride-based modules with the maximum hot side operating temperature of 300 °C [5 – 8]. Therefore, despite many advantages that such TEGs possess, as compared to other autonomous power sources, there are significant disadvantages that limit their capabilities, namely low efficiency, excess of operating temperature of modules, which leads to a decrease in TEG service life, the need in overheating protection systems which substantially complicate generator design [9].

The use of cascade modules optimized for the hot temperatures of 500 °C as thermoelectric converters for household TEGs allows solving the above problems, which, in our opinion, is a rather obvious fact. However, there are no real applications of cascade designs in this direction as yet.

The idea of creating a generator cascade module of Bi_2Te_3-*PbTe*-TAGS-based materials with electric power output 20 W for thermoelectric generators using the heat of heated surfaces of solid fuel furnaces was proposed in [10]. Using computer design methods, the authors developed the design and found the optimal conditions whereby the maximum electrical power of the module and thermoelectric conversion efficiency are achieved.

The purpose of this work is fabrication of a thermoelectric generator two-stage module of Bi_2Te_3-*PbTe*-TAGS-based materials and experimental research on its characteristics.

Special aspects of hot stage manufacturing

For creation of the high-temperature (hot) stage, the n-type legs of *PbTe* and p-type legs of TAGS (Fig. 1) were used which were obtained by joint hot pressing method [11].

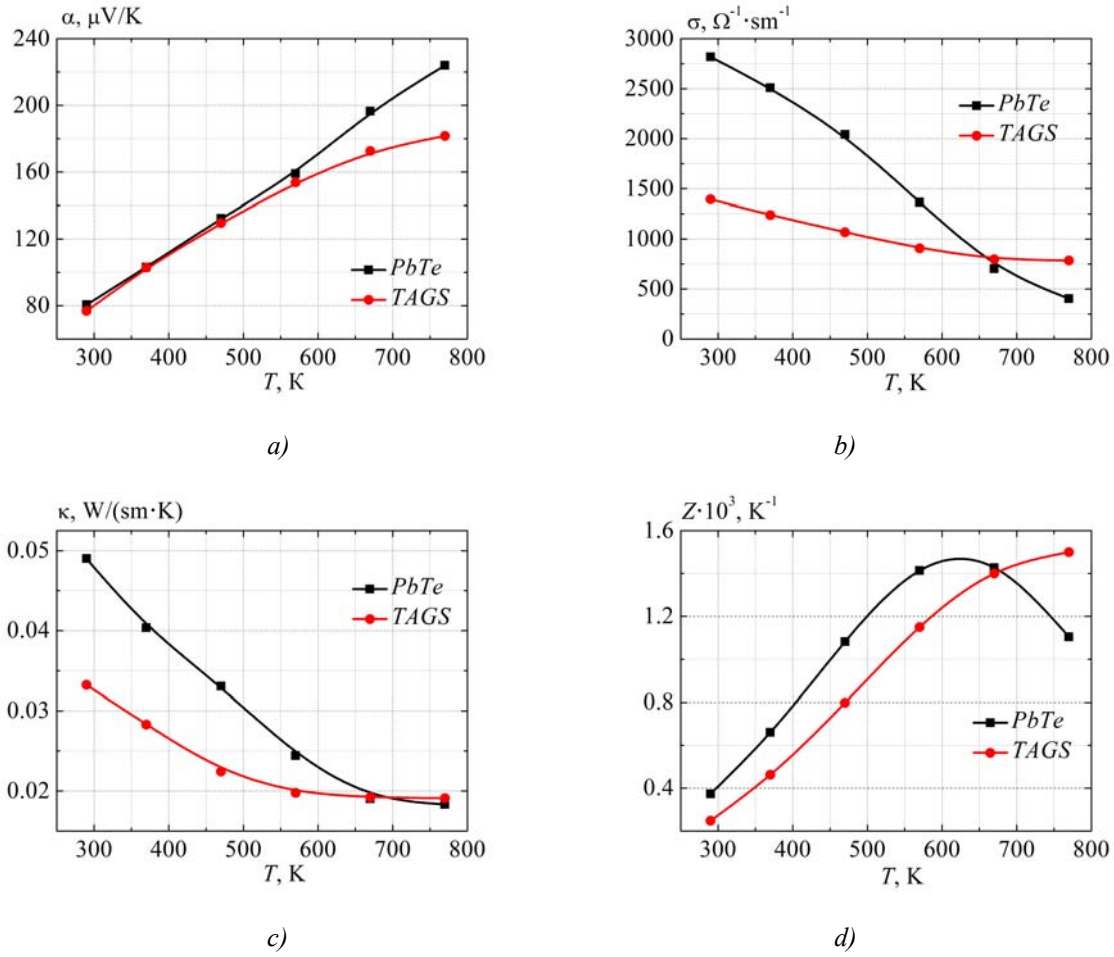

Fig.1. Temperature dependences of parameters of n-PbTe and p-TAGS-based thermoelectric materials: a) the Seebeck coefficient; b) the electrical conductivity; c) the thermal conductivity; d) the figure of merit.

Connection of thermoelement legs of *PbTe* and TAGS-based materials was made by silver connecting plates using diffusion welding method. Schematic of a device for connection of the hot stage thermoelements is shown in Fig. 2.

The device consists of a demountable lattice toolset 1, in which thermoelement legs 2 and silver connecting plates 3 are inserted. The toolset with the legs and connecting plates is placed into heater 4 and pressed by pressure mechanism 5. To reduce the temperature of pressure elements, the intermediate plate 6 was cooled by running water. In order to prevent the base 7 from warming, the heater 4 is located on a perforated heat-insulating support 8.

The design feature of the connecting device is the use of hydroplastic pressing method, which allows creating pressure on each leg of thermoelectric material separately. This is important, especially in the cases when it is necessary to connect legs with different plastic deformation ability. Moreover, hydroplastic pressing method allows device modification for the cases of connection of different number of legs.

Connection of thermoelement legs of *n*- and *p*-types with silver plates was done in vacuum at a temperature of 500 °C. The lines of 16 in-series connected legs of the same height, obtained by diffusion welding method, were mounted into the hot stage module.

Due to possible sublimation of thermoelectric material components at operating temperatures 450 – 500°C, a layer of thermally stable anti-sublimation coating based on silicone resins and composites of low- melting enamels was applied on the lateral surfaces of legs.

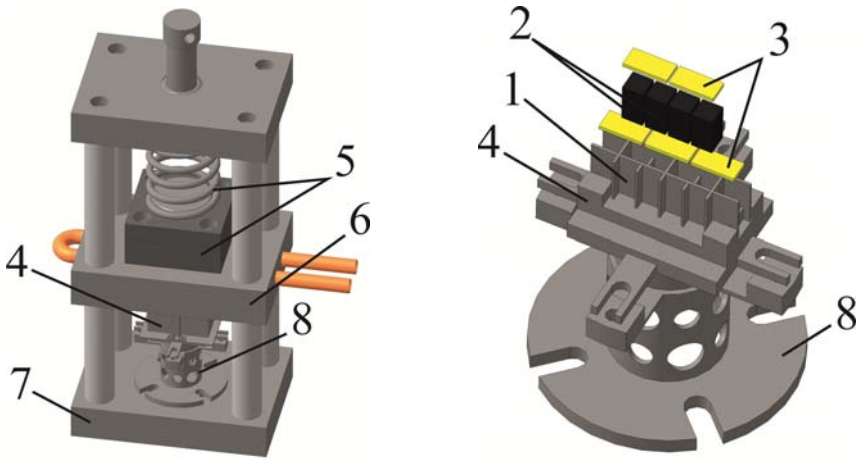

Fig.2. Schematic of a device for connection of the hot stage thermoelements:
1 – lattice toolset, 2 – thermoelement legs; 3 –connecting plates; 4 – heater;
5 – pressure mechanism; 6 –intermediate plate; 7 – base, 8 – heat insulator.

Anti-sublimation coatings were applied on the lateral surfaces of legs by spraying method. The coating was dried in two steps: in the air at a temperature of 20-30°C and in thermostat at a temperature of 170 – 180°C.

For connection of the hot stage, the lines with the applied anti-sublimation layers were placed into a special toolset, schematically shown in Fig. 4. The lines were placed in parallel according to a schematic shown in Fig. 5.

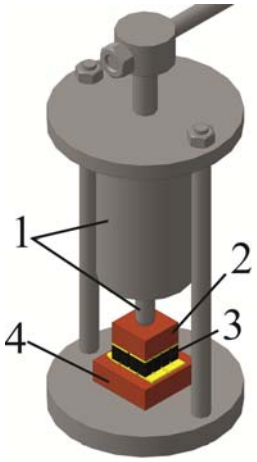

Fig.3. Toolset for the hot stage connection: 1 – pressure mechanism; 2 – upper pressure plate;
3 – thermoelectric module; 4 – lower heat insulating pressure plate.

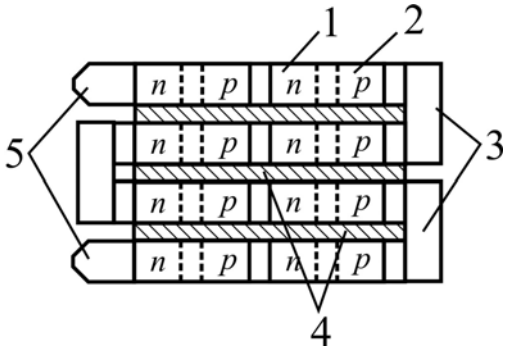

Fig. 4. Schematic of lines arrangement in the hot stage: 1 – n-type conductivity legs;
2 – p-type conductivity legs; 3 – connecting plates; 4 – electrical insulation; 5 – electrical contacts.

Connection of lines into the hot stage module was done by means of connecting plates 3 using soldering method with high-temperature solder and aqueous solution of $ZnCl_2$.

Special aspects of cold stage manufacturing

For creation of thermoelement legs of the low-temperature (cold) stage, the n- and p-type Bi_2Te_3–based materials were used, the temperature dependences of whose thermoelectric parameters are given in Fig. 5. The thermoelement legs were obtained from a single-crystal sample grown by the zone melting method.

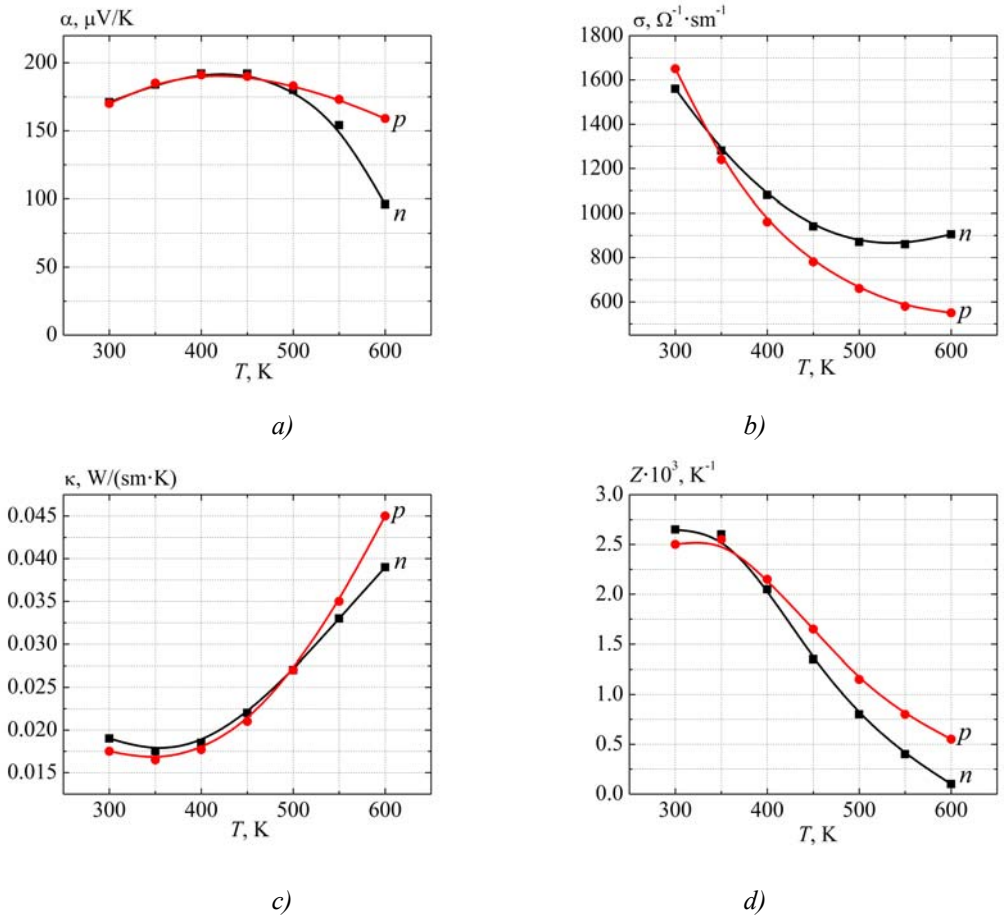

*Fig.5. Temperature dependences of parameters of thermoelectric n- and p- type Bi_2Te_3-*based legs*:*
a) the Seebeck coefficient; b) the electrical conductivity; c) the thermal conductivity; d) the figure of merit.

Connection of the cold and hot sides was done by copper plates in a special toolset, schematically shown in Fig. 6.

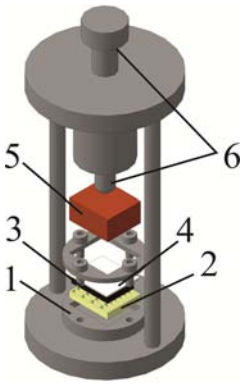

Fig.6. Toolset for the cold stage connection:
1 – base; 2 – silicone matrix;
3 – thermoelement legs; 4 – ceramic plate;
5 – heater; 6 – pressure mechanism.

For this purpose, base 1 with matrix 2 and module legs 3 were arranged in the toolset and ceramic plate 4 with applied connecting plates were placed on the end of the legs. On soldering of connecting plates, the hot side of the module was levelled by grinding method.

Measurement results

Fig.7a shows a schematic design of the resulting two-stage generator module of Bi_2Te_3-PbTe-TAGS-based materials.

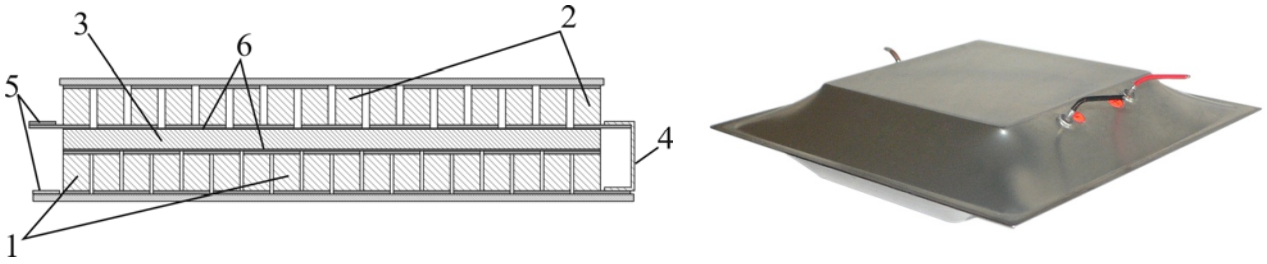

a) *b)*

Fig.7 –Thermoelectric two-stage generator module of Bi_2Te_3-PbTe-TAGS-based materials for solid fuel TEG: a). schematic representation; b). external view in a sealed package: 1 – low-temperature stage; 2 – high-temperature stage; 3 – heat conducting plate; 4 – connecting bus; 5 – electrical contacts; 6 – electrically insulating mica gaskets.

A two-stage module consists of low-temperature stage 1, high-temperature stage 2 and interstage heat conducting plate 3. The stages are connected in series into an electrical circuit by means of a connecting bus 4. To connect the electrical energy user or the modules into thermopiles, the electrical contacts 5 are outside the module. Electrical insulation of the hot and cold stages from plate 3 is done by mica gaskets 6.

The low-temperature and high-temperature stages comprise 72 and 64 thermoelements, respectively. The cross-section of legs is 4x4 mm, the height of which with regard to the applied layers is 6 mm.

In order to prevent degradation of contacts due to oxidation processes at operating temperatures, the cascade module is sealed in a thin-walled metal package, the internal volume of which is filled with inert gas (Fig. 7b).

Research on parameters of a cascade module was done at the cold side temperature T_c = 30°C and the hot side temperature T_h from 200 to 500°C. The results of measurements are given in Figs.8, 9

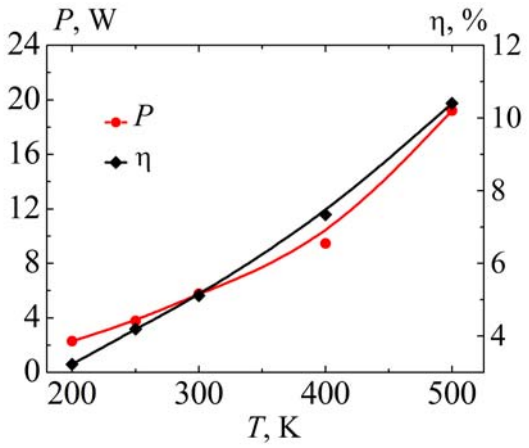

Fig.8. Dependence of electrical power P and efficiency η of two-stage generator module of Bi_2Te_3-PbTe-TAGS-based materials on temperature T_h

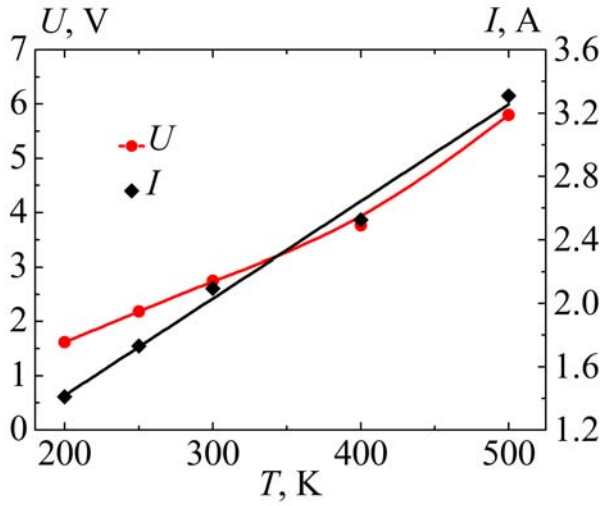

Fig.9. Dependence of electrical voltage U and current strength I of generator module of Bi_2Te_3-PbTe-TAGS-based materials on temperature T_h

Experimental temperature dependences of the energy characteristics of the module of Bi_2Te_3-*PbTe*-TAGS-based materials were obtained on automated equipment "Altec-10002" developed at the Institute of Thermoelectricity [12].

From the above data it is seen that maximum output electrical power and voltage of the module are achieved at the hot side temperature 500 °C and make P = 19.2 W and U = 5.8 V, respectively. In so doing, the thermoelectric conversion efficiency η is 10.4 %.

With a further rise in T_h for the level of temperatures 550 °C, there was increase in the electrical power and efficiency up to 24 W and 12.5 %. However, such temperatures are objectionable for the operation of the module, especially for TAGS-based *p*-leg, due to acceleration of degradation processes.

Conclusion

1. A technological scheme for manufacturing thermoelements of the high-temperature stage of *n-PbTe* and *p*-TAGS-based materials was developed, which includes diffusion welding of pre-pressed legs with connecting plates into thermoelement "lines", application of anti-sublimation layers on the lateral surfaces of legs and connection of the "lines" into the high-temperature stage module.
2. A technology of creating the low-temperature stage of *n*- and *p*-type Bi_2Te_3–based materials is shown, which includes joint connection of thermoelement legs into the low-temperature stage module.
3. It is determined that maximum output electrical power and voltage of the resulting two-stage generator module of Bi_2Te_3-*PbTe*-TAGS-based materials are achieved at the hot side temperature 500 °C and make 19.2 W and 5.8 V, respectively. In so doing, the thermoelectric conversion efficiency is 10.4 %.

References

1. Strutynska L.T., Bilinsky-Slotylo V.R., Mykhailovsky V.Ya. (2012). Proektuvannia sektsiinykh moduliv na osnovi *PbTe*/TAGS dlia termoelektrychnykh heneratoriv [Design of segmented modules based on *PbTe*/TAGS for thermoelectric generators]. *Fizyka i khimiia tverdoho tila – Physics and Chemistry of the Solid State*, 13 (4), 1032 – 1036 [In Ukrainian].

2. Vikhor L.M., Mykhailovsky V.Ya., Mocherniuk R.M. (2014). Optymizatsiia materialiv ta otsinka kharakterystyk heneratornykh moduliv dlia rekuperatoriv tepla [Optimization of materials and performance evaluation of generator modules for heat recuperators]. *Fizyka i kmimiia tverdoho tila – Physics and Chemistry of the Solid State*, 15(1), 206 – 213 [in Ukrainian].
3. Mykhailovsky V.Ya., Bilinskyi-Slotylo V.R. (2013). Dvukhkaskadnyie moduli na osnove Bi_2Te_3 i SiGe dlia termoelektricheskikh generatorov [Two-stage modules based on Bi_2Te_3 i *SiGe* for thermoelectric generators]. *Tekhnologiya i Konstruirovaniie v Elektronnoi Apparature*, 2 – 3, 39 – 42 [in Russian].
4. Mykhailovsky V.Ya., Bilinskyi-Slotylo V.R. (2012). Termoelektrychni kaskadni moduli iz materialiv na osnovi Bi_2Te_3-*PbTe*-TAGS [Thermoelectric cascade modules of Bi_2Te_3-*PbTe*-TAGS based materials]. *Termoelektryka- J.Thermoelectricity*, 4, 67 – 74 [in Ukrainian].
5. Champier D., Favarel C., Bedecarrats J.P., Kousksou T., Rozis J.F. (2013). Prototype combined heater/thermoelectric power generator for remote applications. *Journal of Electronic Materials*, 42, 1888 – 1899.
6. Montecucco A., Siviter J., Knox A.R. (2017). Combined heat and power system for stoves with thermoelectric generators. *Applied Energy*, 185(2), 1336 – 1342.
7. Goudarzi A.M., Mazandarani P., Panahi R., Behsaz H., Rezania A., Rosendahl R.A. (2013). Integration of thermoelectric generators and wood stove to produce heat, hot water, and electric power. *Journal of Electronic Materials*, 42, 2127 – 2133.
8. Anatychuk L.I., Mocherniuk R.M., Havryliuk M.V., Andrusiak I.S. (2017). Termoelektrychnyi henerator shcho vykorystovuie teplo nahritykh poverkhon [Thermoelectric generator using the heat of heated surfaces]. *Termoelektryka – J.Thermoelectricity*, 2, 84 – 95 [in Ukrainian].
9. Juanico L.E., Rinalde F., Taglialavore E., Molina M. (2013). Novel heat controller for thermogenerators working on uncontrolled stoves. *Journal of Electronic Materials*, 7, 1776 – 1780.
10. Vikhor L.M., Maksimuk M.V. (2017). Proektuvannia termoelektrychnykh kaskadnykh moduliv dlia TEG na tverdomu palyvi [Design of thermoelectric cascade modules for solid fuel TEG]. *Termoelektryka – J.Thermoelectricity*, 4, [in Ukrainian].
11. Mykhailovsky V.Ya., Lysko V.V., Antoniuk V.V., Maksimuk M.V. (2017). Doslidzhennia termoelementiv z materialiv na osnovi *n-PbTe* and *p*-TAGS termoelektrychnoho heneratornoho kaskadnoho modulia [Research on thermoelements based on *n-PbTe* and *p*-TAGS materials for thermoelectric genertaor cascxade module]. *Termoelektryka- J.Thermoelectricity,* 3, [in Ukrainian].
12. Anatychuk L.I. and Havrylyuk M.V. (2011). Procedure and equipment for measuring parameters of thermoelectric generator modules. *Journal of Electronic Materials*, 5, 1292 – 1297.

Submitted 19.11.2017

Михайловський В.Я., *доктор фіз-мат. наук,*
Разіньков В.В., Максимук М.В., Гаврилюк М.В.

Інститут термоелектрики НАН і МОН України, вул. Науки, 1,
Чернівці, 58029, Україна*, e-mail: anatych@gmail.com*

ЕКСПЕРИМЕНТАЛЬНІ ДОСЛІДЖЕННЯ ТЕРМОЕЛЕКТРИЧНОГО ГЕНЕРАТОРНОГО КАСКАДНОГО МОДУЛЯ ДЛЯ ТЕГ НА ТВЕРДОМУ ПАЛИВІ

Наведено результати експериментальних досліджень термоелектричного генераторного каскадного модуля із матеріалів на основі Bi_2Te_3-PbTe-TAGS для використання в термоелектричних генераторах на твердому паливі. Описано технологічні аспекти виготовлення низькотемпературного і високотемпературного каскадів, представлено загальну конструкцію модуля, наведено результати вимірювання енергетичних характеристик каскадного модуля за температур холодної сторони 30°С і гарячої 200-500°С. Бібл. 12, Рис. 9.
Ключові слова: каскадний модуль, термоелектричний генератор, термоелемент, ефективність.

Михайловский В.Я., *доктор физ-мат. наук,*
Разиньков В.В., Максимук Н.В., Гаврилюк Н.В.

Институт термоэлектричества, ул. Науки, 1, Черновцы, 58029, Украина
e-mail: anatych@gmail.com

ЭКСПЕРИМЕНТАЛЬНЫЕ ИССЛЕДОВАНИЯ ТЕРМОЭЛЕКТРИЧЕСКОГОГЕНЕРАТОРНОГО КАСКАДНОГО МОДУЛЯ ДЛЯ ТЭГ НА ТВЕРДОМ ТОПЛИВЕ

Приведены результаты экспериментальных исследований термоэлектрического генераторного каскадного модуля из материалов на основе Bi_2Te_3-PbTe-TAGS для использования в термоэлектрических генераторах на твердом топливе. Описаны технологические аспекты изготовления низкотемпературного и высокотемпературного каскадов, представлена общая конструкция модуля, приведены результаты измерения энергетических характеристик каскадного модуля при температурах холодной стороны 30°С і горячей 200-500°С. Библ. 12, Рис. 9.
Ключевые слова: каскадный модуль, термоэлектрический генератор, термоэлемент, эффективность.

References

1. Strutynska L.T., Bilinsky-Slotylo V.R., Mykhailovsky V.Ya. (2012). Proektuvannia sektsiinykh moduliv na osnovi *PbTe*/TAGS dlia termoelektrychnykh heneratoriv [Design of segmented modules based on *PbTe*/TAGS for thermoelectric generators]. *Fizyka i khimiia tverdoho tila – Physics and Chemistry of the Solid State*, 13 (4), 1032 – 1036 [In Ukrainian].
2. Vikhor L.M., Mykhailovsky V.Ya., Mocherniuk R.M. (2014). Optymizatsiia materialiv ta otsinka kharakterystyk heneratornykh moduliv dlia rekuperatoriv tepla [Optimization of materials and performance evaluation of generator modules for heat recuperators]. *Fizyka i kmimiia tverdoho tila – Physics and Chemistry of the Solid State*, 15(1), 206 – 213 [in Ukrainian].
3. Mykhailovsky V.Ya., Bilinskyi-Slotylo V.R. (2013). Dvukhkaskadnyie moduli na osnove Bi_2Te_3 i SiGe dlia termoelektricheskikh generatorov [Two-stage modules based on Bi_2Te_3 i *SiGe* for thermoelectric generators]. *Tekhnologiya i Konstruirovaniie v Elektronnoi Apparature*, 2 – 3, 39 – 42 [in Russian].
4. Mykhailovsky V.Ya., Bilinskyi-Slotylo V.R. (2012). Termoelektrychni kaskadni moduli iz materialiv na osnovi Bi_2Te_3-*PbTe*-TAGS [Thermoelectric cascade modules of Bi_2Te_3-*PbTe*-TAGS based materials]. *Termoelektryka- J.Thermoelectricity*, 4, 67 – 74 [in Ukrainian].

5. Champier D., Favarel C., Bedecarrats J.P., Kousksou T., Rozis J.F. (2013). Prototype combined heater/thermoelectric power generator for remote applications. *Journal of Electronic Materials*, 42, 1888 – 1899.
6. Montecucco A., Siviter J., Knox A.R. (2017). Combined heat and power system for stoves with thermoelectric generators. *Applied Energy*, 185(2), 1336 – 1342.
7. Goudarzi A.M., Mazandarani P., Panahi R., Behsaz H., Rezania A., Rosendahl R.A. (2013). Integration of thermoelectric generators and wood stove to produce heat, hot water, and electric power. *Journal of Electronic Materials*, 42, 2127 – 2133.
8. Anatychuk L.I., Mocherniuk R.M., Havryliuk M.V., Andrusiak I.S. (2017). Termoelektrychnyi henerator shcho vykorystovuie teplo nahritykh poverkhon [Thermoelectric generator using the heat of heated surfaces]. *Termoelektryka – J.Thermoelectricity*, 2, 84 – 95 [in Ukrainian].
9. Juanico L.E., Rinalde F., Taglialavore E., Molina M. (2013). Novel heat controller for thermogenerators working on uncontrolled stoves. *Journal of Electronic Materials*, 7, 1776 – 1780.
10. Vikhor L.M., Maksimuk M.V. (2017). Proektuvannia termoelektrychnykh kaskadnykh moduliv dlia TEG na tverdomu palyvi [Design of thermoelectric cascade modules for solid fuel TEG]. *Termoelektryka – J.Thermoelectricity*, 4, [in Ukrainian].
11. Mykhailovsky V.Ya., Lysko V.V., Antoniuk V.V., Maksimuk M.V. (2017). Doslidzhennia termoelementiv z materialiv na osnovi *n-PbTe* and *p*-TAGS termoelektrychnoho heneratornoho kaskadnoho modulia [Research on thermoelements based on *n-PbTe* and *p*-TAGS materials for thermoelectric genertaor cascxade module]. *Termoelektryka- J.Thermoelectricity,* 3, [in Ukrainian].
12. Anatychuk L.I. and Havrylyuk M.V. (2011). Procedure and equipment for measuring parameters of thermoelectric generator modules. *Journal of Electronic Materials*, 5, 1292 – 1297.

Submitted 19.11.2017


P.D. Mykytiuk

P.D.Mykytiuk, *Candidate Phys.-math. Sciences*

Institute of Thermoelectricity of the NAS and MES of Ukraine, 1, Nauky str, Chernivtsi, 58029, Ukraine; *e-mail: anatych@gmail.com*
Yurii Fedkovych Chenivtsi National University, 2, Kotsiubynskyi str., Chernivtsi, 58012, Ukraine); *e-mail: anatych@gmail.com*

FACTORS OF INFLUENCE ON THE ACCURACY OF THERMAL CONVERTERS

Analysis of thermal operating mode of semiconductor thermal converter (TC) has been made. The temperature distribution in the TC heater with regard to the environmental effect has been calculated. A method for determination of the coefficient of heat exchange of the TC heater with the environment has been proposed.
The results obtained can be used in the design of TC with improved parameters and characteristics. Bibl. 8, Fig. 2, Table 1.
Key words: thermal converter, heater, thermocouple, environment.

Introduction

Widespread introduction of energy saving technologies in all sectors of the national economy requires more qualitative control of energy quantities of alternating current of different frequency and signal shape.

Despite the rapid development of measuring instruments based on other principles, devices based on thermal converters occupy a prominent place, and leading metrology centers of different countries [1 – 3] carry out works aimed at developing and refining thermal converters for state standards and reference devices for measuring current strength, voltage, power and power factor.

The absence in Ukraine of a primary state standard of electrical voltage necessitates the use of standards from other countries (Russia) for the metrological assurance of a unit of electrical voltage, in particular, for the frequency range in which the major part of military equipment of the Armed Forces of Ukraine operates. The lack of a primary standard negatively affects the quality of such equipment.

An important component of the standard is thermoelectric alternating current converter [4] the quality of which determines the quality of the standard as a whole. Moreover, for creation of state standards, thermal converters (TC) of high accuracy are required.

The research and development of alternating current TC for measuring equipment is a traditional direction of research pursued by Institute of Thermoelectricity. At the Institute, the theory of thermoelectric converters and thermoelectric materials for measuring instruments has been created; the physical, mathematical and computer models of TC have been developed and investigated using multi-factor computer simulation [5]. The influence of physical effects, phenomena and processes on the parameters and characteristics of direct current and alternating current TC has been studied. In particular, the influence on the accuracy of TC of the Thomson effect [6] has been investigated, which leads to a disturbance of symmetry in the distribution of the heater temperatures and to the displacement of the maximum heating area depending on the direction of current through the heater. The influence of the Peltier effect at the heater junctions with current-carrying blocks has been studied which leads to a redistribution of

temperature in the heater. The temperature dependences of the properties of thermocouple and heater materials have been studied.

However, the accuracy of TC is essentially affected by many other factors caused by the features of structural members of TC, heat exchange between them, heat exchange with the environment, whose research is the purpose of this work.

Thermal operating mode of TC

The sensitivity of TC $S_W = \alpha/\kappa^*$, where α is the Seebeck coefficient of the thermocouple, and $\kappa^* = W/\Delta T$, where W is the power on the heater at the operating temperature difference ΔT, can be increased either due to increasing the thermoelectric figure of merit of thermocouple material Z, or due to improving the efficiency of heat use in TC. Since the real increase in Z should not be expected in the near future, we will analyze the thermal operating mode of TC.To do this, first of all, we need to know the distribution of temperature along the heater and its value in the centre thereof, taking into account the various mechanisms of heat losses that occur in TC. Calculation was made for the model shown in Fig. 1.

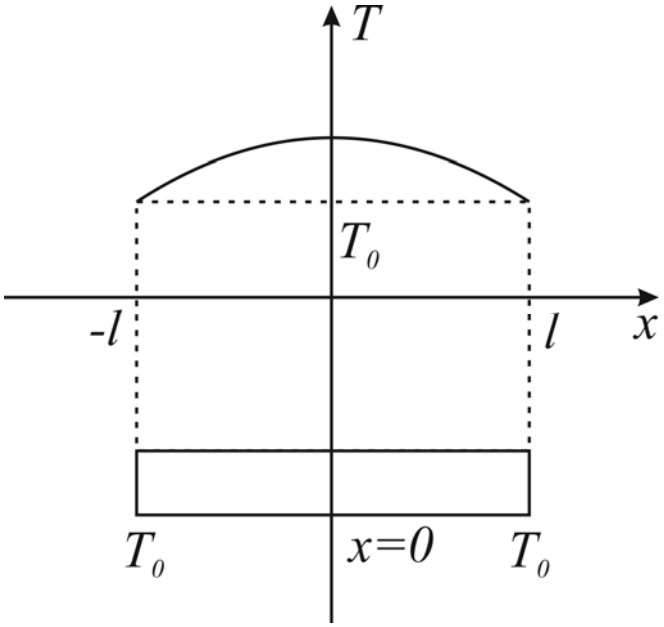

Fig.1. Model for calculation of temperature distribution in the TC heater.

Under steady-state conditions the value and distribution of temperatures in the heater is found from the heat balance equation [1, 2].

$$\kappa_{\text{н}} S_{\text{н}} \frac{d^2T}{dx^2} - C_0 P_{\text{н}} (T - T_0) - \varepsilon\sigma_{\text{б}} P_{\text{н}} (T^4 - T_0) + \frac{\rho_0 I_{\text{н}}^2}{S_{\text{н}}} [1 + \beta(T - T_0)], \qquad (1)$$

where: κ_h is coefficient of thermal conductivity of the heater material;

S_h is cross-section of the heater;

T is absolute temperature determined by running coordinate x;

C_0 is coefficient of heat exchange with the environment;

P_h is perimeter of cross-section S_{h};

ε is emissivity;

$\sigma_б$ is the Boltzmann constant;

$\rho(\rho_0)$ is the heater material resistivity at a temperature of $T_0(T)$;

I_h is current flowing through the heater;

ρ is temperature coefficient of resistance (TCR) of the heater material.

In Eq. (1) the first term describes thermal flux due to material thermal conductivity; the second term takes into account the presence of heat exchange of the heater surface with the environment; the third term – heat losses due to radiation; the fourth term – the Joule heat released when the current passes through the heater.

The boundary conditions for Eq. (1) were written with regard to the fact that current leads of the heater are thermostated at the ambient temperature of T_0, *K*.

Solution of Eq. (1) with regard to the boundary conditions yields the expression for temperature difference in the heater of length 2*l*.

$$T_x - T_0 = \frac{\rho_0 I_h^2}{P_h S_h (C_0 + \varepsilon\sigma_б 4T_0^3 - \frac{\rho_0 \beta I_h^2}{P_h S_h})} \cdot (1 - \frac{chNal_x}{chNal}), \tag{2}$$

where T_x is temperature of the heater at point l_x located at a distance x from the middle of the heater, and

$$N = \sqrt{\frac{C_0 P_h + \varepsilon\sigma_б 4T_0^3 P_h - \frac{\rho_0 \beta I_h^2}{S_h})}{xS}} \tag{3}$$

We will analyze the contribution of various mechanisms of heat transfer which influence the temperature in the centre of the heater whose value determines the sensitivity of TC.

Calculations were performed for manganin heater in glass insulation. The resistance of the heater was 16 Ω. The thermophysical properties of glass were taken into account by the introduction of "effective" values of thermal conductivity and other characteristics of the heater.

In the simplest case, heat losses in the heater are due to its thermal conductivity. Then, formula [4] will be valid

$$\Delta T_{max} = \frac{U_н^2}{8 x_н \rho_н} \tag{4}$$

where U_h is electrical voltage on the heater.

Substituting the parameters for the heater, for current I_h = 5 mA, we find that the maximum temperature difference in the heater ΔT_{max} = 44.

In real constructions of TC, other mechanisms of heat losses also have essential influence. Taking into account heat losses due to material thermal conductivity and convective heat exchange yields the following expression:

$$\Delta T_{max} = \frac{\rho_0 I_h^2}{S_h P_h C_0} \cdot (1 - \frac{1}{\mathrm{ch} Na' l}) \tag{5}$$

where $Na' = \sqrt{\frac{C_0 P_h}{\kappa_h S_h}}$.

Formula (5) includes coefficient of heat exchange C_0, the exact value of which should be determined

for each specific case.

Determination of coefficient of heat exchange with the environment

The expression is known [7, 8] for coefficient of heat exchange with the environment C_0 of infinite thin wire of diameter *d,* arranged in the unlimited space filled with gas of thermal conductivity κ_Γ.

$$C_0 = \frac{\kappa_\Gamma}{2d} \tag{6}$$

However, expression (6) for coefficient of heat exchange was obtained under a number of assumptions which are difficult to be executed in real systems. Moreover, coefficient of heat exchange is greatly affected by the specific conditions (the shape and geometric dimensions of the heater and TC package, their mutual arrangement, orientation with respect to gravitational field, pressure and ambient temperature, etc.), that are difficult to be taken into account in theoretical calculations. Calculations show that in the air in the alternate designs of TC the radiation losses are much lower than the losses due to convective heat exchange which accounts for the major share of heat losses. So, a method for determining the coefficient of heat exchange with the environment C_0 was developed. The essence of the method is as follows: the dependence of the heater temperature on the value of heat exchange coefficient C_0 is theoretically calculated, and the heater temperature is experimentally determined (by the temperature dependence of resistance). Comparison of the experimental data with the theoretical calculations yields the numerical value of coefficient C_0.

The validation of the proposed method for determining C_0 was as follows.

On passing of current through the conductor, the resistance of linear homogeneous heater 2*l* with thermostated ends can be determined from the expression

$$R = \frac{1}{S_h}\int_0^{2l} \rho_0[1+\beta(T(x)-T_0)]dx\,, \tag{7}$$

and temperature distribution along the heater length is given by expression (2). If we substitute (2) into (7) and make certain transformations, we will get

$$\Delta R_{\text{H}} = \frac{I_{\text{H}}^2 R_0 l\beta}{\kappa_{\text{H}} S_{\text{H}} y^2}\left[1-\frac{\text{th}(y)}{y}\right], \tag{8}$$

where $y = Na\cdot l$, $R_0 = \rho_0 \dfrac{2l}{S_h}$, $\Delta R_h = R_h - R_0$

Eq.(8) is a transcendental equation for unknown value of *y*. Finding experimentally a change in resistance ΔR_h depending on the value of current strength I_h and solving Eq. (8), one can determine the value of *y*, hence of C_0.

Fig. 2 shows the experimentally obtained dependences of ΔR_h on I_h^2 for three heaters whose parameters are given in the table.

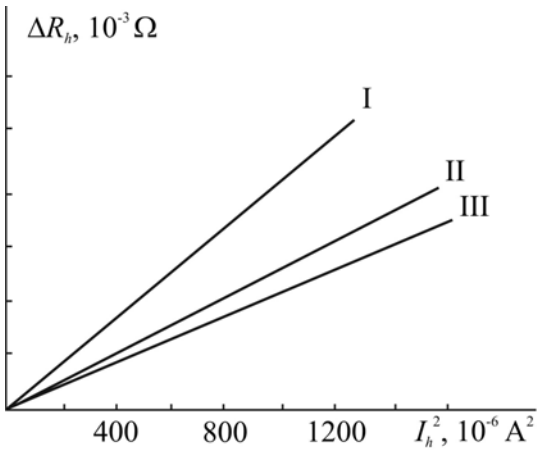

Fig. 2. Dependence of change in resistance ΔR_h on the square of current strength I_h: I – silver microwire, R_h = 1 Ω; II – copper microwire, R_h = 0.51 Ω; III – copper microwire, R_h=0.57 Ω;

As can be seen from Fig. 2, ΔR_h depends on I_h^2 in a linear fashion, which agrees well with Eq. (8) on condition that Na does not depend on I_h, that is, instead of (3), the following expression is valid

$$Na = \sqrt{\frac{C_0 P_h + \varepsilon\sigma_б 4T_0^3}{\kappa_h S_h}} \tag{9}$$

The evaluations confirm the correctness of the assumption in the derivation of formula (9). Note that the presence of a linear relationship between ΔR_h and I_h^2 simplifies determination of a coefficient of heat exchange C_0. For this purpose, one can use another transcendental equation, namely:

$$\frac{d(\Delta R_н)}{d(I_н^2)} = \frac{R_0 l\beta}{\kappa_н S_н y^2}\left[1 - \frac{\mathrm{th}(y)}{y}\right] \tag{10}$$

The obtained C_0 values are given in the Table.

Table

Parameters of the heaters

Type of heater in glass insulation	Diameter of metal wire d, 10^{-6} m	Diameter of microwire in insulation d_c, 10^{-6} m	Electric resistance of the heater R, Ω	TRC, $10^{-3}K^{-1}$	Coefficient of heat exchange with the environment, 10^{-3} W/m^{2}K
Silver microwire	7	18	1	4.033	1.8
Copper microwire	10	20	0.51	4.033	2.3
Copper microwire	9.6	20	0.57	4.033	2.4

$$C_0 = \frac{\kappa_г}{2d} = 0.5\cdot 10^{-3}\,\frac{\mathrm{W}}{\mathrm{m}^2\cdot\mathrm{K}}, \tag{11}$$

(numerical value is indicated for the air).

The higher C_0 value obtained for a limited linear heater testifies to the influence of closely spaced current-carrying wires and small dimensions of TC package on the process of heat exchange between the heater and the environment. The difference in the C_0 values for different heaters is within the error of the experiment.

Conclusion

1. Significant increase in the sensitivity of TC can be achieved due to minimization of heat losses between its structural members.
2. Among the factors that influence the parameters of TC, a prominent place is held by the environmental effect.
3. An efficient method for determining coefficient of heat exchange between the TC heater and the environment is proposed.
4. The results obtained can be used in the design of specific TC constructions.

References

1. H. Sasaki, N. Fujiki, K. Shimizume, S.Hidaka. Development of a Thermal Voltage Converter With Calculable High - Frequency Characteristics // IEEJ Trans 2011; 6: 293 – 298.
2. Lee Y.H., Kwon S.W., Kim K.J., Park S.I., Ihm Y.E. Performance improving of KRISS Micromachined Multijunction Thermal Converter // Conference of Precision Electromagnetic Measurements Digest, 2004.
3. Klonz M., Laiz H., Kessler E. Development of Thin - Film Multijunction Thermal Converters at PTB/IPHT // IEEE Transactions of Instrumentation and Measurement, vol. 50, no. 6, December, 2001.
4. Термоэлементы и термоэлектрические устройства: Справочник / Л.И.Анатычук.– К.: Наук. думка, 1979 – 768 с.
5. Анатичук Л.І. Диференційний термоелектричний перетворювач змінного струму в режимі різночасового компарування. / Анатичук Л.І., Кузь Р.В., Тащук Д.Д. // Термоелектрика. – 2015. – № 4. – С. 77 – 82.
6. Тащук Д.Д. Оптимізація розподілу температури у термоелектричному вимірювальному перетворювачі. / Тащук Д.Д. // Термоелектрика. – 2012.– №4. – С. 95 – 98.
7. Анатычук Л.И., Андрусяк С.А., Боднарук В.И., Готра З.Ю. Анализ тепловых условий работы дифференциальных полупроводниковых термопреобразователей // Радиодетали и радиокомпоненты. – вып.4(29). – 1978. – с.72 – 77.
8. Михеев М.А. Основы теплопередачи: учеб. для вузов .-М.; Л.:Госэнергоиздат,1949 – 396 с.

Submitted 22.11.2017

Микитюк П.Д., *канд. фіз.-мат. наук*

Інститут термоелектрики НАН і МОН України, вул. Науки, 1,
Чернівці, 58029, Україна*, e-mail: anatych@gmail.com*
Чернівецький національний університет імені Юрія Федьковича,
вул. Коцюбинського 2, Чернівці, 58012, Україна; *e-mail: anatych@gmail.com*

ПРО ФАКТОРИ ВПЛИВУ НА ТОЧНІСТЬ ТЕРМОПЕРЕТВОРЮВАЧІВ

Проведено аналіз теплового режиму роботи напівпровідникового термоперетворювача (ТП). Розраховано розподіл температури в нагрівнику ТП з врахуванням впливу оточуючого середовища. Запропоновано метод визначення коефіцієнту теплообміну нагрівника ТП з оточуючим середовищем. Отримані результати можуть бути використані при конструюванні ТП з підвищеними параметрами і характеристиками. Бібл. 8, Рис. 2, Табл. 1.
Ключові слова: термоперетворювач, нагрівник, термопара, оточуюче середовище.

Микитюк П.Д., *канд. физ.-мат. наук*

Институт термоэлектричества, ул. Науки, 1, Черновцы, 58029, Украина
e-mail: anatych@gmail.com

О ФАКТОРАХ ВЛИЯНИЯ НА ТОЧНОСТЬ ТЕРМОПРЕОБРАЗОВАТЕЛЕЙ

Проведен анализ теплового режима работы полупроводникового термопреобразователя (ТП). Рассчитано распределение температуры в нагревателе ТП с учетом влияния окружающего среды. Предложен метод определения коэффициента теплообмена нагревателя ТП с окружающей средой.
Полученные результаты могут быть использованы при конструировании ТП с повышенными параметрами и характеристиками. Библ. 8, Рис. 2, Табл. 1.
Ключевые слова: термопреобразователь, нагреватель, термопара, окружающая среда.

References

1. Sasaki H., Fujiki N., Shimizume K., Hidaka S. (2011). Development of a thermal voltage converter with calculable high-frequency characteristics. *IEEJ Trans*, 6, 293 – 298.
2. Lee Y.H., Kwon S.W., Kim K.J., Park S.I., Ihm Y.E. (2004). Performance improving of KRISS micromachined multijunction thermal converter. *Conference of Precision Electromagnetic Measurements Digest* (London, England, 27 June – 2 July 2004).
3. Klonz M., Laiz H., Kessler E. (2001). Development of thin - film multijunction thermal converters at PTB/IPHT. *IEEE Transactions of Instrumentation and Measurement, 50(6).*
4. Anatychuk L.I. (1979). *Termoelementy i termoelektricheskiie ustroistva: spravochnik [Thermoelements and thermoelectric devices: handbook]*. Kyiv: Naukova dumka [in Russian].
5. Anatychuk L.I., Kuz R.V., Taschuk D.D. (2015). Dyferentsiinyi termoelektrychnyi peretvoriuvach zminnoho strumu v rezhymi riznochasovoho komparuvannia [Differential thermoelectric AC converter in the non-simultaneous comparison mode]. *Termoelektryka- J.Thermoelectricity*, 4, 77 – 82 [in Ukrainian].
6. Taschuk D.D. (2012). Optymizatsiia rozpodilu temperatury u termoelektrychnomu vymiriuvalnomu peretvoriuvachi [Optimization of temperature distribution in thermoelectric measuring transducer]. *Termoelektryka- J.Thermoelectricity,* 4, 95 – 98 [in Ukrainian].
7. Anatychuk L.I., Andrusiak S.A., Bodnaruk V.I., Hotra Z.Yu. (1978). Analiz teplovykh uslovii raboty

differentsyalnykh poluprovodnikovykh termopreobrazovatelei [Analysis of thermal operating conditions of differential semiconductor thermal converters]. *Radiodetali i radiokomponenty – Radio Details and Radio Components*, 4(29), 72 – 77 [in Russian].

8. Mikheiev M.A. (1949). *Osnovy teploperedachi: uchebnik dlia vuzov [Fundamentals of heat transfer: manual for higher educational institutions]*. Moscow, Leningrad: Gosenergoizdat [in Russian].

Submitted 22.11.2017

L.I.Anatychuk

L.I. Anatychuk, *acad. National Academy of Sciences of Ukraine*,
O.J. Luste, *Doctor Phys.-math. Sciences*

O.J.Luste

Institute of Thermoelectricity of the NAS and MES of Ukraine, 1, Nauky str, Chernivtsi, 58029, Ukraine;
Yu.Fedkovych Chernivtsi National University, 2, Kotsiubynskyi str., Chernivtsi, 58000, Ukraine*, e-mail: anatych@gmail.com*

THE EFFECT OF DEGRADATION ON THE SERVICE LIFE PROPERTIES OF THERMOELECTRIC MATERIALS

Obtaining improved functional thermoelectric materials and near-contact structures of increased service life for thermoelectric devices with a long-term operation under extreme conditions, including in space environment, requires thorough study of generalized time functions of temperature, mechanical and other effects during long-term operation of thermoelectric materials and near-contact structures, research on their degradation mechanisms, development of methods for carrying out accelerated life tests and determination of statistic laws of degradation of thermoelectric materials and near-contact structures. These investigations are based on modern reliability theory. *Bibl. 19, Fig. 5, Tables 3.*
Key words: *reliability, degradation, thermoelectric materials*.

Introduction

Peculiarities of using reliability theory in thermoelectricity

Modern reliability theory is part of applied mathematics. What features distinguish modern, "working" applied mathematics from traditional, "classical"? They are: new methodology, a new set of techniques, new research structure. Recall how a "classical" research using mathematical methods was built. The scheme is as follows: a clear statement of the problem is taken, assumptions are formulated, and then the problem is solved using irreproachably accurate formal mathematical transformations. Disputes, if they arise, concern only the correctness of the computations made (if they are incorrect, the work is discarded), or whether the author has chosen the most successful of the mathematical methods. The arbitrariness that is unavoidable in the formulation of the problem (since it fits into strictly formulated conditions) is allowed only once (most often by the author himself) and remains outside the discussion.

Once specified (note, arbitrarily!), confidence level (that is, the probability that an event can be considered reliable) "is final and binding" in the future. If an event with a probability of, say, 99 % is considered to be practically reliable, all subsequent calculations are carried out irreproachably accurately and strictly, and the question of where this 99% come from is considered even improper.

The intonation of reasoning is approximately like this: let an outsider specify confidence level. Where did he take it is not the matter of theory; the task of theory is to answer the question: does such and such hypothesis contradict the research data according to the established confidence level?

Another example. The problem of optimal planning of reliability tests is being solved. Any parameter is selected as an indicator of test effectiveness, and then absolutely strict methods are used to search for that version of the test, which makes this indicator the maximum.

Why this particular indicator or target function has been specified is not discussed.

The study begins with classical wording: "Let there be given..." and then the parameters are listed that are supposed to be "known". Where do they come from, from which source, with what precision? Such an issue is not even raised. Known – and that's all there is to it. And now the models appear that, from the applied point of view, are "informationally inadequate" – that is the only word for it.

This classical research scheme, separating the "customer" and the "executor", becomes obsolete before our eyes.

For modern applied mathematics another thing is typical: the unity of those who set the tasks and solve them. Let us pay attention to one more circumstance. In traditional mathematics, after the task is set and the assumptions are formulated, the solution is always sought at the maximum available level of accuracy. Modern applied mathematics, on the contrary, is characterized by the requirement of all equally accurate research elements. The accuracy of the apparatus must correspond to the accuracy with which the initial data may be known to us. If calculations according to this model require knowledge of parameters and functions that cannot be obtained in the foreseeable future, we must abandon this model and replace it with another, even less accurate, but based on available information. The application of reliability theory in situations where statistical stability is available and information is needed is fully justified and can yield good results. This is not the case in the situations where we do not have any information at all about unknown factors. Such problems (the choice of a solution under conditions of total uncertainty) are dealt with by the theory of statistical solutions. It is impossible to completely deny the benefit of this theory, it allows some estimates to be made, but its possibilities should not be overestimated. Where there is no information, the solution comes inevitably bad, and it is better not to pore over its rationale, but to try to get the required information in accessible scope. However, the lack of information is the researcher's trouble, rather than his advantage, although it is precisely in the absence of information that he has a chance to use the most exquisite mathematical methods. Sensibly formulated tasks require relatively simple solutions. It is a sad situation when mathematics begins to suppress common sense. Of the two extremes: "mathematics without common sense" and "common sense without mathematics" preference, certainly, should be given to the latter. Naturally, the best thing is when both are in effect, and mathematical calculations are checked all the time by "common sense".

But this is not always the case. The mathematical apparatus has some kind of hypnotic property, and researchers are often inclined to believe without doubt in their calculations, and the more complex mathematical apparatus is applied, the more they believe.

The real work is aimed at pointing out the importance of avoiding traditional mistakes in the use of mathematical methods of reliability theory. For this purpose, two problems of the reliability of thermoelectric devices and systems are considered below as an example: determination of the minimum allowable size of test sample and building reliable complex systems out of unreliable elements [1].

Determination of the minimum size of test sample.

Determination of the minimum allowable size of test sample is a task of mathematical statistics on constructing a confidence interval with a small number of experiments. To do this, a rather delicate apparatus was developed, based on the assumption that we know the law of the distribution of the sign in the general population (normal or exponential). And again, the question arises: from where is this information known? How accurate it is? And what is finally the practical value of the "product" itself - the confidence interval? Few experiments mean little information and our things look blue. But whether the confidence interval is a little wider or narrower is not so important (especially since the confidence probability is arbitrarily specified). Yet, more often than not, this problem is given undeservedly great attention. Here, there is a clear discrepancy between the inaccuracy of the statement of the problem, the low value of the findings and the perfection of the apparatus. In general, the abuse of the formal side of the

theory of probability is to the detriment of common sense - the problem of many applied works, where the mathematical apparatus is not a means but a goal.

Theory of reliability is often regarded as a sort of magic wand allowing you to get information from complete ignorance. But this is impossible - theory is only a tool for converting one piece of information to another.

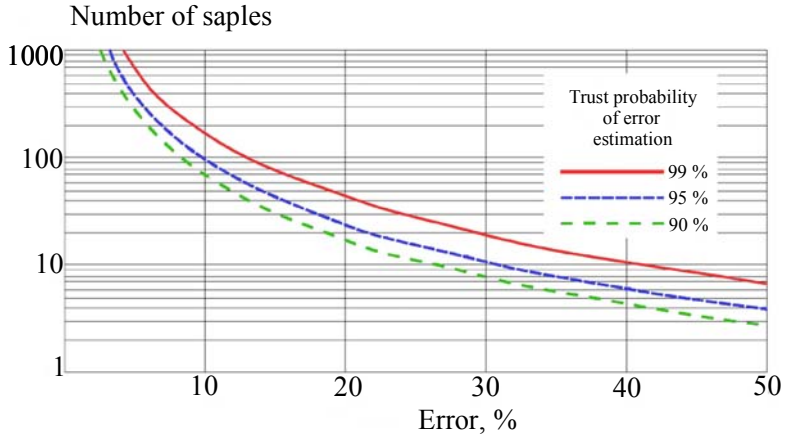

Fig.1. Relationship between the number of samples in the lot under study, the error in the determination of reliability and confidence probability parameters.

However, there is another approach, which is illustrated in Fig. 1. The figure shows the estimates obtained in [2] of the number of samples of thermoelectric modules in the lot under study, the error in the determination of reliability and confidence probability parameters. In so doing, both the law of distribution in general population and all parameters calculated and represented in Fig.1 are determined for given number of samples, and the curves illustrate the possibility of a free choice by the customer of confidence level for this error in the determination of parameters. The fundamental difference between these estimates is that, with a small number of samples, the details of the distribution law in the general population, as shown in [3], are insignificant for these estimates.

Building reliable complex systems out of unreliable elements

The task of building reliable complex systems out of unreliable elements can be formulated as finding such system structure, which provides the necessary level of reliability of the system at an arbitrarily small level of reliability of its elements. An example is the choice of the electric circuit of a thermoelectric generator, the variants of which are given in Table 1.

Table 1.

Examples of variants of electric circuits of thermoelectric generator

Variants of circuits	Structural levels			
	Lower		Upper	
	Number of connections			
	parallel	series	parallel	series
1	-	126	4	8
2	-	126	16	4
3	-	126	32	2
4	-	126	64	1

Continuation of Table 1

5	63	2	16	4
6	63	2	32	2
7	63	2	64	1

The electric power output of TEG *W(t)* on the matched load is determined from the expression $W(t) = W_0 w_0(t) W_f(t)$, where W_0 is generator power in the initial state, *w(t)* is relative power loss due to natural aging processes, $W_f(t)$ is power loss due to random failures of generator components. $w_0(t) = 1 - Kt$, where K is a constant which is determined from the results of investigation of aging processes. Power loss due to random failures $W_f(t)$ was calculated from the results of failure statistics based on the theory of reliability of complex systems with the use of the following relation of operational state probability $R(t)$:

$$R(t) = \sum \left[C_M^n \cdot R_m(t)^{M-n} \left(1 - R_m(t)\right) + \sum_{nD} \left[C_M^n - \frac{L}{n} C_k^{a+1} C_{M-(a+1)}^{n-(a+1)} \right] \left(R_m(t)(1 - R_m(t)\right)^n \right] \quad (1)$$

where k is the number of parallel connections in generator circuit, L is the number of series connections, M is the total number of modules in the generator, N is permissible number of failures, where D is total number of failures, and m – the number of permissible failures with к.

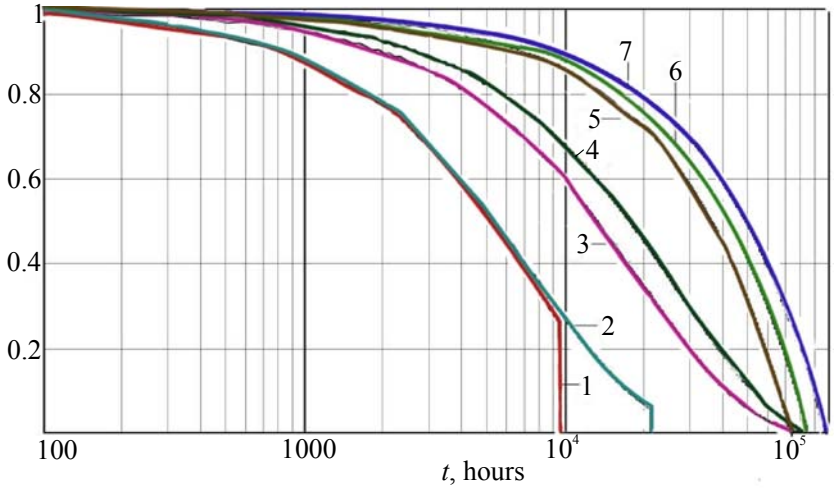

Fig. 2. Drop in TEG power with time due to failures of structural elements.

Calculations were made by the method of discrete elements using specially developed computer program. The program allows taking into account any types of failures of TEG elements, simulating them as branching Markov processes. It is possible to calculate and optimize the electrical circuit of the device not only for any number of standard sizes of TEG structural elements, but also for any restrictions on cost efficiency, dimensions, and other parameters. The results clearly show (Fig. 2) that the introduction of excessive parallel connections at increasingly lower levels of the structure hierarchy with transition from circuit 1 to circuits 2, 3, 4, 5, 6, 7 leads to a drastic improvement of the system reliability.

Thus, the necessary condition for reliability improvement is the availability of reliable information on failure statistics. Such statistically stable information can be obtained even with a small size of test sample.

Optimal choice of complex system structure allows considerable improvement of system reliability for any reliability level of components.

Elasticity limits and cyclic stability

In [3], the diagonal components of the tensor of elastic components C_{ijkl} of Bi_2Te_3 based materails doped with isovalent impurities are determined. The values of C_{ijkl} were used to study mechanical stresses arising in thermoelectric cooling modules during thermal cycling, as well as to establish the limits of elastic and plastic strains.

Cyclic stability is a fundamental operational parameter of cooling modules. Recently, the attention of researchers has been focused on increased requirements to cyclic stability due to creation of equipment which employs multiple cooling, as well as positional temperature control. The results of numerous tests have shown that conventional single-stage Peltier modules of size 40×40×4 mm under temperature cycling in the range 0÷100 °C are destroyed after several hundreds of cycles. From this standpoint, increasing the cyclic stability of thermoelectric cooling modules is certainly relevant. Significant here is determination of the elastic constants C_{ijkl} of thermoelectric materials as the initial data for calculating the cyclic stability of modules. The elastic properties of perfect Bi_2Te_3 single crystals were studied in [2 – 4]. It was noted that improvement of thermoelectric figure of merit of materials by introducing isovalent impurities alongside with reduction of phonon component of thermal conductivity leads, naturally, to the deterioration of mechanical properties of crystals.

Acoustic studies of the elastic properties of thermoelectric materials $Bi_2Te_3 + 1\ \%SbI_3$ and $Bi_{0.5}Sb_{1.5}Te_3 + 2.5\ \%Te$ (space group R3m, trigonal syngony) were performed. The anisotropic structure of these materials (the ratio $c/a = 7$) is also reflected on the high elastic anisotropy of materials having six independent components C_{ijkl} [4, 5]. The measurements of adiabatic C_{ijkl} were made by ultrasonic pulse method with a discrete delay at a frequency of 10 MHz at room temperature. The results of measurements for $Bi_2Te_3 + 1\ \%SbI_3$ are given in Table 1 (C_{ij} in W.Voigt notation in the units 10^{11} dyn/sm^2), where for comparison the C_{ij} of undoped Bi_2Te_3 crystals are given. [2, 3]. Comparing the C_{ij} measured in [2, 3] to our results, we see that introduction of isovalent impurities reduces the C_{ij} of doped crystals: longitudinal rigidity constants C_{11} and C_{33} decrease by 20 % and 4 %, respectively, and shear constant C_{44} – by 9 %. Based on the elastic constants C_{ijkl} one can calculate a number of widely used elastic parameters – Young's modulus E, shear modulus G, etc. for any orientation $\vec{q}$ in a crystal. For instance, Young's moduli $E(\vec{q})$ depend on the direction of in-plane extension as follows [4, 5]

$$E^{-1}(\vec{q}) = S_{11}\left(1-q_3^2\right)^2 + S_{33}q_3^4 + \left(2S_{13}-S_{44}\right)q_3^2\left(1-q_3^2\right) + 2S_{14}\left(3q_1^2-q_2^2\right)q_2q_3\,, \qquad (2)$$

where S_{ij} are corresponding elastic compliances, reciprocal to tensor of elastic constants C_{ij}.

Table 2

Elastic constants of thermoelectric materials based on bismuth telluride

c_{mn}	Source of data		
	ITE	[2]	[3]
	$Bi_2Te_{2.7}Se_{0.3}$+1%SbI_3	Bi_2Te_3	Bi_2Te_3
C_{11}	5.747	6.46	6.847
C_{66}	-	2.88	2.335
C_{33}	4.573	4.73	4.768
C_{44}	2.487	2.50	2.738
C_{13}	-	-	2.703
C_{14}	-	-	1.325

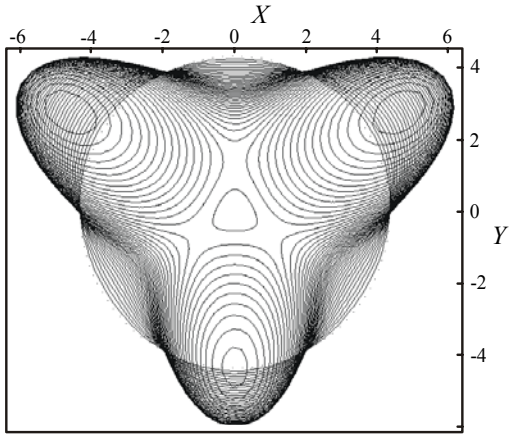

Fig. 3. Sections of characteristic Young's modulus surface by the (001) planes.

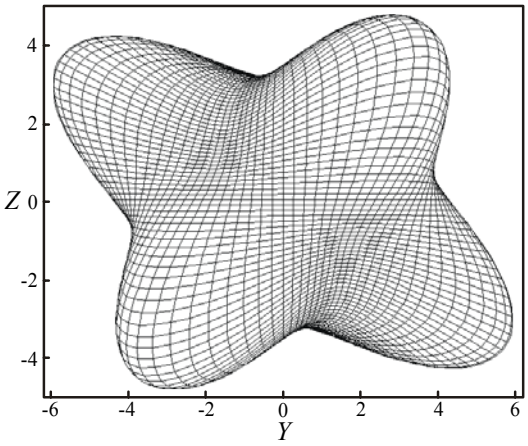

Fig. 4. Sections of characteristic Young's modulus surface by the (100) planes.

The results of calculation of the orientation dependences of Young's modulus according to (1) are shown in Figs. 1 – 2, clearly demonstrating the anisotropy of elasticity on stretching. Unlike Young's modulus, the shear modulus $G(\vec{p},\vec{q})$ in crystals depends on two directions: normal vector to slide plane $\vec{p}$ and perpendicular to it slide direction vector $\vec{q}$

$$G(\vec{p},\vec{q}) = \frac{1}{S_{im}(\vec{p}\vec{q}+\vec{q}\vec{p})_i(\vec{p}\vec{q}+\vec{q}\vec{p})_j}, \tag{3}$$

where

$$(\vec{p}\vec{q}+\vec{q}\vec{p}) = p_i q_j + p_j q_i \,(i,j \leftrightarrow 1,...6)\,. \tag{4}$$

The type of angular dependences of shear modulus for the (001) and (100) planes is shown in Fig.3. Comparing Figs.1-2 and Fig.3, it is easily seen that the anisotropy of shear modulus *G* is of the same type as *E*. The (001) plane is the plane of elastic isotropy, however, in the (100) plane the anisotropy of the shear modulus is essential: $G(\vec{p},\vec{q})$ has a maximum at shear efforts $\vec{p}$ and $\vec{q}$ along the [010] and [001] axes and a minimum at the angle bisector between these axes. In so doing, the maxima of shear modulus in the (100) plane are three times less that isotropic modulus $G(\vec{p},\vec{q})$ for the (001) plane. This result was confirmed by direct static measurements of shear moduli on the samples that have the shape and geometry in the ranges corresponding to legs of thermoelectric cooling modules. Direct static measurements of shear strains and the respective tangential shear stresses on such samples were also used to determine elasticity

limits and strength limits. It was established that for shear strains the ratio of elasticity limit in the (001) plane to elasticity limit in the (100) plane lies in the range 4.5 ÷ 4.9. For strength limits such ratio is close to 1.9.

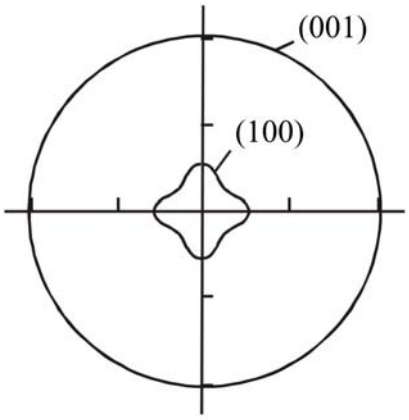

Fig.5. Angular dependences of shear modulus in the (100) and (001) planes.

Leg strains. Known parameters of elasticity and strength of thermoelectric materials allow calculating strains and mechanical stresses during cyclic switching on/off of the power supply to cooling modules and determining their cyclic stability.

As long as the rigidity of ceramic plates is much higher than that of legs, for calculations it is sufficient to consider a separate leg of thermoelectric module, and to take into account mechanical interaction between the leg and ceramics in the boundary conditions for mechanical stresses on the leg ends.

Local equilibrium equations of strained leg of anisotropic material are of the form

$$\frac{\partial \sigma_{xx}}{\partial x}+\frac{\partial \sigma_{xy}}{\partial y}+\frac{\partial \sigma_{xz}}{\partial z}=0, \tag{5}$$

$$\frac{\partial \sigma_{xy}}{\partial x}+\frac{\partial \sigma_{yy}}{\partial y}+\frac{\partial \sigma_{yz}}{\partial z}=0, \tag{6}$$

$$\frac{\partial \sigma_{xz}}{\partial x}+\frac{\partial \sigma_{yz}}{\partial y}+\frac{\partial \sigma_{zz}}{\partial z}=0, \tag{7}$$

where $\hat{\sigma}=\hat{S}\hat{u}$ is tensor of stresses, $\hat{u}$ is tensor of strains, $\hat{S}$ is tensor of elastic compliance coefficients. Directing the z axis along the longitudinal axis of legs of length l and locating the x, y axes in the cross-section of leg of area ab, let us write the boundary conditions on the faces $z = 0$ and $z = l$, assuming that the leg is rigidly fixed on the face $z = 0$, and a distributed tangential shear stress $\Sigma(x, y)$ is applied to the face $z = 0$.

$$u_{xx}\big|_{z=0}=u_{yy}\big|_{z=0}=u_{zz}\big|_{z=0}=0, \tag{8}$$

$$\sigma_{xz}\big|_{z=l}=\Sigma(x,y),\quad \sigma_{xy}\big|_{z=l}=0\quad \sigma_{zz}\big|_{z=0}=0. \tag{9}$$

The solution of the problem (4) – (8) for homogeneous anisotropic legs can be reduced to the boundary problem for a biharmonic type equation with anisotropic coefficients for the highest derivatives of the strain potential. Since the general analytical theory of such problems does not exist, numerical methods and a corresponding computer program were developed for their solution, which allows,

depending on the profile of the cross-section, the size and the effect of shear forces, to determine the strain of each leg and thus calculate the cyclic stability of the entire module, taking into account the limits of elasticity and strength.

Experimental procedure for testing of modules. In [3], a measuring complex was developed for cyclic testing of cooling modules, which allows determination of cyclic stability of 20 modules simultaneously. The complex can implement a broad spectrum of test modes. Usually, we conducted tests in harsh conditions, when the temperature on the working surface of the module varied in the range of 0 ÷ 100 °C. In so doing, the temperature of the heat-removing plate was maintained in the range of 30 ÷ 40 °C. The heating cycle time and the cooling cycle time are 5 minutes each. All modules during the tests were in conditions close to operational. For this purpose, standard heat conducting pastes were used, as well as the compression of the module with a force of 50 kg.

Testing was performed on the modules 40×40×3.5 mm of the type ALTEC-22. To ensure statistical probability, 30-50 modules were tested in each lot. Testing was performed on the modules made of materials obtained by different methods, namely the Czochralski and zone recrystallization techniques.

The following results were obtained. The correlation between the perfection of thermoelectric materials and the cyclic stability of modules made of them was established. Modules made of large-block materials with a value of ΔT_{max} from 66 – 68 K to 300 K, under normal conditions have the best cyclic stability of 400 to 1500 cycles. For materials with ΔT_{max} 72 – 74 K the cyclic stability is decreased to 200 – 400 cycles. In so doing, a reliable contact of legs with connecting plates was maintained, so breaking of legs always took place in thermoelectric material. Standard legs for modules 1.4×1.4×1.6 mm are broken at shear loads between 0.5 ÷ 1 kg. In this case, the most pronounced is the anisotropy of elasticity limits and strength limits, which is in the ratio 1:2 ÷ 1:4 and essentially depends on the structural perfection of materials, trigonal plane orientation and the size of crystalline blocks. Conspicuous is the fact that between the results of calculation and the results of testing there is a significant difference, though qualitatively these results correlate well, particularly with regard to the anisotropy of parameters. This testifies that, apart from elastic strains, there are other mechanisms in the modules that have a considerable impact on cyclic stability. Despite the fact that during cyclic tests the destruction of legs occurs inside the thermoelectric material, it always takes place in the near-contact area. This is a qualitative proof that these areas, obviously due to technological operations, have a lower mechanical strength. These circumstances will be the subject of further research.

During cyclic tests, as a rule, peripheral legs are subject to destruction, which corresponds to the results of computer calculations of stress distribution in modules. Naturally, the value of cyclic stability increases with decreasing dimensions of ceramic plates. Testing in the range 0÷100 °C creates in the legs shear strains, which are beyond the limits of elasticity, so measures were taken to reduce the strain of legs. For this purpose, the working ceramic plates were fastened to connecting plates with heat-conducting rubbers 3÷10 μm thick. The damping effect of such rubber gaskets allowed improving the cyclic stability of modules by a factor of more than 10. The result of such studies and tests was creation of design and technology for manufacturing modules of increased cyclic stability. The parameters of some of them are given in Table 3.

Table 3

Characteristics of thermoelectric modules of increased cyclic stability

Catalog №	T_h = 27°C				Dimensions (mm)						
	I_{max} (A)	Q_{max} (W)	V_{max} (V)	ΔT_{max} (K)	A	B	C	D	E	G	H
Altec-CM-1-S-IR-127-1.4×1.4-2.5	3.6	31.9	15.00	72	40	40	46	46	43	43	4.9

Continuation of Table 3

Altec-CM-1-S-IR-127-1.6×1.6-2.0	5.9	51.7	15.00	71	40	40	46	46	43	43	4.4
Altec-CM-1-S-IR-127-1.8×1.8-1.3	11.4	97.0	15.00	69	40	40	46	46	43	43	4.3
Altec-CM-1-S-IR-127-2.0×2.0-1.15	15.9	141.1	15.00	68	40	40	46	46	43	43	4.7

The guaranteed cyclic stability for the temperature range of 0 ÷ 100 °C is 10 thousand ÷ 15 thousand cycles. With increasing the amplitude of temperature change, the cyclic stability drastically grows to 150 thousand ÷ 200 thousand cycles. Significant is the fact that parameters ΔT_{max} of cyclically stable modules are retained with the use of damping layers, and Q_{max} decreases by not more than 3 %.

Conclusion

1. The necessary condition for reliability improvement is availability of real information on failure statistics. Such statistically stable information can be obtained even with a small size of test sample. Optimal choice of complex system structure allows considerable improvement of system reliability for any reliability level of components.
2. The correlation between the perfection of thermoelectric materials and cyclic stability of modules made of them is established. In so doing, the most pronounced is the anisotropy of elasticity limits and strength limits, which is in the ratio 1:2 ÷ 1:4 and essentially depends on the structural perfection of materials, trigonal plane orientation and the size of crystalline blocks.

References

1. O.J.Luste. Reliability of Thermoelectric Devices , Journal of Thermoelectricity, v.4, N 1, 1996
2. 2.L.I.Anatychuk, O.J.Luste, Journal of Thermoelectricity, , N 1, 2001
3. L.I. Anatychuk, V.N. Balazyuk, O.J. Luste, V.V. Malyshko, V.P. Mikhalchenko , Journal of Thermoelectricity, N 4, 2003 p 72
4. P.Click, R.Marlow, “Reliability and failure modes of thermoelectric heat pumps”, Proc. 2nd Intl. Conf. On Thermoelectric Energy Conversion, Arlington, Texas 1978, pp. 115-120.
5. H.T.Leong, R.T.Martorana, “Finite element stress analysis of a thermoelectric cooler”, Proc. 3rd Intl. Conf. On Thermoelectric Conversion, Arlington, Texas, 1980, pp. 86-91.
6. David D.Allred, On Van Nguyen, “Accelerated life test for thermoelectric junctions: solder element interactions”, Proc. 7th Intern. Conf. On Thermoelectric Energy Conversion, Arlington, Texas, 1988, pp. 137-140.
7. D.A.Johnson, J.S.Kendrick, “Improvements in reliability of thermoelectric coolers through the use of redundant elements”, Proc. 7th Intern. Conf. On Thermoelectric Energy Conversion, Arlington, Texas 1988 Ed. K.R.Rao, Ph.D., pp. 95-100.
8. P.A.Dillon, L.McCarthy, M.I.Stephenson, “Effects of thermal cycling on thermoelectric modules”, Proc. 9th Intern. Cons. On Thermoelectrics CIT, Pasadena, 1990, JPL, pp. 136-142.
9. Richard N.Alonso, Dwight A.Johnson, Roger Devilibiss, “Predicting thermoelectric cooler reliability for the telecommunications industry”, Proc. XI Intern. Conf. Thermoelectrics, Univ. Texas, Arlington, 1992, pp. 312-318.
10. J.H.Kiely, D.V.Morgan, D.M.Rowe “Failure Analysis of a Thin Film Thermoelectric Generator”, Proc. XIII Intern. Conf. On Thermoelectrics, Kansas City, Missouri, USA, 1994.
11. R.M.Redstall, R.Studd, “Reliability of Peltier Coolers in Fiber-Optic Laser Packages”, in *CRC*

Handbook of Thermoelectrics, Ed. D.M.Rowe, CRC Press, Inc., pp. 641 - 645, 1995.
12. K. Reinschke, *Modelle zurZuverlassigkeits undEmpfindlichkietsanalyse von System,* bd.1, Berlin VEB Verlag Technik,1973; bd.2, Berlin VEB Verlag Technik, 1974.
13. *N.Wiener.,* Extrapolation, interpolation and smoothing of stationary time series, *J.Willey, N-Y,1950.*
14. А.Н.Колмогоров, "Интерполяция и экстраполяция пространственно-однородных случайных последовательностей", Изв.АН СССР,сер.мат.т.5,№ 11, 1941, с. 3-11.
15. Илисавский Ю.В. Упругие постоянные Bi_2Te_3 при 300 К // ФТТ. – 1961. – № 3. – С.3555.
16. Jenkins J.O., Rayne J.A. Elastic Moduli of Bi_2Te_3 from 4.2 K to 300 K // Phys. Letters. – 1969. – Vol. A 30. – № 6. – P.349.
17. Jenkins J.O., Rayne J.A. Ure. Elastic moduli and phonon properties of Bi_2Te_3 // Phys. Rev. – B6, 1609, 1972.
18. Voigt W. Lehrbuch der Kristallphysik. – Leipzig: B. Teubner, (1910, 1928), 1966 (Nachdruck). – 978 p.
19. Nye J. F. Physical properties of crystals. – Oxford: Clarendon Press, 1964. – 362 p.

Submitted 15.11.2017

Анатичук Л.І. *ак. НАН України*,
Лусте О.Я. *доктор фіз.-мат. наук*

Інститут термоелектрики НАН і МОН України, вул. Науки, 1,
Чернівці, 58029, Україна*, e-mail: anatych@gmail.com*
Чернівецький національний університетім. Юрія Федьковича,
вул. Коцюбинського 2, Чернівці, 58000, Україна,
e-mail: anatych@gmail.com

ВПЛИВ ДЕГРАДАЦІЇ НА РЕСУРСНІ ВЛАСТИВОСТІ ТЕРМОЕЛЕКТРИЧНИХ МАТЕРІАЛІВ

Одержання вдосконалених функціональних термоелектричних матеріалів та приконтактних структур підвищеної ресурсної стійкості для термоелектричних пристроїв з довготривалим терміном експлуатації в екстремальних умовах, в тому числі в космічному середовищі вимагає ретельного вивчення узагальнених часових функцій впливу температурних, механічних та інших дій при довготривалій експлуатації термоелектричних матеріалів та приконтактних структур, дослідження механізмів їх деградації, розробки методів проведення прискорених ресурсних випробувань та визначення статистичних закономірностей деградації термоелектричних матеріалів та приконтактних структур. В основу цих досліджень покладено сучасну теорію надійності. Бібл. 19, Рис. 5, Табл. 3.
Ключові слова: .

Анатычук Л.И. *ак. НАН Украины*,
Лусте О.Я. *доктор физ.-мат. наук*

Институт термоэлектричества, ул. Науки, 1, Черновцы, 58029, Украина
e-mail: anatych@gmail.com

Черновицкий национальный университет им. Юрия Федьковича,
ул. Коцюбинського 2, Черновцы, 58000, Украина
e-mail: anatych@gmail.com

ВЛИЯНИЕ ДЕГРАДАЦИИ НА РЕСУРСНЫЕ СВОЙСТВА ТЕРМОЭЛЕКТРИЧЕСКИХ МАТЕРИАЛОВ

Получение усовершенствованных функциональных термоэлектрических материалов и приконтактных структур повышенной ресурсной стойкости для термоэлектрических устройств с продолжительным сроком эксплуатации в экстремальных условиях, в том числе в космической среде, требует тщательного изучения обобщенных временных функций влияния температурных, механических и прочих воздействий при продолжительной эксплуатации термоэлектрических материалов и приконтактных структур, исследования механизмов их деградации, разработки методов проведения ускоренных ресурсных испытаний и определения статистических закономерностей деградации термоэлектрических материалов и приконтактных структур. В основу этих исследований положена современная теория надежности. Библ. 19, Рис. 5, Табл. 3.

Ключевые слова: .

References

1. Luste O.J. (1996). Reliability of thermoelectric devices. *J. Thermoelectricity*, 1, 5-13.
2. Anatychuk L.I., Luste O.J. (2001). Osobennosti primeneniia teorii nadezhnosti v termoelektrichestve [Peculiarities of using reliability theory in thermoelectricity]. Termoelektrichestvo - *J. Thermoelectricity*, 1, 60-65 [in Russian].
3. Anatychuk L.I., Balazyuk V.N., Luste O.J., Malyshko V.V., Mikhalchenko V.P. (2003). Povysheniie tsiklicheskoi ustoichivosti termoelektricheskikh modulei okhlazhdeniia [Increase of cyclic stability of cooling thermoelectric modules]. Termoelektrichestvo - *J. Thermoelectricity*, 4, 72-76 [in Russian].
4. Click P., Marlow R. (1978). Reliability and failure modes of thermoelectric heat pumps. *Proc. 2nd Intl. Conf. On Thermoelectric Energy Conversion* (Arlington, Texas, 1978) (pp. 115-120).
5. Leong H.T., Martorana R.T. (1980). Finite element stress analysis of a thermoelectric cooler. *Proc. 3rd Intl. Conf. On Thermoelectric Conversion* (Arlington, Texas, 1980) (pp. 86-91).
6. Allred David D., Nguyen On Van. (1988). Accelerated life test for thermoelectric junctions: solder element interactions. *Proc. 7th Intern. Conf. On Thermoelectric Energy Conversion* (Arlington, Texas, 1988) (pp. 137-140).
7. Johnson D.A., Kendrick J.S. (1988). Improvements in reliability of thermoelectric coolers through the use of redundant elements. *Proc. 7th Intern. Conf. On Thermoelectric Energy Conversion* (Arlington, Texas, 1988). K.R.Rao (Ed.) (pp. 95-100).
8. Dillon P.A., McCarthy L., Stephenson M.I. (1990). Effects of thermal cycling on thermoelectric modules. *Proc. 9th Intern. Conf. On Thermoelectrics* (Pasadena, JPL, 1990) (pp. 136-142).
9. Alonso Richard N., Johnson Dwight A., Devilibiss Roger. (1992). Predicting thermoelectric cooler reliability for the telecommunications industry. *Proc. XI Intern. Conf. Thermoelectrics* (Univ. Texas, Arlington, 1992) (pp. 312-318).
10. Kiely J.H., Morgan D.V., Rowe D.M. (1994). Failure analysis of a thin film thermoelectric generator. *Proc. XIII Intern. Conf. On Thermoelectrics* (Kansas City, Missouri, USA, 1994).

11. Redstall R.M., Studd R. (1995). Reliability of Peltier coolers in fiber-optic laser packages. *CRC Handbook of Thermoelectrics.* D.M.Rowe (Ed.). CRC Press, Inc. (pp. 641 – 645).
12. Reinschke K. (1973, 1974). *Modelle zur Zuverlassigkeits und Empfindlichkeitsanalyse von System,* Bd.1. Berlin: VEB Verlag Technik, 1973; Bd.2. Berlin: VEB Verlag Technik, 1974.
13. Wiener N. (1950). *Extrapolation, interpolation and smoothing of stationary time series*. New York: J.Wiley.
14. Kolmogorov A.N. (1941). Interpolation and extrapolation of spatially-inhomogeneous random sequences. *Izvestiia Akademii Nauk SSSR. Matematika – Bulletin of the USSR Academy of Sciences. Mathematics*, 5(11), 3-11 [in Russian].
15. Ilisavskii Yu.V. (1961). Uprugiie postoiannyie Bi_2Te_3 pri 300 K [Elastic constants of Bi_2Te_3 at 300 K]. *Fizika tverdogo tela – Physics of the Solid State*, 3, 3555 [in Russian].
16. 16. Jenkins J.O., Rayne J.A. (1969). Elastic moduli of Bi_2Te_3 from 4.2K to 300 K. *Phys.Letters A*, 30 (6), 349.
17. Jenkins J.O., Rayne J.A., Ure R.W. (1972). Elastic moduli and phonon properties of Bi_2Te_3 . *Phys. Rev. B,* 6, 1609.
18. Voigt W. (1966). *Lehrbuch der Kristallphysik*. Leipzig: B. Teubner.
19. Nye J. F. (1964). *Physical properties of crystals*. Oxford: Clarendon Press.

Submitted 15.11.2017

ARTICLE SUBMISSION GUIDELINES

For publication in a specialized journal, scientific works are accepted that have never been printed before. The article should be written on an actual topic, contain the results of an in-depth scientific study, the novelty and justification of scientific conclusions for the purpose of the article (the task in view).

The materials published in the journal are subject to internal and external review which is carried out by members of the editorial board and international editorial board of the journal or experts of the relevant field. Reviewing is done on the basis of confidentiality. In the event of a negative review or substantial remarks, the article may be rejected or returned to the author(s) for revision. In the case when the author(s) disagrees with the opinion of the reviewer, an additional independent review may be done by the editorial board. After the author makes changes in accordance with the comments of the reviewer, the article is signed to print.

The editorial board has the right to refuse to publish manuscripts containing previously published data, as well as materials that do not fit the profile of the journal or materials of research pursued in violation of ethical norms (for instance, conflicts between authors or between authors and organization, plagiarism, etc.). The editorial board of the journal reserves the right to edit and reduce the manuscripts without violating the author's content. Rejected manuscripts are not returned to the authors.

Submission of manuscript to the journal

The manuscript is submitted to the editorial office of the journal in paper form in duplicate and in electronic form on an electronic medium (disc, memory stick). The electronic version of the article shall fully correspond to the paper version. The manuscript must be signed by all co-authors or a responsible representative.

In some cases it is allowed to send an article by e-mail instead of an electronic medium (disc, memory stick).

English-speaking authors submit their manuscripts in English. Russian-speaking and Ukrainian-speaking authors submit their manuscripts in English and in Russian or Ukrainian, respectively. Page format is A4. The number of pages shall not exceed 15 (together with References and extended abstracts). By agreement with the editorial board, the number of pages can be increased.

To the manuscript is added:

1. Official recommendation letter, signed by the head of the institution where the work was carried out.

2. License agreement on the transfer of copyright (the form of the agreement can be obtained from the editorial office of the journal or downloaded from the journal website – Dohovir.pdf). The license agreement comes into force after the acceptance of the article for publication. Signing of the license agreement by the author(s) means that they are acquainted and agree with the terms of the agreement.

3. Information about each of the authors – full name, position, place of work, academic title, academic degree, contact information (phone number, e-mail address), ORCID code (if available). Information about the authors is submitted as follows:

authors from Ukraine - in three languages, namely Ukrainian, Russian and English;

authors from the CIS countries - in two languages, namely Russian and English;

authors from foreign countries – in English.

4. Medium with the text of the article, figures, tables, information about the authors in electronic form.

5. Colored photo of the author(s). Black-and-white photos are not accepted by the editorial staff. With the number of authors more than two, their photos are not shown.

Requirements for article design

The article should be structured according to the following sections:

- *Introduction*. Contains the problem statement, relevance of the chosen topic, analysis of recent research and publications, purpose and objectives.
- *Presentation of the main research material* and the results obtained.
- *Conclusions* summing up the work and the prospects for further research in this direction.
- *References*.

The first page of the article contains information:

1) in the upper left corner – UDC identifier (for authors from Ukraine and the CIS countries);

2) surname(s) and initials, academic degree and scientific title of the author(s);

3) the name of the institution where the author(s) work, the postal address, telephone number, e-mail address of the author(s);

4) article title;

5) abstract to the article – not more than 1 800 characters. The abstract should reflect the consistent logic of describing the results and describe the main objectives of the study, summarize the most significant results;

6) key words – not more than 8 words.

The text of the article is printed in Times New Roman, font size 11 pt, line spacing 1.2 on A4 size paper, justified alignment. There should be no hyphenation in the article.

Page setup: "mirror margins" – top margin – 2.5 cm, bottom margin – 2.0 cm, inside – 2.0 cm, outside – 3.0 cm, from the edge to page header and page footer – 1.27 cm.

Graphic materials, pictures shall be submitted in color or, as an exception, black and white, in .opj or .cdr formats, .jpg or .tif formats being also permissible. According to author's choice, the tables and partially the text can be also in color.

Figures are printed on separate pages. The text in the figures must be in the font size 10 pt. On the charts, the units of measure are separated by commas. Figures are numbered in the order of their arrangement in the text, parts of the figures are numbered with letters – a, b, .. On the back of the figure, the title of the article, the author (authors) and the figure number are written in pencil. Scanned images and graphs are not allowed to be inserted.

Tables are provided on separate pages and must be executed using the MSWord table editor. Using pseudo-graph characters to design tables is inadmissible.

Formulae shall be typed in Equation or MatType formula editors. Articles with formulae written by hand are not accepted for printing. It is necessary to give definitions of quantities that are first used in the text, and then use the appropriate term.

Captions to figures and tables are printed in the manuscript after the references.

Reference list shall appear at the end of the article. References are numbered consecutively in the order in which they are quoted in the text of the article. References to unpublished and unfinished works are inadmissible.

Attention! In connection with the inclusion of the journal in the international bibliographic abstract database, the reference list should consist of two blocks: CITED LITERATURE and REFERENCES (this requirement also applies to English articles):

CITED LITERATURE – sources in the original language, executed in accordance with the Ukrainian standard of bibliographic description DSTU 8302:2015. With the aid of VAK.in.ua (http://vak.in.ua) you can automatically, quickly and easily execute your "Cited literature" list in conformity with the requirements of State Certification Commission of Ukraine and prepare references to scientific sources in Ukraine in understandable and unified manner. This portal facilitates the processing of scientific sources when writing your publications, dissertations and other scientific papers.

REFERENCES – the same cited literature list transliterated in Roman alphabet (recommendations according to international bibliographic standard APA-2010, guidelines for drawing up a transliterated reference list "References" are on the site http//www.dse.org.ua, section for authors).

To speed up the publication of the article, please adhere to the following rules:

- in the upper left corner of the first page of the article – the UDC identifier;
- family name and initials of the author(s);
- academic degree, scientific title;

begin a new line, Times New Roman font, size 12 pt, line spacing 1.2, center alignment;

- name of organization, address (street, city, zip code, country), e-mail of the author(s);

begin a new line 1 cm below the name and initials of the author(s), Times New Roman font, size 11 pt, line spacing 1.2, center alignment;

- the title of the article is arranged 1 cm below the name of organization, in capital letters, semi-bold, font Times New Roman, size 12 pt, line spacing 1.2, center alignment. The title of the article shall be concrete and possibly concise;
- the abstract is arranged 1 cm below the title of the article, font Times New Roman, size 10 pt, in italics, line spacing 1.2, justified alignment in Ukrainian or Russian (for Ukrainian-speaking and Russian-speaking authors, respectively);
- key words are arranged below the abstract, font Times New Roman, size 10 pt, line spacing 1.2, justified alignment. The language of the key words corresponds to that of the abstract. Heading "Key words" - font Times New Roman, size 10 pt, semi-bold;
- the main text of the article is arranged 1 cm below the abstract, indent 1 cm, font Times New Roman, size 11 pt, line space spacing 1.2, justified alignment;
- formulae are typed in formula editor, fonts Symbol, Times New Roman. Font size is "normal" – 12 pt, "large index" – 7 pt, "small index" – 5 pt, "large symbol" – 18 pt, "small symbol" – 12 pt. The formula is arranged in the text, center aligned and shall not occupy more than 5/6 of the line width, formulae are numbered in parentheses on the right;
- dimensions of all quantities used in the article are represented in the International System of Units (SI) with the explication of the symbols employed;
- figures are arranged in the text. The figures and pictures shall be clear and contrast; the plot axes – parallel to sheet edges, thus eliminating possible displacement of angles in scaling; figures are submitted in color, black-and-white figures are not accepted by the editorial staff of the journal;
- tables are arranged in the text. The width of the table shall be 1 cm less than the line width. Above the table its ordinary number is indicated, right alignment. Continuous table numbering

throughout the text. The title of the table is arranged below its number, center alignment;

- references should appear at the end of the article. References within the text should be enclosed in square brackets behind the text. References should be numbered in order of first appearance in the text. Examples of various reference types are given below.

Examples of LITERATURE CITED

Journal articles

Anatychuk L.I., Mykhailovsky V.Ya., Maksymuk M.V., Andrusiak I.S. Experimental research on thermoelectric automobile starting pre-heater operated with diesel fuel. *J.Thermoelectricity*. 2016. №4. P.84–94.

Books

Anatychuk L.I. *Thermoelements and thermoelectric devices. Handbook.* Kyiv, Naukova dumka, 1979. 768 p.

Patents

Patent of Ukraine № 85293. Anatychuk L.I., Luste O.J., Nitsovych O.V. Thermoelement.

Conference proceedings

Lysko V.V. *State of the art and expected progress in metrology of thermoelectric materials.* Proceedings of the XVII International Forum on Thermoelectricity (May 14-18, 2017, Belfast). Chernivtsi, 2017. 64 p.

Authors' abstracts

Kobylianskyi R.R. *Thermoelectric devices for treatment of skin diseases*: extended abstract of candidate's thesis. Chernivtsi, 2011. 20 p.

Examples of REFERENCES

Journal articles

Gorskiy P.V. (2015). Ob usloviakh vysokoi dobrotnosti i metodikakh poiska perspektivnykh sverhreshetochnykh termoelektricheskikh materialov [On the conditions of high figure of merit and methods of search for promising superlattice thermoelectric materials]. *Termoelektrichestvo - J.Thermoelectricity,* 3, 5 – 14 [in Russian].

Books

Anatychuk L.I. (2003). *Thermoelectricity. Vol.2. Thermoelectric power converters*. Kyiv, Chernivtsi: Institute of Thermoelectricity.

Patents

Patent of Ukraine № 85293. Anatychuk L. I., Luste O.Ya., Nitsovych O.V. Thermoelements [In Ukrainian].

Conference proceedings

Rifert V.G. Intensification of heat exchange at condensation and evaporation of liquid in 5 flowing-down films. In: *Proc. of the 9th International Conference Heat Transfer.* May 20-25, 1990, Israel.

Authors'abstracts

Mashukov A.O. *Efficiency hospital state of rehabilitation of patients with color carcer.* PhD (Med.) Odesa, 2011 [In Ukrainian].